THE UNIVERSITY OF CHICAGO

DEVELOPMENTAL AND EVOLUTIONARY MECHANISMS THAT SHAPE RODENT MOLARS

A DISSERTATION SUBMITTED TO

THE FACULTY OF THE DIVISION OF THE BIOLOGICAL SCIENCES

AND THE PRITZKER SCHOOL OF MEDICINE

IN CANDIDACY FOR THE DEGREE OF

DOCTOR OF PHILOSOPHY

COMMITTEE ON EVOLUTIONARY BIOLOGY

BY

ROBERT WAYNE BURROUGHS

CHICAGO, ILLINOIS

AUGUST 2021

Table of Contents

List of Figures

List of Tables

Acknowledgements

I thank the collections managers for access to specimens, specifically Adam Ferguson (FMNH), Chris Conroy (MVZ), Erick Rickhart (UMNH), Patricia Holroyd (UCMP), Chris Sagebiel (TMM), and Chris Sidor (UW).

I thank April Isch-Neander, Lisa Lichty, and Jacob Wiley, and Francesca Socki for help in collecting μCT data.

I thank Jukka Jernvall, Ophir Klein, Pauline Marangoni, Santiago Herrera-Alvarez, David Jablonski, P. David Polly, Anjali Goswami, Charles Marshall, Scott Lidgard, Larry Heaney, Kevin Feldheim, Erica Zahnle, Izzy Distefano, Christopher Bell, Christopher Jass, Natasha Vitek, Kelsey Stilon, James Proffitt, Leslie Hlusko, and Graham Slater for helpful conversations regarding ideas, methods, and concepts presented in this thesis.

I thank the staff and faculty of the Committee on Evolutionary Biology for emotional and financial support.

Finally, I thank my family, Catherine Burroughs, Nora Burroughs, Wayne Burroughs, Angela Macias, Liz Mitha, Rasheed Mitha, and Jett, Ronan, Aziz, and Ayah for their love and support.

Forward

I constructed this thesis to integrate developmental and morphological data to understand evolutionary mechanisms. I recognized that in order to integrate both developmental and morphological data, I would need an empirical system which met a number of criteria. Those criteria were that the system in question:

1. Have a substantial fossil record;
2. Have individuals that can be diagnosed to a reasonable taxonomic level based on isolated fossils;
3. Encompass a substantial evolutionary transition in an anatomical system that has received substantial studies from both evolutionary and developmental perspectives;
4. Be phylogenetically close to a developmental model species with substantial studies already conducted.

Based on my own background as a vertebrate paleontologist, I chose to focus on a vertebrate system. I quickly recognized that one such system was rodent teeth, in particular the lower first molar (m1) of rodents, which has a huge volume of studies dedicated to it from both evolutionary and developmental perspectives. The fossil record of mammal teeth is quite robust and rodent teeth are quite common in the late Cenozoic (e.g., Quaternary) fossil record. Among those fossils, voles are commonly studied from evolutionary and biostratigraphic perspectives. Ultimately, I chose *Lemmiscus curtatus*, the sagebrush vole, as my evolutionary system of choice, because it has a substantial fossil record in the Pleistocene-Holocene and is still extant (Nowak 1999; Bell et al.

2019). A substantial evolutionary transition has been described in *L. curtatus*, consisting of an increase in the number of closed enamel triangles on the anterior end of the m1 (Barnosky and Bell 2003; Figure F.1).

The apices of the enamel triangles of voles (such as *Lemmiscus*) are homologous with cusps (Keränen et al. 1998), and thus developmental mechanisms that can explain the formation of new cusps on the m1 of rodents generally also have the potential to explain the formation of new enamel triangles on the m1 of voles. One question I was forced to answer initially was whether there was a developmental limit on the number of cusps that could be present on the m1 of *Lemmiscus*. Because there is limited work on the development of vole teeth, I chose to focus broadly on determining if there were developmental limitations to the number of cusps found on the m1s of rodents as a whole. To this end, I identified two constraints: 1) a phylogenetic constraint, where absent the evolutionary loss of the fourth premolar (p4), more than six cusps cannot occur on the m1 of rodents (Burroughs 2019; Chapter 1 this work); and 2) a developmental constraint, where it appears that for rodent m1s to have fewer than four cusps, substantial changes in developmental regimes must occur that are lethal to embryonic individuals (Burroughs 2019; Chapter 1 of this work).

In the course of uncovering these constraints, I proposed hypothetical mechanisms that can serve to explain why loss of the p4 is necessary to produce more than six cusps on the m1. It was identified that early in development, primordial developmental buds of third and fourth premolars (both lost evolutionarily in different clades during

rodent evolutionary history) are present (Prochazka et al. 2010; Figure F.2). This discovery, combined with evidence that the m1 tooth bud has signaling center expansion that begins to include a portion of the p4 served as the basis of the 'Rudimentary Tooth Buds' hypothesis (Prochazka et al. 2010; Burroughs 2019; Figure F.2). This hypothesis stipulates that expansion of the m1 to include portions of the presumptive p4 results in the ability to form additional cusps on the m1 (Burroughs 2019; Chapter 1 this work). Thus, the loss of the p4 served to release the previously-identified phylogenetic constraint (Burroughs 2019; Chapter 1 this work). As a result, it can be hypothesized that individuals without a p4 that show substantial evolutionary shifts at the anterior end of the m1 (such as the addition of anterior cusp homologues described for *Lemmiscus*) represent the incorporation of increasing amounts of the p4 into the m1 (Chapters 2 and 3 this work).

Subsequent developmental experiments on m1 toothbuds grown in culture found that it was possible to recover a p4-like morphology via bisection of the m1 to separate the anterior and posterior portions of the tooth bud (Sadier et al. 2019). As a result, it could be hypothesized that more cusps can be added evolutionarily to m1 in individuals that do not have a p4; thus it could be that an m1 made up of two distinct developmental modules, something that was initially postulated by Prochazka et al. (2010). However, Sadier et al. (2019) discovered that the presumptive p4 morphology can be experimentally rescued from their bisection experiments, a surprising finding that shows the presumptive p4 may not be fully merged into m1 in muroid evolution as previously postulated by Prochazka et al (2010). Sadier et al. (2019) have hypothesized that down-

stream developmental repatterning would result in complete integration of p4-components into the m1. During this late stage repatterning, the ‘p4-components’ of an earlier stage have since lost their p4 identity and become entirely ‘m1’ in identity (Sadier et al. 2019; Figure F.2).

Because development serves as the basis of phenotype, it is anticipated that increased developmental integration should result in downstream morphological integration (Klingenberg 2008). The mechanism behind this is that as developmental traits become more tightly integrated, covariation between developmental traits and phenotypic traits increases (Klingenberg 2008). I have shown that development serves to limit cusp number on the m1 (Burroughs 2019; Chapter 1 of this work). Therefore, it is possible to utilize a phenotypic system that is directly tied to a developmental system to investigate developmental modularity and integration, by looking at patterns of phenotypic integration and modularity.

As a result, here, I utilized the proposed evolutionary patterns of *Lemmiscus*, and the identification of developmental and phylogenetic constraints, to test the hypothesis that the m1 includes two modules reflecting the distinct contributions of the p4 and m1 during development (Prochazka et al. 2010). Alternatively, Sadier et al.’s (2019) results raise the possibility that re-patterning of the m1 later in development overprints the original p4 and m1 identities of the different portions of the tooth, resulting in a phenotypically integrated m1.

I found that there is a strong signal of morphological integration in the m1 across the evolutionary history of *Lemmiscus*, supporting that hypothesis that there is downstream repatterning of the m1 that results in complete integration of the p4 into the m1 (Chapters 2 and 3 of this work). The substantial phenotypic shifts in the m1 of *Lemmiscus* over the course of its evolutionary history are primarily limited to the regions of the m1 that appear to be more developmentally labile (Chapter 1 of this work). This suggests that developmental integration is the dominant evolutionary mechanism for m1s within *Lemmiscus*, and that natural selection has only been able to act on traits that have the largest amount of developmental lability over that time.

Cited

Barnosky A. D., and Bell C. J. 2003. Evolution, climatic change, and species boundaries: Perspectives from tracing *Lemmiscus curtatus* populations through time and space. Proceedings of the Royal Society of London B 270: 2585-2590.

Bell, C. J., Jass, C. N. Burroughs, R. W. 2019. Dental variation in a collection of *Lemmiscus curtatus* from the northern plains of southern Saskatchewan: implications for morphological evolution. *Western North American Naturalist* 79:219–232.

Burroughs, R.W. 2019. Modeling rodent tooth morphogenesis reveals constraints on mammalian tooth evolution. *Scientific Reports* 9:10902 doi:10.1038/s41598-019-47469-x

Keranen SV, Aberg T, Kettunen P, Thesleff I, Jernvall J (1998) Association of developmental regulatory genes with the development of different molar tooth shapes in two species of rodents. Dev Genes Evol 208, 477–486.

Klingenberg, C. 2008. Morphological integration and developmental modularity. Annual Review of Ecology Evolution and Systematics 39: 115-132.

Nowak, R. M. 1999. Walker's Mammals of the World; 2-Volume Set, Johns Hopkins University Press; 6th Edition.

Prochazka, J., Pantalucci, S., Churava, S., Rothova, M., Lambert, A., Lesot, H., Klein, O., Peterka, M., Laudet, V., and Peterkova, R. 2010. Patterning by heritage in mouse molar row development. PNAS 107, 15497-15502.

Sadier, A., Twarogowska, M., Steklikova, K., Hayden, L., Lambert, A., Schneider, P., Laudet, V., Hovorakova, M., Calvez, V., and Pantalacci, S. 2019. Modeling Edar expression reveals the hidden dynamics of tooth signaling center patterning. PLoS Biol. 17, e3000064. doi: https://doi.org/10.1371/journal.pbio.3000064

Figure F.1: Evolutionary History of *Lemmiscus curtatus*

Line drawings of theoretical m1s of *Lemmiscus curtatus* showing evolutionary transitions of increasing numbers of closed enamel triangles.

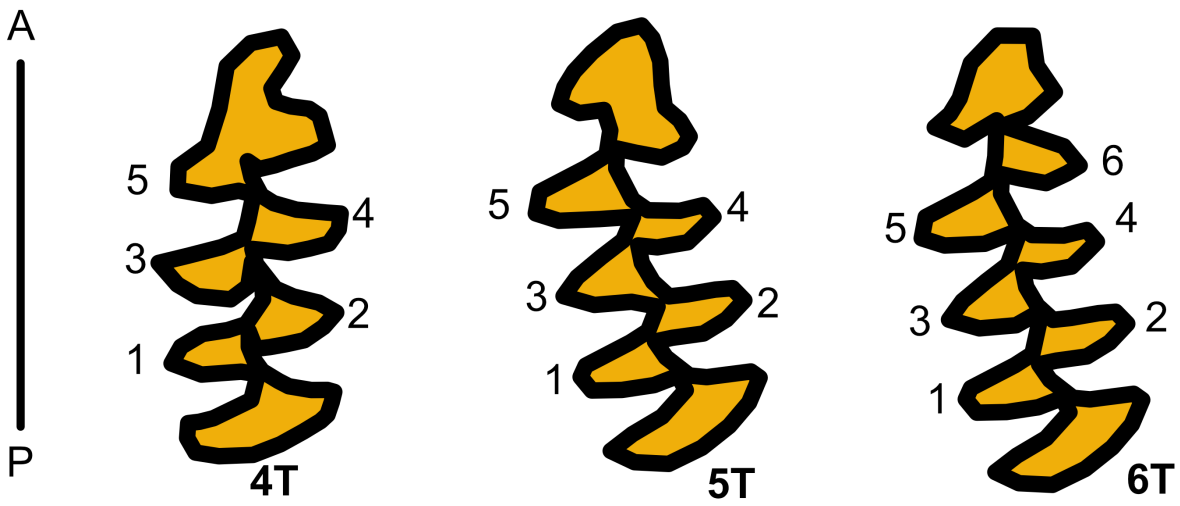

Figure F.2: Diagram of Muroid Molar Development

Diagram showing developmental of m1 from stages E13-E15+. Initial conception (Prochazka et al. 2010) was that after stage E14 there would be inclusion of the p4 primordial bud into the m1, but that the both the p4 and m1 modules could be separated experimentally at all developmental stages E14-onward. Alternative hyopthesis of Sadier et al. (2019) is that after from E15-onward there would be developmental repatterning which resulted in total integration of the p4 into the m1.

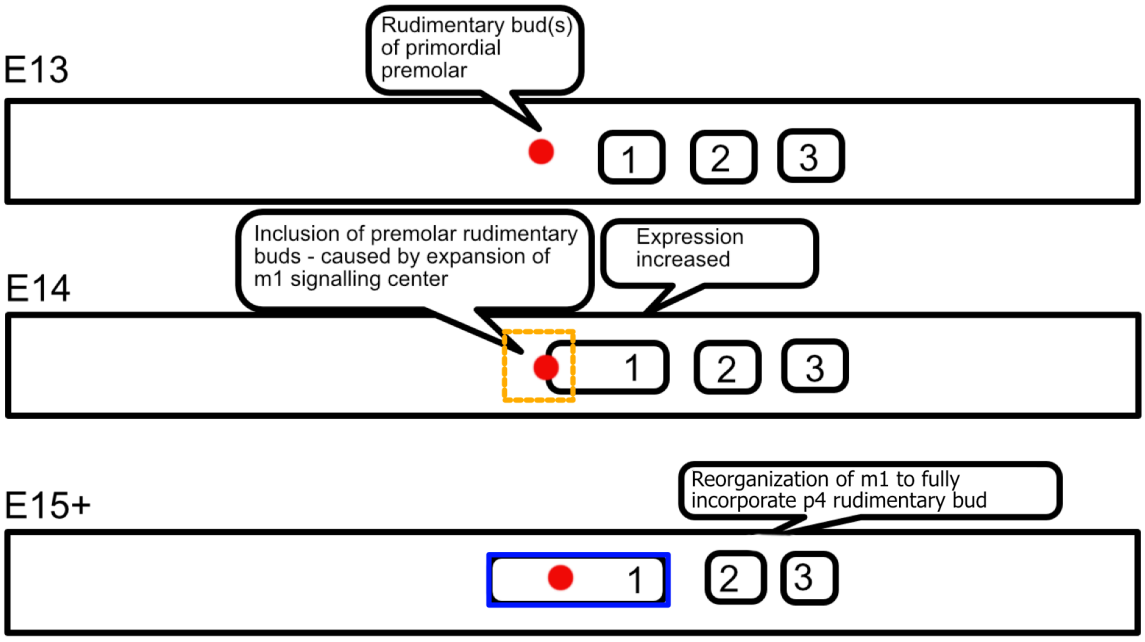

Chapter 1: Phylogenetic and Developmental Constraints Dictate the Number of Cusps on Molars in Rodents

Author Note: The following text is edited from the accepted, revised, manuscript version of my publication: Burroughs, R.W. 2019. Modeling rodent tooth morphogenesis reveals constraints on mammalian tooth evolution. *Scientific Reports* 9:10902 doi:10.1038/s41598-019-47469-x. Edits are limited to formatting changes to conform to the style of the remaining chapters of this work.

Introduction

Mammal teeth show great diversity in morphology and function, which is directly correlated with dietary ecology and evolution (Ungar 2010, Luo 2007, Luo et al. 2015). Convergence is a major feature of mammalian tooth evolution, but the mechanisms underlying this homoplasy are unclear. For instance, function and dietary ecology alone are insufficient to explain phenotypic convergence because convergent phenotypes appear to share structural components that are thought to be homologous (Ungar 2010). To understand convergence in any morphology, it is necessary to understand the constraints that affect it. Here, I investigate constraints on a major structural feature of tooth morphology in rodents, cusp number. I use an *in silico* modeling approach and empirical data from a broad sample of rodents to determine these constraints. In the course of identifying these constraints, I uncover rules that underlie morphogenesis (morphogenetic rules), which appear to be at least as ancient as the clade Glires.

Constraint is most readily recognized in three major forms; functional,

developmental, and phylogenetic. Functional constraints exist where the phenotype interacts with the environment and are typically revealed through the study of functional morphology. Developmental and phylogenetic constraints are more difficult to separate, but clear definitions, are available, the ones I use here are *sensu* (McGhee 2007). A developmental constraint exists when it is embryologically possible to make a specific phenotype but genesis of the phenotype results in a fatal outcome for the organism. A phylogenetic constraint is where the ability to make a specific phenotype has not yet evolved or has been lost; therefore the organism has no mechanistic way of producing the phenotype.

It is possible to begin to differentiate developmental and phylogenetic constraints from functional ones by constructing a theoretical morphospace based on morphogenetic interactions, and then comparing empirical data to determine where morphologies overlap (McGhee 2007). Here, I construct a theoretical morphospace for rodent molars using morphogenetic interactions modeled *in silico.* When compared to the reported empirical data, this morphospace allows the identification of potential developmental or morphogenetic constraints on cusp number in rodents.

Rodents are the most taxonomically diverse group of living mammals, encompassing some 40% of extant mammalian species. They are characterized by a wide range of functionally specialized tooth forms, contributing to the success of their ecological radiations (Ungar 2010). Substantial previous work has focused on detailing the process by which mammal teeth (in particular rodent teeth) develop embryologically, in-

cluding the construction of ‘staging’ schemes that demarcate the emergence of the substantial morphological features of a tooth (see: Caton and Tucker 2009 for review). Research on rodent tooth development provides an understanding of how tooth structures form and are constrained by interactions between developing morphological structures and the genetics that underlie them (e.g., Thesleff et al. 1995, Jernvall et al. 1998).

Rodent odontogenesis is broadly characterized by five main stages that follow one another in embryonic days (Caton and Tucker 2009). First, the ‘thickening’ stage (embryonic day 12.5 or E12.5) is when an invagination of the dental epithelium becomes visible. Second, the “bud” stage (E13.5), where the invagination of the dental epithelium has formed a bud-like structure and condensing neural-crest based mesenchyme is present at the base of this bud (the tooth is referred to a bud from this point until it erupts). Third, the “cap” stage (E14.5) is where the mesenchyme has sufficiently condensed that the bud is now capped by one or several primary enamel knots. Fourth, the “early bell” stage (E16.5): here further expansion of the epithelium into the mesenchyme has occurred and differentiation of tooth layers (inner enamel epithelium, dental papilla, and dental follicle) has begun, along with the differentiation of primary enamel knot(s) into secondary enamel knots on the tooth cap. Fifth, the “late bell” stage (E20), where ameloblasts are now differentiated into the distinct tooth layers commonly recognized (e.g., pulp, dentin, and enamel) and the tooth is ready to erupt. Each of these stages are initiated and limited by a host of genetic factors that control organogenesis and odontogenesis (see: Ungar 2010 and Caton and Tucker 2009 for review). It is within these five stages where minute changes to the developmental regime occur

most readily and simultaneously produce substantial morphological differences. For example, reorganization of tissues surrounding developing tooth buds that causes less compression of the bud during cap and bell stages results in the characteristic “zig-zag” or “Christmas tree” patterns of vole molars (Renvoise et al. 2017). Because all rodents, and all mammals, share this developmental staging, the basic structures of mammalian teeth are homologous. This fact is of critical importance when we investigate the changes to these structures that result in distinct tooth morphologies (and functions).

Empirical observations of cusp numbers in the fossil record show apparent trends characterized by the addition of cusps on the anterior end of the lower first molar in distantly related rodents such as voles (Barnosky and Bell 2003); muskrats (Chaline et al. 1999); and caviomorphs (Vucetich et al. 2005). These cusp additions are homoplastic, but consistent in their location, suggesting that they are constrained in some way. Constraint can take multiple forms, developmental, morphogenetic, or functional, and disentangling one type of constraint from another is exceptionally difficult. This is because constraints are fundamentally linked to one another. For example, developmental and morphogenetic constraints can be thought of as the product of the interactions between *morphogenetic rules* (*sensu* Marshal 2014). In turn, morphogenetic rules are simply the *interactions* between two or more morphology-forming genetic controls, which function to produce a *limited set of morphologies* from what is otherwise an infinite morphospace (in other words, morphogenetic rules define theoretical morphospaces; McGhee 2007, Marshall 2014). Identification of developmental or morphogenetic constraints is possible through the construction of a morphogenetic landscape, which

is itself a type of theoretical morphospace. This is done by plotting potential (or known) morphogenetic interactions on the X and Y axes and the resulting morphologies on the Z axis; further addition of modeled morphogenetic interactions results in the space becoming hyper-dimensional. The result is a landscape where morphology is defined by the interactions of two or more genetic controls. It is then necessary to compare empirical data to the theoretical morphospace. The resulting phenotypic limitations inferred from this analysis are interpreted to be constraints (morphospace limiting factors).

To understand the role of development in constraining phenotype, and therefore to disentangle developmental and morphogenetic constraint from functional constraint, I used *in silico* modeling to build a morphogenetic landscape based on the interactions of two genetic factors in odontogenesis as it relates to the lower first molars (m1) of rodents. After identifying two potential morphogenetic rules, I used empirical studies of adult rodent cheekteeth to confirm that there is a constraint placed on rodent cheekteeth by either morphogenetic interactions or developmental regimes, independent of function. My approach uses the modeling program ToothMaker (Harjunmaa et al. 2014), which models aspects of the embryological development of rodent molars, by generating enamel-knot signaling centers on an epithelial-mesenchyme interface (ToothMaker does not model deposition of mineralized tissues). One feature of embryological tooth development that allows prediction of adult tooth morphology is the number of primary and secondary enamel knots (EKs). This is because EKs are the embryological precursors of adult cusps (Caton and Tucker 2009, Vaahtokari et al. 1996); the number of EKs can serve as a proxy for the number of cusps and vice versa. The relationship between

numbers of EKs and cusps provides a link between *in silico* modeling.

Here, through the use of *in silico* modeling of enamel knots (EKs) and comparison with counts of cusps on empirical samples, I identify two broad morphogenetic rules that help constrain the number of cusps on rodent molars. One rule is identified as a developmental constraint (the minimum number of cusps found on molars), the other is identified as an phylogenetic constraint (the maximum number of cusps found on molars).

Methods

Cusps and cusp counting - Because cusps can serve as a proxy for the number of enamel knots (EKs) during development, counting cusps allows approximate quantification of the number of EKs present in a given tooth during embryological development. I counted cusp numbers and collected measurement data on the adult post-canine dentition of 40 fossil and extant rodent species. Extant specimen data was collected from the Field Museum of Natural History (FMNH) Mammal Collection (specimen numbers provided in Supplemental Dataset 1, photographs showing cusp counts are provided in Appendix 1.1). Fossil data were collected from images associated with publications (specimen numbers and publication citations provided in Appendix 1.2). Additionally, I utilized reported cusp count data from Harjunmaa et al. (2014) to add nine species and 17 specimens to my dataset, to provide a total of 57 specimens across 48 species of extant and fossil rodents. This sample represents multiple species from all living rodent families (based on Fabre et al. 2012) and the oldest definitive stem Glires (Asher et al.

2005) (Appendix 1.2).

In silico modeling - Lower first molars were modeled in ToothMaker (v 0.47) described by Harjunmaa et al. (2014) and available for download at: http://www.biocenter.helsinki.fi/bi/evodevo/toothmaker.html. ToothMaker incorporates 26 variable parameters to model embryological development of the lower first molar (Harjunmaa et al. 2014, Salazar-Ciudad and Jernvall 2010, Salazar-Ciudad and Marin-Riera 2013). Importantly, ToothMaker models embryological teeth, not adult dentition. Thus size, shape, and occlusal patterns should not be interpreted as representative of adult morphology. Instead, the models represent early stage teeth (stages E12 through ~E20 are modeled). The results of Harjunmaa et al. (2014) demonstrate that the modeled teeth are sufficiently late stage that the final number of EKs in a given model should approximate the number of cusps found on the adult lower first molar.

Default parameters in ToothMaker are those designated to represent a wild-type (WT) *Mus musculus* molar, with five enamel knots present (parameters and results Supplemental Data 2; WT designation by Harjunmaa et al. 2014). I altered two of the 26 parameters available in ToothMaker, Initial Activator Concentration (ACT) and Inhibitory Effect (INH), to assess the potential lability of EK (i.e., cusp) addition or removal. I varied ACT and INH based on published experimental results of rodents indicating that ACT directly correlates with cusp number. In particular, developmental experiments utilizing various ACT-null lines have rescued cusp morphology only after the application of an activator (e.g., Harjunmaa et al. 2014, Kangas et al. 2004). Overexpression of an activator can produce supernumerary cusps (e.g., Harjunmaa et al. 2014, Salazar-Ciudad

and Jernvall 2010, Salazar-Ciudad and Marin-Riera 2013). Simultaneously, impedance of inhibitor signaling, when an activator is present, will allow supernumerary cusp formation on occlusal surfaces (e.g.,Jarvinen et al. 2006). The expectation is that simultaneously varying ACT and INH will produce the highest numbers of supernumerary cusps in models.

I applied three schemes for altering parameters: ACT was varied while INH was held constant (at the WT designation), INH was varied while ACT was held constant (at the WT designation), and ACT and INH were varied simultaneously. To determine how sensitive the model was to minor perturbations, I adjusted ACT and INH individually and counted resulting enamel knots.

For ACT, I compared the results of adjusting ACT in 0.05 unit increments versus 0.1 unit increments, and 0.1 versus 0.2. I found no difference between 0.05 and 0.1, but found that increases of 0.2 resulted in an averaging of changes, which did not show some of the movements back and forth between enamel knot numbers. For the final analyses, I increased ACT in 0.1 unit increments from 0.5 to 3.6.

For INH, I adjusted by increments of 50 units and 100 units. No difference was found between these two increments, except at very low levels (<300) of INH. Below this point, INH produces teeth that are interpreted as not biologically realistic (SI Figure 1).

With my sampling schemes established, each model was run for 14000 iterations and all other parameters were default as defined by Harjunmaa et al. (13). The resulting

morphogenetic landscape is shown in Figure 1, a table of results and ACT-INH values is provided in Supplemental Dataset 2.

Biologically 'non-viable' models - I made efforts to explore the limitations of ToothMaker models and as a result identify several ranges which I interpret as 'biologically non-viable'. Increasing ACT or decreasing INH individually can induce seven or more supernumary cusps, but these models are interpreted as non- viable. Non-viabilty is assumed because the initial domain of ACT does not differentiate into additional EKs during any of the 14000 iterations at higher ACT levels (> 4.0) (Supplemental Figure 1A in Appendix 1.3) or lower INH levels (< 300) (SI Figure 1B), nor do they differentiate if the simulation is run longer (i.e., 28000 iterations) (SI Figure 1C). The lack of differentiation would, if biologically viable, produce a tooth with a single, large, centrally-located cusp surrounded by a sea of undiffer- entiated enamel (e.g., SI Figure 1C). Simultaneous manipulation of high ACT levels (>4.0) and low INH levels (<300) run for a standard 14000 iterations produces the same result as running for 28000 iterations (i.e., SI Figure 1C) It is also possible that at high ACT/low INH levels the mathematical model underlying these ToothMaker parameters is not capable of differenting this initial domain.

Statistical Analyses - To investigate the correlation between empirical m1 cusp number and length variables, I performed a series of Pearson's Correlation Coefficient analyses. Pearson's Correlation Coefficient uses a linear model to compare the correlation between two variables and outputs an r value between 0 and 1, with 0 being no correlation between variables and 1 being complete correlation between variables. Higher r values between two variables are interpreted as being stronger, with lowers values be-

ing “weak”. In addition, P-values are provided to determine if “weak” correlations are non-significant. Here, I use a 95% confidence interval ($P < 0.05$ is significant). In addition to comparison of empirical m1 cusp number and length variables, I investigated whether or not m1 cusp numbers collected from the empirical dataset and those from *in silico* simulations are drawn from the same distribution using a two-sample Kolmogorov-Smirnov test. The two-sample Kolmogorov-Smirnov test outputs two critical values, a D value, which is the maximum vertical deviation between two samples, and a P value, which informs us if the D value is statistically significant. A significant result, allows us to reject the null hypothesis that both samples are drawn from the same distribution.

Results

Both *in silico* and empirical data indicate that the lower first molars (m1) are limited to a minimum four cusps and predominantly a maximum of nine cusps, with complete toothrows limited to 28 cusps.

In silico modeling reveals that increasing initial activator (ACT) concentration over wild-type (WT) conditions can induce additional enamel knots (EKs) on a modeled tooth, but there appears to be a limit of six EKs that can be added by modeling ACT alone (Figure 1). Doubling of WT-ACT adds one additional cusp (from five to six); Tripling WT-ACT produces what is interpreted as a non-biologically viable tooth (see: Methods, *Biologically ‘non-viable’ models*; Supplemental Information (SI) Figure 1). Decreasing the initial inhibitory effect (INH) by lowering INH also induces additional cusps, again with a limit of six cusps total before becoming non-viable. Simultaneous

manipulation of ACT and INH produces supernumerary cusps, with a maximum number of nine cusps among the biologically-viable models (Figure 1.1).

Cusp counts of cheekteeth of 48 extant and extinct rodent species ranged between 12-28 cusps total in the toothrow (SI Table 1 in Appendix 1.3). Lower m1s consistently have 4-9 cusps. To investigate the potential influence of size of the m1 and/or toothrow length on cusp number in extant species, I used a Pearson's Correlation Coefficient to investigate the relationship between; m1 cusp number and m1 length, m1 cusp number and dentary length, and m1 cusp number and total toothrow length in 37 specimens. The results reveal a weak, significant, positive correlation between m1 cusp number and m1 tooth length ($r=0.35194$, $P=0.0254$). A weak, non-significant, positive correlation between m1 cusp number and toothrow length ($r=0.24793$, $P=0.1392$) and m1 cusp number and dentary length ($r=0.17351$, $P=0.3198$) is also recovered (Figure 1.2A). I also investigated the correlation between total cheek-toothrow cusp number and m1 cusp number, to consider if total cheektooth cusp number potentially influenced m1 cusp number; I recovered a weak, significant, positive correlation between m1 cusp number and total cheek-toothrow cusp number ($r=0.41083$, $P=0.009$). Because length data were not available for fossils, only cusp numbers are reported here; phylogenetically early rodents represented by fossils have similar counts to those in extant species, with estimated total cusp numbers between 12-25, and cusp numbers of m1s between 4-9 (SI Table 1).

Discussion

The results identify genetic interactions that define some of the morphogenetic rules for rodent (and potentially all mammal) teeth. Genetic interactions that limit enamel knot number embryologically result in a constraint on cusp number in adults. In particular, modeling indicates that there is a minimum of four enamel knots (morphogenetic rule 1) and a maximum limit of nine enamel knots (morphogenetic rule 2) that can be formed on the m1; 84% (n = 205) of simulations recover 4-9 cusps; suggesting that 4-9 cusps on m1 should be the most common form. This result is supported by cusp counts on extant and extinct rodents, where 97% of observed specimens (n=51) have between 4-9 cusps. The rarity of recovering more than nine cusps in simulations (13%, n=39) suggests that empirical examples with greater than nine cusps should be rare. Only one taxon in this study sample (*Hydrochoerus hydrochaeris*; capybara) has more than nine cusps present. Biologically viable simulation models with less than four cusps are exceptionally rare (<1%, n=2), providing an expectation that few, if any, empirical examples will be recovered. Only transgenic *Mus musculus* specimens showed fewer than 4 cusps (n=2), and both specimens have such low doses of ACT that they are considered effectively non-viable (Harjunmaa et al. 2014). Comparison of *in silico* and empirical cusp counts using a Kolmogorov-Smirnov test suggests different underlying distributions of cusp counts for the simulation and empirical data (D = 0.2321, P = 0.011). A cumulative fraction plot (Figure 1.2B) reveals that the fraction of cusps found in the empirical data is actually less than recovered in simulations, with the maximum deviation between the two occurring between seven and eight cusps. Simulations suggest we should find more empirical specimens with seven

and eight cusps than we do; implying that the patterns revealed by the simulations are conservative relative to biological reality.

The identification of minimum and maximum cusp numbers does not explain the variation in cusp number present across rodents. One potential explanation is that the number of enamel knots available for inclusion in m1 is itself variable, and is perhaps driven by the absence and presence of premolars. Previous studies have, controversially, demonstrated that expansion of gene signaling centers localized to the m1 shift anteriorly and include portions of primordial lower fourth premolars (p4) in *Mus* (Prochazka et al. 2010). More recent studies have directly investigated the potential of rescuing these primordial buds and demonstrating that they are locationally homologous to p4s (Sadier et al. 2019). This suggests that m1s may become more complex by "borrowing" enamel knots from p4 rudimentary buds that are resorbed and never fully develop. Examining the empirical cusp counts between species with p4s present and absent reveals distinct averages for m1 cusp number. Mean m1 cusp number for murids (which lack p4) is 7.48 whereas mean m1 cusp number for non-murids with p4 present is 5.47, a significant difference (Welch's T-test, P=0.00008). If m1s are "borrowing" enamel knots from p4s that do not develop, our expectation is that the mean for p4 + m1 would be higher than the m1 mean. This is the case, with the p4 + m1 mean being 10.60 whereas the m1 alone is 7.48, a significant difference (Welch's T-test, P=0.00004). Additionally, animals with and without p4s present should have total cusp count means that are different. This is also true: 21.9 with p4, 17.14 without, also a significant difference (Welch's T-test, P=0.000038). Additionally, the weak correlation

between m1 cusp number and total cheek-toothrow cusp number supports the idea that the p4 + m1 complex may well be functioning as a separate developmental module from the remaining cheekteeth. Together, these observations suggest that variation in enamel knot number for the m1 is not only a function of the morphogenetic factors modeled here, but is also related to the presence/absence of the p4, suggesting that the evolutionary loss of the p4 may be necessary for the m1 to develop more than six cusps in many scenarios.

The evolutionary consequences of the results described here are significant. Rodent lower first molars, despite numerous forms and functions, is fundamentally limited by the minimum (four) and maximum (nine) number of cusps that can be formed embryologically. Many developmental pathways exist to reach the limit of nine cusps; but far fewer surpass this limit, and even fewer allow the formation of less than four cusps. These minima and maxima are a reflection of morphogenetic rules interacting during development which serve to constrain occupied morphospace. These constraints are likely more ancient than crown Rodentia, as evidenced by an apparent hard minimum of four cusps within Glires. It would appear that uni-cuspid cheek teeth, the inferred ancestral condition within Synapsida (Ungar 2010), are not able to be developed within Glires. This suggests that the evolution of the morphogenetic rules defining the minimum number of cusps predates the origin of Glires some 65 million-plus years ago (Asher et al. 2005). The timing of the origin of the morphogenetic rules providing a maximum of nine cusps is less clear, but it appears to have been present for at least a few million years in some lineages. For instance, arvicoline rodents (e.g.,

muskrats) have evolutionarily “stalled” at nine cusps for more than two million years (Chaline et al. 1999). Molar cusp count results from this and other studies (e.g., Polly 2008) suggest that these rules may apply more broadly to many, if not all, crown eutherians; though this remains to be investigated and is beyond the scope of this study. These constraints may also be applicable to more ancient molar crown patterns that evolved convergently in different clades; such as the tribosphenic teeth that underlie the Mesozoic evolution of modern mammal clades (Luo 2007).

In this study, it appears that one developmental and one phylogenetic constraint are each present. The constraint on minimum cusp number appears to be developmental because fewer than four cusps is rare in the morphogenetic landscape and only non-viable transgenic *Mus* lines (per Harjunmaa et al. 2014) produce fewer than four cusps on the molars. The constraint on maximum cusp number appears to be phylogenetic. While it is uncommon to recover more than nine cusps in the morphogenetic landscape, at least one species, *Hydrochoerus hydrochaeris*, the capybara, does have more than nine cusps present.

Capybara may turn out to be the exception that enforces or “proves” the rule. Recent work sequencing the genome of capybara has discovered high synonymous mutation load, significant protein evolution within the Insulin-Insulin-like or Insulin-growth-factor signaling pathway (IIS/IGF1), and a potentially novel t-cell anti-cancer enhancer that functions on a tumor suppression pathway (Herera-Alvarez et al. 2018). The IIS/IGF1 pathway has been identified as playing a role in odontogenesis, including

being able to promote Fibroblast-Growth-Factor-4 (FGF4) producing enamel knots in human dental pulp cells (Oyanagi et al. 2019). It is also known that the Ectodysplasin-Activator-Ectodysplasin-Receptor (EDA-EDAR) pathway plays a critical role in activating and maintaining a tumor necrosis pathway in mammals (Mikkola and Thesleff 2003). And though entirely speculative at this stage, it is possible that the novel capybara anti-cancer enhancer may increase EDA expression in some fashion. None-the-less within capybara, it appears that the rules are broken likely be the increased expression of IIS and/or potential for a novel anti-cancer enhancer to play a role in influencing enamel knot number and formation. Importantly, it appears that, in the lone case of a rodent exceeding nine cusps on its m1, this exception required substantial regulatory and developmental evolution. Therefore the conclusion is that addition of cusps must be a phylogenetic constraint. The additional data offered by cusp number variance in the presence and absence of a p4 (itself a phylogenetically distinct character) further suggests that the ability to add cusps to the m1 is a function of phylogeny and not only development and thus is a phylogenetic constraint (*sensu* McGhee 2007).

It is important to acknowledge that the factors modeled here are a fraction of the genetic factors controlling odontogenesis. The morphogenetic rules identified here indicate that genetic interactions between ACT and INH serve to constrain a portion of the lower first molar (m1) morphology. This is not the sum total of the factors influencing molar morphology or even cusp number (see discussion of the potential role of p4 above). This means that the morphogenetic rules defining cusp number are multidimensional and potentially hierarchical in nature. The rules described here

conservatively apply only to the lower first molar of Rodentia. The rules may apply more broadly phylogenetically (e.g., across Glires) and spatially (e.g., the entirety of the lower/mandibular cheekteeth), however this remains to be tested. Importantly, the rules described here do not apply to any teeth outside of the cheekteeth (i.e., incisors or canines). It may seem counter-intuitive that morphogenetic rules can apply to only a narrow anatomical system, but there is currently evidence to suggest that cheekteeth and non-cheekteeth are maintained in separate developmental and evolutionary modules (Hlusko et al. 2011).

Conclusions

Modeling reveals that multiple developmental pathways produce the same limited numbers of cusps, despite extensive variation in cusp morphologies. These constraints on tooth structure (and by proxy morphospace) are the results of developmentally linked morphogenetic rules that fundamentally limit the number of enamel knots. The rules are minimally, but unlikely totally, defined by the interactions between two genetic factors, the physical concentration of the activator gene(s) (ACT) and the strength of the initial inhibitory effect (INH) of other products that interact with the activator(s).

In identifying morphogenetic rules controlling molar cusp number within Rodentia, I have provided a substantial step forward in the study and application of morphogenetic rules and theoretical morphospaces to studying evolution. This approach facilitates mapping the interactions between genetic factors and their morphological products, and the use of *empirical* data to confirm our findings, an approach advocated by other

researchers (e.g., McGhee 2007, Vucetich et al. 2005, Hlusko et al. 2011, Raup 1966, Niklas 1994, Niklas 1997, and Niklas 2004). Through the identification of morphogenetic rules we can further develop predictive models of morphological evolution.

Future work should focus on investigating the role of other morphogenetic factors, such as the role of buccal and lingual bias on tooth shape and cusp number; and investigation of the mechanistic (genetic and selective) implementation of enamel knot limitations (i.e., how are morphogenetic rules applied?). Rarely are we able to map genotype-to-phenotype, but in the case presented here, we have a compelling starting point. Beginning with the genetic basis of mammalian odontogenesis, there is a short list of potential gene interactions and products to investigate that influence resulting morphology, and study of these in light of the morphogenetic rules identified here should provide insight into how limitations are implemented. The *in silico* modeling approach used here has generated testable hypotheses with respect to how much activator and inhibition effect (should be present for any given potential pathway to produce a given morphology within Rodentia and potential Glires (i.e., researchers can perform experimental applications of values of ACT and INH modeled here). Continued methodological advances in real-time quantification of gene expression and transcriptomes will allow these hypotheses to be tested in the near future. Empirical data collection from across mammalia should also prove insightful, providing context for understanding the phylogenetic depth of the morphogenetic rules identified here and for allowing the identification of potential ‘rule breakers’. ‘Rule breakers’ will, in many respects allow researchers to identify both the limits of morphogenetic rules and points

where substantial evolution within the dental system (i.e., both genomic and phenomic) has occurred.

Cited:

Asher, R. J., Meng, J., Wible, J.R., McKenna, M.C., Rougier, G.W., Dashzeveg, D., Novacek, M.J. 2005. Stem Lagomorpha and the Antiquity of Glires. Science 302: 1091-1094.

Barnosky, A.D., Bell, C.J. 2003. Evolution, Climatic Change and Species Boundaries: Perspectives from tracing Lemmiscus curtatus populations through time and space. Procs. Royal Soc. Lon. B 270, 2585-2590.

Catón, J., Tucker, A.S. 2009. Current knowledge of tooth development: pattering and mineralization of the murine dentition. J. Anat. 214: 502-515.

Chaline, J., Brunet-Lecomte, P., Montuire, S., Viriot. L.,Courant, F. 1998. Anatomy of the arvicoline radiation (Rodentia): palaeogeographical, palaeoecological history and evolutionary data. Ann. Zool. Fennici 36: 239-267.

Fabre, P-H., Hautier, L., Dimitrov, D., Douzery, E.J.P. 2012. A glimpse on the pattern of rodent diversification: a phylogenetic approach. BMC Ev. Bio. 12: 88.

Harjunmaa, E., Seidel, K., Häkkinen, T., Renvoise, E., Corfe, I., Kallonen, A., Zhang, Z-Q., Evans, A., Mikkola, M., Salazar-Ciudad, I., Klein, O., Jernvall, J. 2014, Replaying the evolutionary transitions from the dental fossil record. Nature 512: 44-48.

Herrera-Álvarez, S. Karlsson, E., Ryder, O.A., Lindblad-Toh, K., Crawford, A.J. 2018. How to make a rodent giant: Genomic basis and tradeoffs of gigantism in the capybara, the world's largest rodent. *bioRxiv* 424606.

Hlusko, L.J., Sage, R.D., Mahaney, M.C. 2011. Modularity in the mammalian dentition: Mice and monkeys share a common dental genetic architecture. J. Exp. Zool. B. Mol. Dev. Evol. 316: 21-49.

Jarvinen, E., Salazar-Ciudad, I., Birchmeier, W., Taketo, M., Jernvall, J., Thesleff, I. 2006. Continuous tooth generation in mouse is induced by activated epithelial Wnt/beta-catenin signaling. PNAS 103: 18627-18632.

Jernvall, J., Åberg, T., Kettunen, P., Keränen, S., Thesleff, I. 1998. The life history of an embryonic signaling center: BMP-4 induces p21 and is associated with apoptosis in moust tooth enamel knot. Development 125: 161-169.

Kangas, A. T., Evans, A. R., Thesleff, I., Jernvall, J. 2004. Nonindependence of mammalian dental characters. Nature 432: 211-214.

Luo, Z-X. 2007. Transformation and diversification in early mammal evolution. Nature 450: 1011-1019.

Luo, Z-X., Gatesy, S., Jenkins, F., Amaral, W., Shubin, N. 2015. Mandibular and dental characteristics of Late Triassic mammaliaform *Haramiyavia* and their ramifications for mammal evolution. PNAS 112: E7101-E7109.

Marshall, C. 2014. The evolution of morphogenetic fitness landscapes: conceptualising the interplay between the developmental and ecological drivers of morphological innovation. Aust. J. Zoo. 62: 3-17.

McGhee, G.R. 2007. *The Geometry of Evolution: Adaptive Landscapes and Theoretical Morphospaces.* Cambridge University Press.

Mikkola, M.L., Thesleff, I. 2003. Ectodysplasin signaling in development. Cyto. & Grow. Fact. Rev. 14: 211-224.

Niklas, K.J. 1994. Morphological evolution through complex domains of fitness. PNAS 91: 6772-6779.

Niklas, K.J. 1997. Effects of Hypothetical Developmental Barriers and Abrupt Environmental Changes on Adaptive Walks in a Computer-Generated Domain for Early Vascular Land Plants. Paleobio. 23: 63-76.

Niklas, K.J. 2004. Computer Models of Early Land Plant Evolution. Ann. Rev. Earth and Planet. Sci. 320: 47-66.

Oyanagi, T., Takeshita, N., Hara, M., Ikeda, E., Chida, T., Seki, D., Yoshida, M., Seiryu, M., Takano, I., Kimura, S., Oshima, M., Tsuji, T., Takano-Yamamoto, T. 2019. Insulin-like growth factor 1 modulates bioengineered tooth morphogenesis. Sci. Rep. 9: Article Number 368.

Polly, P.D. 2008. Developmental dynamics and G-matrices: can morphometric spaces

be used to model evolution and development? Evol. Biol. 35: 83-96.

Prochazka, J., Pantalucci, S., Churava, S., Rothova, M., Lambert, A., Lesot, H., Klein, O., Peterka, M., Laudet, V., Peterkova, R. 2010. Patterning by heritage in mouse molar row development. PNAS 107: 15497-15502.

Raup. D.M. 1966. Geometric Analysis of Shell Coiling: General Problems. J. Paleo. 40: 1178-1190.

Renvoise, E., Kavanagh, K., Lazzari, V., Häkkinen, T., Rice, R., Pantalacci, S., Salazar-Ciudad, I., Jernvall, J. 2017. Mechanical constraint from growing jaw facilitates mammalian dental diversity. PNAS 114: 9403-9408.

Sadier, A., Twarogowska, M., Steklikova, K., Hayden, L., Lambert, A., Schneider, P., Laudet, V., Hovorakova, M., Calvez, V., Pantalacci, S. 2019. Modeling Edar expression reveals the hidden dynamics of tooth signaling center patterning. PLoS Biol. 17: e3000064. doi: https://doi.org/10.1371/journal.pbio.3000064

Salazar-Ciudad, I., Jernvall, J. 2010. A computational model of teeth and the developmental origins of morphological variation. Nature 464: 583-586.

Salazar-Ciudad, I., Marin-Riera, M. 2013. Adaptive dynamics under development-based genotype-phenotype maps. Nature 497: 361-364.

Thesleff, I. Vaahtokari, A., Kettunen, P.. Aberg, T. 1995. Epithelial-mesenchymal signaling during tooth development. Conn. Tiss. Res. 32: 9-15.

Ungar, P. 2010. *Mammal teeth, origin, evolution, and diversity.* Johns Hopkins University Press.

Vaahtokari, A., Åberg, T., Jernvall, J., Keränen, S., Thesleff, I. 1996. The enamel knot as a signaling center in the developing mouse tooth. Mech. Dev. 54: 39-43.

Vucetich, M.G., Deschamps, C.M., Olivares, A.I., Dozo, M.T. 2005. Capybaras, shape, size and time: a model kit. Acta Paleo. Pol. 50: 259–272.

Figure 1.1: Morphogenetic Landscape of Molars

Morphogenetic landscape generated by *in silico* modeling. Multiple optima are present that could produce a 5-6 cusp occlusal morphology like shown by *Lemmiscus curtatus* m1 (solid arrows). *Mus musculus* wildtype location (dashed arrow) per Harjunmaa et al. (2014).

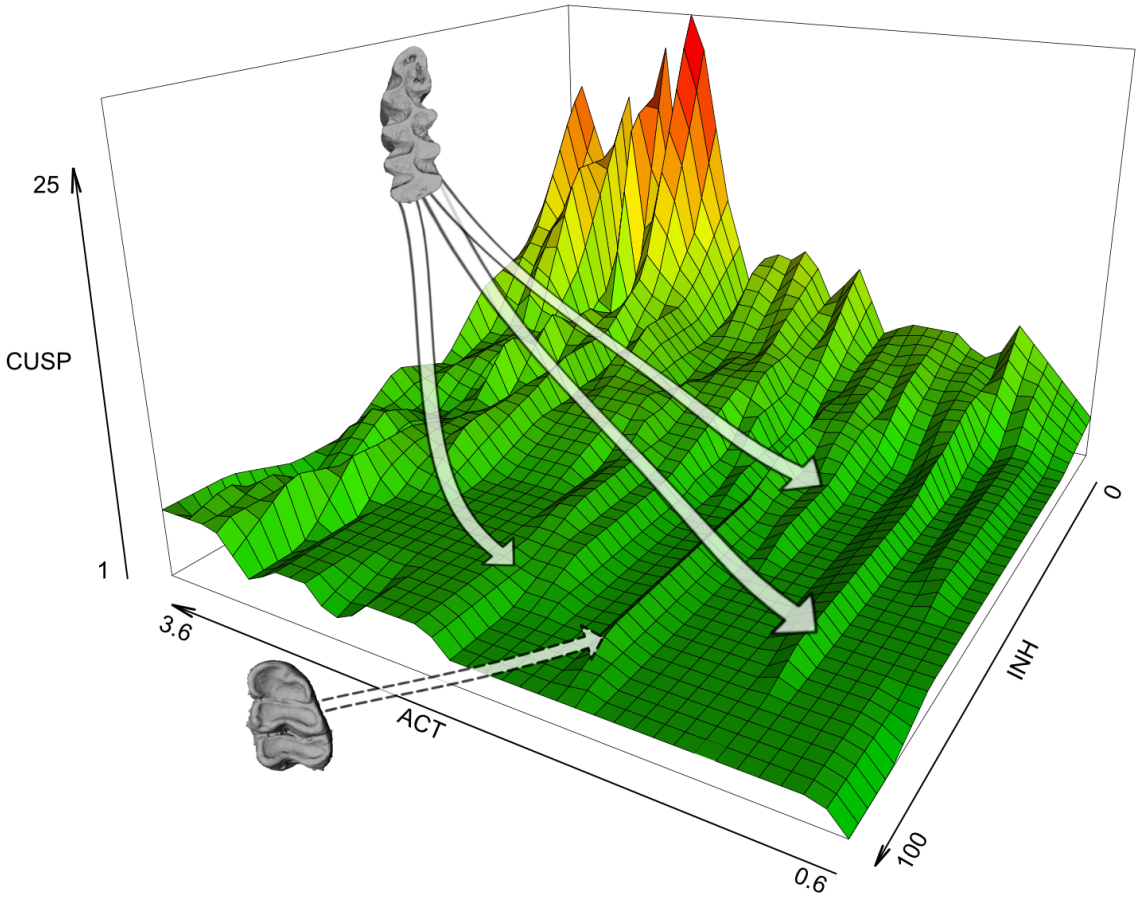

Figure 1.2: Cusp Counts and K-S Test of Results

(A) m1 cusp number compared to m1 length of extant and fossil rodents*. (B) Cumulative fraction plot of Kolmogorov-Smirnov test of empirical (solid line) and simulation (dotted line) cusp counts. See Supplemental Table 1 for full taxonomic sampling.

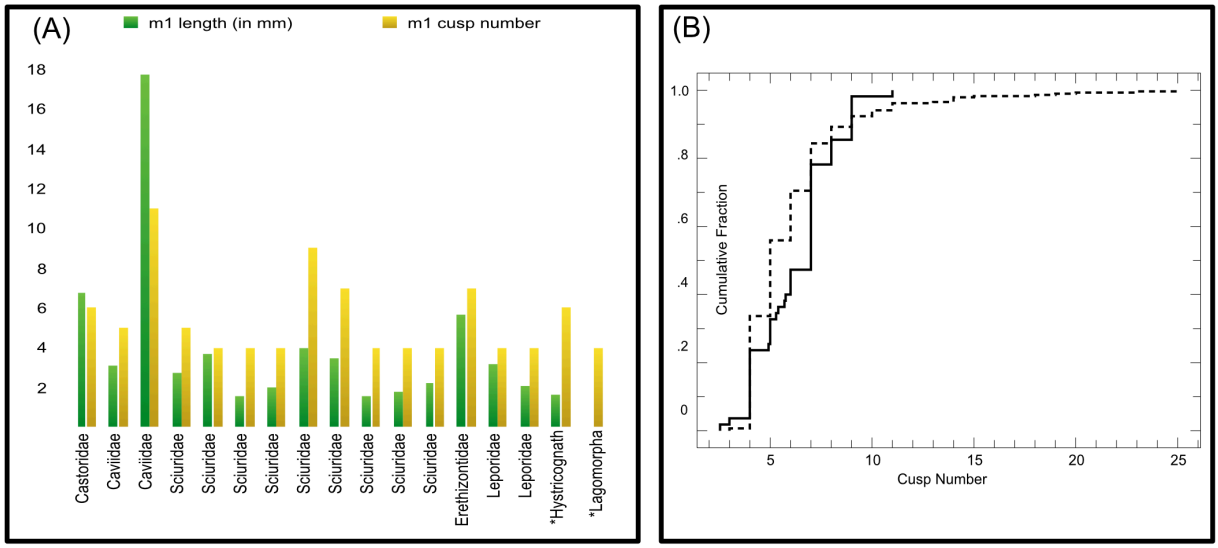

Figure 1.3: Evolution of *Lemmiscus* molars

Evolution of *Lemmiscus curtatus* lower m1 over approximately the last two million years.

(A)Relative distributions of fossil morphotypes from San Antonio Mountain Cave in New Mexico, Porcupine Cave in Colorado, Kennewick Road Cut in Washington between <1 MYA and ~6600 YA, and distribution of morphotypes from a modern population in Saskatchewan reported by Bell et al. (In Review).
(B)Potential evolutionary trajectories of 4T-5T-6T evolutionary transitions. Solid lines are the inferred trajectories based on modeling results, dotted lines are potential trajectories not ruled out by modeling or fossil data.
(C)Morphogenetic landscape evolution of *Lemmiscus* derived from *in silico* modeling based on three factors, activator concentration (ACT), inhibitor effect (INH), and cusp number (Cusp Number).

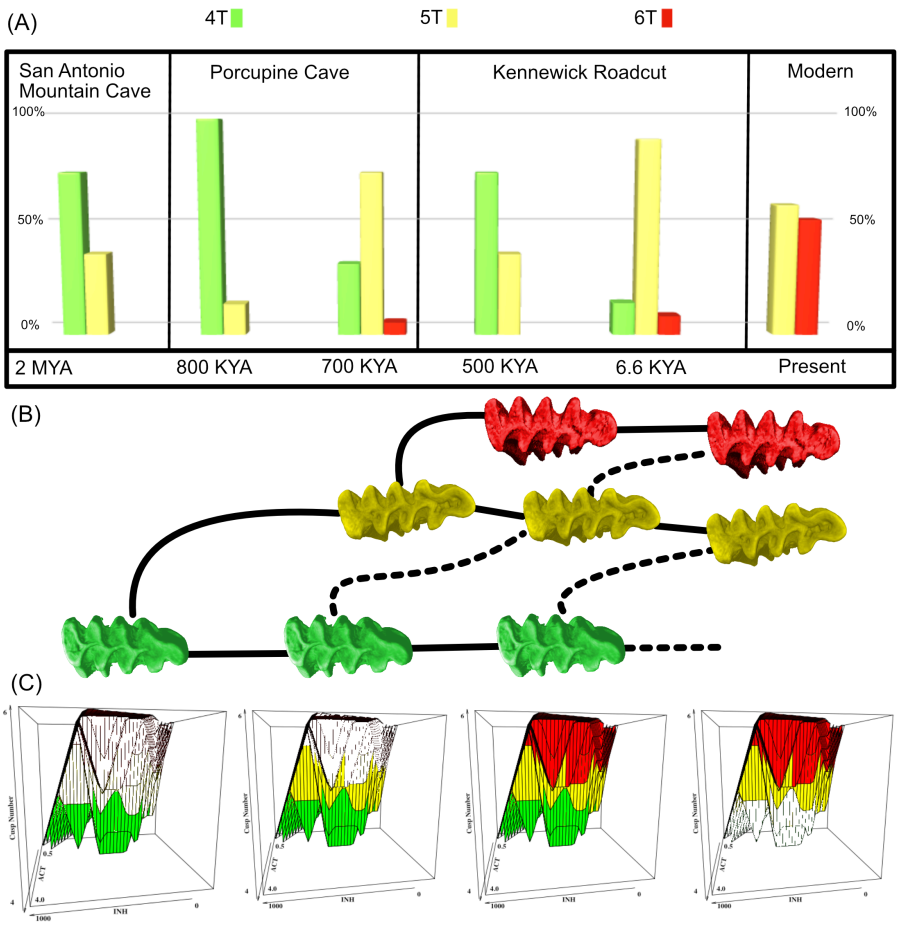

Chapter 2: Tooth Triangles: A Tale of Modularity and Integration

Introduction

The evolution of mammals is often characterized by analysis of changes within the sensory and masticatory systems (Luo 2007). In particular, teeth are often studied due to their frequent occurrence and abundance in the fossil record and the plethora of forms, and functions associated with those forms, seen in Mammalia both today and in the past (Lucas, 2004; Ungar 2010). For these reasons, mammalian dentition represents a hallmark study system for evolutionary dynamics on both macro and micro scales (Evans et al. 2007; Luo et al. 2015). On a microevolutionary scale, the study of asymmetric variation of tooth occlusal surfaces has been proposed to represent both small scale (within population) genetic and/or non-genetic changes to reflect ecology (Polly 2008). In addition to their use in studying evolutionary and ecological dynamics, mammalian teeth are frequently used to study biogeographic shifts (e.g.,Bell and Mead 1998, Ruez and Gensler 2006, Bell and Jass 2004, Jass 2011), and in geochronology as biostratigraphic markers in the Cenozoic (e.g., Barnosky and Bell 2003, Bell and Jass 2004, Jass 2011, Woodburne 2004).

Given the emphasis on mammalian teeth in evolutionary studies it is unsurprising that there also is a robust literature on their embryological development (for review: Polly 2007, Rodrigues et al. 2013). The intersection of development and evolution (devo-evo) of mammalian teeth is a rapidly growing field that is already more than 30-years old (Jernvall and Thesleff 2000; Salazar-Cuidad and Jernvall 2013). The most recent

work in this area, focuses on utilizing an understanding of developmental potential vs. realized morphologies to highlight macroevolutionary dynamics (e.g., Burroughs 2019; Morita et al. 2020). With respect to tooth evolution, rodents and their lower first molars (m1s) are critical nexus points where developmental data and evolutionary data come together to generate novel devo-evo insights. The majority of developmental data on mammalian tooth odontogenesis is derived from work on *Mus* and *Rattus* with other important contributions coming from the study of voles belonging to the genus *Microtus* (for review see: Jernvall and Thesleff 2000; Salazar-Ciudad and Jernvall 2013; Rodrigues et al. 2013).

The pattern of dental evolution recognized across distantly related rodent groups is one characterized by the addition of cusps, or lophs that are derived from cusps, and increasing complexity, at the anterior, or mesial, end of the tooth (Burroughs 2019). Although the evolution of these cusps is homoplastic, they appear to be consistent in location, suggesting a similar developmental basis (Burroughs 2019). Studies aimed at investigating the nature of this developmental mechanism have revealed that there appears to be a combination of developmental limits, in the form of morphogenetic rules and constraints (e.g. Burroughs 2019), and developmental lability at the anterior end of the developing m1 (e.g., Prochazka et al. 2010, Sadier et al. 2019).

In particular, studies of the developmental pathways underlying these morphological shifts indicate that the m1 tooth bud grows larger in individuals in which the premolars are absent in the adult form (Prochazka et al. 2010). The hypothesized mechanism

underlying this size increase is that the anterior end of the developing m1 is able to capture the signaling center of the last premolar, which is subsequently resorbed during development (Prochazka et al. 2010). From here it becomes less clear how development proceeds and whether or not there are distinct developmental modules within this 'combined' m1 tooth bud. For example, Prochazka et al. (2010) hypothesized that the p4 and m1 are connected but are distinct, thus creating modularity (the P10 hypothesis). Alternatively, there may be subsequent downstream developmental reorganization resulting in the total integration of the p4 components into the m1, resulting in a phenotypically integrated tooth (the S19 hypothesis; Sadier et al. 2019). A graphical representation of these processes is shown in Figure F.2.

In both cases (i.e., P10 or S19), this mechanism to co-opt the signaling center of the presumptive premolar, combined with other evolutionary events, could facilitate evolutionary changes at the anterior end of m1 (Burroughs 2019). This hypothesis provides the basis for investigation of whether or not distinct morphological modules are present in the lower m1. The hypothesis of modularity within rodent molars is not new (e.g., Hlusko et al. 2011). However, the recognition of potential mechanisms to explain the evolution of modules is novel (Prochazka et al. 2010; Sadier et al. 2019). Conceptually, there is a link between covariation in developmental and morphological modules (see: Klingenberg 2008 for review). In particular, where there is variation within development and variation within a morphological trait it can often be assumed that covariation between developmental and morphological traits exists. In the case of teeth, there is no known mechanism for producing different numbers of cusps aside from development. In

other words, it is assumed that all variation in cusp number directly correlates to some aspect of developmental variation. By extension, if developmental modularity (P10) or integration (S19) exists, we would expect there to be a signal for morphological modularity or integration. A signal for morphological modularity would support the P10 hypothesis, whereas a signal for integration would support the S19 hypothesis. It would be possible to investigate the potential for developmental modularity or integration, and their role in shaping the evolution of molars, if a species can be found that has a robust fossil record, diagnosable lower first molars for both extant and fossil specimens, and a described evolutionary transition characterized by m1 evolution.

Lemmiscus curtatus, the Sagebrush Vole*,* is found today in the western United States and into southern Canada, where it occurs primarily in scrubby sagebrush habitat (Nowak 1999) (Figure 2.1). Despite the common name, the strict association of *Lemmiscus* and sagebrush is questionable. *Lemmiscus* is of particular interest due to its stemward position within Arvicolini (Steppan and Schenk 2017), and a purported evolutionary transition in tooth morphology that occurs over approximately the last two million years (Barnosky and Bell 2003; Bell et al. 2019, Figure F.1). This transition consists of the evolution of increased tooth complexity in the lower first molar (m1) and upper third molar (M3) via the addition of enamel cusps and ridges, with the extinction of the least complex morphotype during the last 10,000 years (Bell and Jass 2004, Figure F.1). In particular, this transition is characterized by the addition and closure of the 5th and 6th enamel triangles on the anterior end of lower m1. Individuals with four closed triangles

are referred to as 4T morphotypes and are assumed to represent the plesiomorphic morphology; those with five and six closed triangles are 5T and 6T forms, respectively.

In addition, *Lemmiscus curtatus* is one of the few species of vole with molars that are diagnosable when isolated in both the fossil and extant records (Bell and Jass 2003, Bell et al. 2019). At present, the assumption underlying the evolutionary transition within *L. curtatus* is that fossil and extant individuals of *L. curtatus*, with the increase in tooth complexity, represent an anagenetic change within the lineage (Barnosky and Bell 2003; Bell et al. 2019). Two potential challenges to this assumption exist. First, there are six named sub-species of *Lemmiscus curtatus* (Nowak 1999). The diagnosis for these sub-species is based primarily on geographic location and pelage color (Banfield 1987, Nowak 1999). No skeletal traits are known to be diagnostic of the sub-species, but they raise the possibility of population- or species-level divergences within *Lemmiscus*. Second, it is unclear if there are any morphologically distinct populations across the geographic range of *Lemmiscus curtatus* populations found today. In other words it is unclear if morphological variation found in the m1 of *Lemmiscus* today is representative of population or species-level patterns and processes.

Here, I examine modularity and integration across the lower first molar (m1) of *Lemmiscus curtatus*. Based on expectations from Burroughs (2019) and the proposed evolutionary history of *Lemmiscus* (Barnosky and Bell 2003), I hypothesize that there is signal for modularity within m1s that reflects the intersection of developmental and evolutionary dynamics. Specifically, I hypothesize that the m1 is divided into two modules,

an “anterior” module (AM) and a ‘posterior’ module (PM). The AM consists of all portions of the m1 that are anterior of the fourth triangle (T4) (i.e., triangles five and six (T5 and T6) and the anterior loop (AL)). The AM is consistent with the area of the m1 that is elongated evolutionarily by cooption or inclusion of the signaling center of presumptive p4 and would thus represent a p4 developmental module. The PM consists of triangles one through four (T1, T2, T3, and T4) and the posterior loop (PL) (Figure 2.2). The PM would represent the area of the m1 that is formed without any additional inclusion of the p4 and thus represents the m1 developmental module. To address the potential confounding factors of sub-species and population- or species-level patterns, I also investigate if there are patterns of modularity and integration that vary across the geographic range and five of the six recognized sub-species.

Methods

Sampling

I sampled lower first molars of 28 individuals of *Lemmiscus curtatus* obtained on loan from natural history collections (Appendix 1: Specimen Data). Sample size for this study was limited by two factors. First, for an individual to be used in the patch-based semi-landmark analyses (discussed below) tooth occlusal surfaces must be unbroken. This stringent requirement for landmarking reduces the available specimens that can be examined in landmark-based morphometrics, due to chips, cracks, and damage from dry skeletal preservation. Second, *Lemmiscus curtatus* is an elusive animal to capture

in the field. At present in VertNet only 202 specimens of *Lemmiscus* are recorded as having skeletal preparation and mappable locality information (VertNet search conducted in May 2021).

All individuals were µCT scanned on a GE Phoenix µCT scanner, either at the University of Chicago Paleo-CT facility, or the GE Waygate Technologies Customer Solutions Center (Cincinnati). From these scans, high quality three-dimensional models are generated for downstream geometric morphometric analyses. To facilitate rapid data collection, individuals were scanned in Lego®-brand blocks. The use of Lego® blocks aids in allowing tighter packing of specimens while preventing damage, and aids in rapid post-processing of specimens because separation between the specimens. This facilitates the segmentation of CT scans. Specimens were selected primarily to reflect the potential for capturing population-level dynamics, with 21 of the individuals coming from seven distinct localities (Appendix 1 'Locality'), and to capture a significant portion of the geographic range of *Lemmiscus* that also intersects with the fossil record (Figure 2.1). Post-scan processing was done using VGStudioMax v3.4 (Volume Graphics 2021) for initial model 'extraction' from Lego® blocks, and segmentation was completed in 3DSlicer v.4.11.20210226 (Fedorov et al. 2012; 3D Slicer 2021).

Binning

To address whether m1 shape variation could be explained by sub-species designation, geography, or triangle number, I generated four binning schemes for speci-

mens. I binned specimens based on: 1) the county in which the specimens were collected ('locality'); 2) the state or province in which specimens were collected ('state'); 3) the sub-species designation provided in specimen catalog data ('sub-species'); and 4) the number of closed enamel triangles found on the lower m1 ('triangle number'). For the locality binning scheme, there were ten categories (Appendix 1 'Locality'); for the 'state/province' bin there were four categories (Appendix 1 'State'); for sub-species there were five categories (Appendix 1 'Sub-Species'); and for triangle number there were three bins (Appendix 1 'Triangle Number').

Geometric Morphometrics

To quantify shape variation on the occlusal surface of lower m1s, I utilized high-density combination 3D geometric morphometrics (GMM), which is commonly used to quantify shape variation in cases where surfaces lacking large numbers of homologous landmarks are a focus (e.g., Adams et al. 2004 and 2013; Dumont et al. 2016; Goswami et al. 2019, Rhoda et al. 2020), including tooth morphology (e.g., Morita et al. 2020). I generated a landmarking scheme that consisted of a total of 1008 landmarks; 20 fixed landmarks and 988 sliding semi-landmarks (Figure 2.3). Due to the large number of landmarks and the small sample size, I also conducted analyses using only the fixed landmarks ('Fixed LM') to determine if any differences were detected between the two sets of landmark data.

To generate landmark data, I utilized a combination of modules available in 3D-Slicer and the SlicerMorph Extension for 3DSlicer (Rolfe et al. 2020). I used the **Markups** module in 3DSlicer to generate my initial landmarking template of fixed landmarks (Figure 2.3). From there, I used the fixed landmarks to generate a set of triangular semi-landmark patches to use as a template in the **CreateSemiLMPatches** module in SlicerMorph (Figure 2.3). I manually placed fixed landmarks following my initial template on each specimen and then used the **ProjectSemiLM** module in SlicerMorph to project semi-landmark patches onto each individual based on the above generated template. Finally, I utilized the batch processing function in the **MergeMarkups** module of Slicermorph to combine both the fixed and semi-landmark data into a single file of landmark data output in the .JSON format.

Generalized Procrustes Analysis

I performed Generalized Procrustes Analysis (GPA) on my GMM data in two frameworks. First, I utilized the **GPA** module in SlicerMorph to visualize and make a qualitative evaluation of my results. Then, I utilized the **gpagen** function in the R-package 'geomorph' to conduct in-depth statistical analyses (Collyer and Adams 2018). To easily import data generated in the SlicerMorph **GPA** module, I utilized the **parser** function in the 'SlicerMorphR' R-package. A generalized version of the R-script I used in analyses here is provided in Appendix 2.

Tests of Modularity and Integration

My hypothesis of modularity is based on the *a priori* identification of an anterior module (AM) and a posterior module (PM) (Figure 2.2). The evolutionary history of *Lemmiscus* is characterized by the increase of enamel triangles from a four triangle form to a six triangle form, with a five triangle intermediate form in between (Barnosky and Bell 2003). Both five and six triangle forms are found variably in extant populations, but the four triangle form has been hypothesized to have become extinct about 10,000 years ago (Bell and Jass 2004). Because this transition is assumed to be anagenetic, the first four triangles (T1-T4) and the posterior loop (PL) are hypothesized to be homologous across all *Lemmiscus* m1s. With this in mind, I divided the m1 into two modules, an AM consisting of all structures anterior of T4 (i.e., the anterior loop, T5, and T6 if present), and a PM consisting of all structures from T4 to the posterior end of the m1 (i.e., T4, T3, T2, T1, and the posterior loop) (Figure 2.2).

To test my modularity hypothesis, I utilized the **modularity.test** function 'geomorph' by subsetting all landmarks associated with each module and designating whether they belong to the 'a' (AM) or 'p' (PM) modules. The output of the **modularity.test** function is a covariance ratio (CR) value. Values that are closer to 1 are viewed as representing *less* modularity and values closer to 0 are viewed as representing *more* modularity. To evaluate statistical significance of the CR, the **modularity.test** function uses a random permutation approach and generates a P-value interpreted from a 99% confidence interval (e.g., $P \leq 0.01$ is statistically significant) (Collyer and Adams 2018).

Tests of integration where conducted to evaluate the strength of integration between the two *a priori* defined modules compared to randomized data. In other words, is there a greater amount of integration between the AM and PM than would be expected on a purely random basis. To conduct these tests, I utilizes the **integration.test** function in 'geomorph'. This function utilizes a two-block partial least squares (PLS) analysis and generates a set of random permutations to evaluate the statistical significance of the results. Output values from **integration.test** primarily take the form of the r-PLS value, with values closer to 1 representing *more* integration and values closer to 0 representing *less* integration. P-values are again calculated for a 99% confidence interval (e.g., $P \leq 0.01$ is statistically significant) (Collyer and Adams 2018).

I conducted modularity and integration tests on the total dataset without binning; on the California (n=14) and Nevada (n=11) bins from the 'State/Province' binning scheme; and on the 5T and 6T categories for triangle number. I omitted the individuals with state/province identifications in Idaho (n=1) and Sasketchewan (n=2), and the single 4T individual (see below), due to low sample sizes. Similarly, sub-species and locality by county bins were omitted from modularity tests, due to the low sample sizes for individuals assigned to classes in each of those bins.

ProcrustesANOVA

To determine if categorical variables could help explain shape variation, I conducted a set of ProcrustesANOVAs using the **procD.lm** function within 'geomorph'. In

general, the goal of a Procrustes ANOVA is to determine if a significant amount of variance within Procrustes coordinates can be explained by grouping coordinates based on *a priori* categorization. Under the 'geomorph' framework; after defining categories, random resampling is used to determine if there is a larger difference in the mean shape of the individuals belonging to different categories than would be expected under a random (null) model (Collyer and Adams 2018). The output from Procrustes ANOVAs represent the degrees of freedom (df), sum of squares (SS), mean of squares (MS), R-squared (Rsq), F-statistic (F), Z-score (Z), and P-value for the Rsq values on a 99% confidence interval.

Results

A principal components analysis (PCA) generated from a generalized procrustes analysis (GPA) of the total dataset produced ten principal components (PCs) that capture 1% or more of the total variation. Of those ten the first three PCs represent 69.3% of the total variation (PC1 = 45.9%, PC2 = 17.0%, PC3 = 6.4%), the remaining 30.1% of variation is spread across the remaining seven PCs. A scatter plot of PC1 vs. PC2 is provided in Figure 2.4. Shape variation can be summarized primarily as mesio-lingual shifts in the margins of the anterior and posterior loops for PC1 (Figure 2.5). Disto-buccal shifts of the margins of the posterior and anterior loops are characterized by PC2 (Figure 2.5). Variation in the amount and dipping found in cementum columns between the triangles of each tooth appears to be characterized by PC3 (Figure 2.5).

Tests of modularity for the total dataset, the Nevada and the California datasets, and the 5T and 6T datasets each reflected a weak, but significant, signal for modularity with CRs of 0.966 (total); 0.995 for both Nevada and California; 0.976 (5T); 0.997 (6T); in all cases P = 0.01. The tests of integration for the total dataset, the Nevada and the California, and 5T and 6T subsets all recovered a strong and significant signal for integration. The r-pls values were: 0.987 (total); 0.996 (Nevada); 0.995 (California); 0.990 (5T); 0.997 (6T). In all cases P = 0.001. In the fixed landmark dataset, a very weak signal for modularity was recovered (CR = 0.922) for the total sample but was not significant (P=0.02). A weaker, but still strong signal, for integration was recovered (r-PLS = 0.871, P=0.001).

The ProcrustesANOVAs found no significant mean shape difference between groupings based on sub-species or locality. A significant result was recovered for groupings based on triangle number.

Discussion

Identification of a four-triangle morphotype

In the course of preparing this work, I identified a single 4T individual that came from a modern population of *Lemmiscus*. The individual, UMNH 35651, was collected in Humboldt County, Nevada, in 2012 (Figure 2.6). A second individual, UMNH 35650, collected at the same time and the same location as the 4T form (UMNH35651), presents a ‘typical’ 5T form of *Lemmiscus* (e.g., similar to those described by Bell et al. 2019)

(Figure 2.6). The extant four triangle form of *Lemmiscus* has an incipient fifth and sixth triangle, but neither are fully closed. The entire lower jaw of UMNH 35651, including both the left and right hemimandibles, was available for evaluation; both sides of the jaw show the same 4T form, suggesting this morphotype is not the result of left-right asymmetry or an asymmetrical teratology. No other 4T individual from extant samples is currently known.

Conceptually, this discovery is not completely unexpected. When the first 4T form of *Lemmiscus* was described, it was used as a biostratigraphic marker for designating the age of the Kennewick Roadcut fossil locality (Rensberger et al. 1983). A lack of independent chronological control meant that the age of the 4T form was undetermined at that locality. However, *Lemmiscus* was conceptualized as having evolved from the extinct *Phaiomys,* and the 4T form was believed to be no younger than Irvingtonian based-on faunal assemblages (Repenning 1992). The hypothesis that 4T forms of *Lemmiscus* were Irvingtonian in age persisted until the discovery of a four triangle form at Snake Creek Burial Cave in the Rancholabrean (20-10kya) (Bell and Mead 1998), and then in Kokoweef Cave in the early Holocene (~10-7.5kya) (Bell and Jass 2004). With each discovery, the age of the 4T form has moved closer to the present day. Now, we can recognize that the four triangle form of *Lemmiscus* extends from at least 2.6 million years ago (Rogers et al. 2000) to present day (this study).

Why a recent 4T morphotype has not been identified prior to now is a more difficult question to answer, but relative abundance changes in 4T morphotypes in the fossil

record may provide some insight. Four triangle morphotypes are found in higher abundance than 5T forms in the oldest parts of Kennewick Roadcut (Rensberger et al. 1983), San Antonio Mountain Cave (Rogers et al. 2000), and in Porcupine Cave (Barnosky and Bell 2003). However, as deposits become younger there is a shift in relative abundance, such that the 4T form is no longer dominant and it is replaced by the 5T form in higher abundance, which has led to a number of evolutionary interpretations (e.g., Barnosky and Bell 2004). The low number of 4T individuals found in more recent deposits relative to 5T morphotypes further enforces the idea that the 4T form was in decline in the late Pleistocene or early Holocene, and the absence of identified modern 4T forms led to the conclusion that the morphotype had gone extinct (Bell and Mead 1998, Barnosky and Bell 2003, Bell and Jass 2004). Thus it was to be expected if the 4T form was found in the extant it would be in low abundance, and this hypothesis is corroborated from the observation underlying this study. Evaluation of the majority of the 202 skeletons available in collections have found all *Lemmicus* m1s but one (UMNH 35651) to be 5T or 6T forms (pers. obs.).

Sub-Species, Geography, and Mean Shape Differences

The binning schemes, used here to represent potential geographic and sub-specific groupings, offer little explanatory power for shape variation. The lack of support for groupings based on the identified sub-species of *Lemmiscus* is unsurprising because sub-species in *Lemmiscus* are primarily diagnosed based on pelage color, not on dental or osteological characters (Nowak 1999). Although my results do not directly address

the taxonomic status of the named sub-species of *Lemmiscus*, they indicate that tooth morphology is unlikely to provide support for those distinctions.

Overall, the lack of explanatory power for the binning schemes employed here (e.g., no statistical significance recovered in ProcrustesANOVAs) for the locality and sub-species data is consistent with current hypotheses for species-level evolution in *Lemmiscus curtatus*. This is an important finding, because *Lemmiscus* is conceptualized as being monotypic throughout its entire evolutionary history (see: Bell et al. 2019 for review), and this hypothesis has served as a key underlying assumption in the description of evolutionary dynamics captured in the fossil record (e.g., Barnosky and Bell 2003; Ruez and Gensler 2006; Jass 2011). In particular, the hypothesized evolution of increased tooth 'complexity' characterized by the addition of closed enamel triangles on the anterior end of the tooth, is conceived and presented as representing an anagenetic evolutionary change. The lack of evidence of regional or sub-species divergences in tooth morphology in modern *Lemmiscus* provides support for the idea that the different tooth morphotypes observed in the fossil record belonged to a single panmictic population that was changing over time, not regional variants or distinct subpopulations that were undergoing independent morphological divergence.

Results of the Procrustes ANOVA suggest that the mean shapes differ significantly among forms of different triangle numbers. In this case, only the differences in mean shape between 5T and 6T are viewed as significant, given that there is only a single 4T individual. A difference in mean shapes between 5Ts and 6Ts is not surprising, based on

both the general elongation of the molar and the changes in the detailed shapes of the enamel bands on the tooth as the fifth and sixth triangles are closed off. However, despite these significant differences, it is important to remember that the available sample sizes are still relatively small. The addition of fossil data to include more 4T forms in particular, and more individuals overall, would allow an explicit test of whether 4Ts, 5Ts, and 6Ts each differ in mean shape from one another (see Chapter 3 of this work for such tests).

Given that the evolutionary history of *Lemmiscus* is characterized by significant changes to the anterior end of the tooth (Barnosky and Bell 2003) it is not surprising that a substantial portion of the variation recovered in the PCA reflects shape variation in this region. However, the amount of variation recovered in the posterior loop is more unexpected. Previously, the posterior loop has largely been considered a 'stable' area of the m1s of voles in general (Guthrie 1965), and descriptions of variation of the posterior loop have largely focused on size differences (e.g., one loop is wider or longer than another, see: Bell et al. 2019). The interplay between m1 and m2 may help explain the source of this posterior variation. A cursory examination of the amount of contact between the posterior loop of the m1 and the anterior end of m2, shows variable amounts of contact that appear to be correlated with different shapes of the m1 posterior loop (pers. obs.).

Integration and Modularity

The observation that there is a weak signal for modularity along with a strong signal for integration in the m1 provides support for the S19 (Sadier et al. 2019) hypothesis for developmental integration. I predicted that if the m1 displayed a relatively weak level of integration and high degree of modularity, it would reflect the retention of a pattern of developmental modularity, where the presumptive p4 is included, but not fully subsumed by the m1 (P10 hypothesis). This prediction was based on the combination of both an evolutionary history characterized by changes to the anterior end of the tooth, and a developmental mechanism that could promote, or at least not inhibit, such changes (i.e., that a growing m1 tooth bud can readily capture enamel knots from a primordial premolar tooth bud; Prochazka et al. 2010).

Support for an integrated m1 does not undermine the proposed mechanistic basis of the capture of components of the p4 for inclusion into the m1. A widely accepted idea is that there is a single tooth bud that underlies the formation of the lower m1 within mammals during development (e.g., Evans et al. 2007; Kavanagh et al. 2007; Polly 2007; Polly 2008; Ungar 2010; Rodrigues et al. 2013; Salazar-Ciudad and Jernvall 2013; Sadier et al. 2014; Burroughs 2019; Sadier et al. 2019). As a result, although not usually stated as such, that tooth bud can be viewed as a singe, integrated developmental module.

Similarly, there is a well-established mechanistic understanding for the morphogenesis of anterior part of the tooth (e.g., Burroughs 2019, Sadier et al. 2019). Even though it appears that the absence of a fourth premolar promotes m1 tooth bud growth

developmentally (Prochazka et al. 2010; Sadier et al. 2019), this developmental mechanism does not appear to form a novel developmental module due to the late-stage developmental changes (Sadier et al. 2019). These changes (e.g., developmental repatterning) override the early developmental patterning formed by the combination of a p4 and m1 module (Prochazka et al. 2010; Sadier et al. 2019). As a result, although the m1 tooth bud can get bigger, which may introduce a higher potential for developmental lability (Prochazka et al. 2010), some constraints at a later developmental stage such as those identified by Sadier et al. (2019) can still maintain a strong integration of the m1. The weak signal for morphological modularity suggests that this developmental overprinting might be incomplete, and/or that selection has acted to form evolutionary modules to some degree, although not enough to overcome the limitations set by development. Whether this is because the magnitude of selection changes over time or is due to other factors is beyond the scope of this particular study. However, previous studies indicate that it is likely that selection cannot overcome a relatively strong set of developmental limitations for increasing tooth complexity without significant evolutionary events (e.g., changes in major regulatory gene families via the evolution of novel enhancers; Burroughs 2019).

For example, the capybara, represents a rodent species that has broken a number of potential developmental ‘rules’. The size of this largest living rodent exceeds that of the next largest extant rodent, the North American Beaver, by nearly twice the body length and twice the weight (Nowak 1999). Similarly, although rodents (including the beaver) appear to have an upper limit of nine cusps on their lower m1s, the capybara

has 12 cusps (Burroughs 2019). The capybara, it turns out, has undergone significant regulatory genome evolution. These changes are characterized by the evolution of novel enhancers in the insulin/insulin-like (IIS or IGF) pathway, which appears to explain the capybara's large size (Herrera-Alvárez et al. 2020). It is known from tooth development experiments that enhancers and growth factors associated with the IGF/IIS pathway may also allow supernumery cusps to form on the m1, which can explain why the capybara is able to break the cusp number limit identified in other rodents (Oyanagi et al. 2019; Burroughs 2019). By contrast, no evidence currently exists that indicates *Lemmiscus* has undergone any type of evolutionary event of this magnitude, suggesting that *Lemmiscus* is still constrained by the general developmental rules and modules identified for other rodent species.

Although it is intuitive that stronger modularity can facilitate the generation of morphological novelty, it is somewhat counter-intuitive for well-integrated phenotypic traits to show disparate evolution. This is partly because we anticipate that integration reduces overall variation, but this is not necessarily the case. Instead of variation being reduced, it is that covariation of traits across multiple levels increases (e.g., more developmental integration results in more genetic integration and results in more morphological integration; the traits of each system covary more, not less) (Klingenberg 2008). Thus, in the case of *Lemmiscus* we can anticipate that a signal of morphological integration supports a hypothesis of developmental integration because we expect higher amounts of covariation between morphological and developmental traits when integration is high. How then do we get substantial phenotypic evolution in the face of substan-

tial trait integration? Developmental integration can facilitate phenotypic trait evolution under the right circumstances, as suggested by previous simulation models (Goswami et al. 2014). In particular, Goswami et al. (2014) demonstrated that short-term changes (i.e., generation-scale) can produce a strong selective response, but that phenotypic integration serves to channel that selective response into traits that covary with one another. Because the m1 is integrated and selection must act on the tooth occlusal surface, the areas of the m1 with more potential developmental variation, such as the anterior end of the tooth, would appear to have higher amounts of overall phenotypic evolution, even in the face of strong integration (Goswami et al. 2014, Klingenberg 2008).

Sample Size

One potential confounding factor of these results is the low sample size, combined with the large number of landmarks and semi-landmarks in my analyses. The examination of only the fixed landmarks gives confidence that the general patterns recovered here would hold if the sample size was increased. In all cases, I recover a very weak or non-existent signal of modularity and a strong, significant, signal for integration. Given the similarity of data captured between both the fixed and semi-landmark analyses, a third dataset could be constructed, using sliding semi-landmarks to mark just the enamel ridges of the m1. The best practice for collecting such data would be to virtually slice the occlusal surface off the tooth to reveal a relatively pristine surface for landmarking. This approach would facilitate inclusion of a larger sample of specimens because it would allow specimens previously excluded due to breakage on the occlusal

surface to be included into the overall dataset. Such an approach would also increase the geographic range of *Lemmiscus* that could be sampled.

Conclusions

A single extant individual of the four triangle morphotype, which had been previously thought extinct, was discovered in this study. At present, only this single individual is known. However, this discovery requires a reevaluation of all know 4T forms of *Lemmiscus* to assess how the extant specimen fits with respect to fossil specimens of 4T form. Further collection from the same locality can potentially elucidate the relative abundance of the 4T form in extant populations.

Lack of explanatory power for biological variables suggests that morphological variation within the lower first molar (m1) of *Lemmiscus curtatus* reflects a species-level pattern, not population-level divergences, supporting the underlying assumptions of previous work studying the evolution of *Lemmiscus*. Lack of support for groupings by sub-species does not directly undermine the taxonomic status of these entities, but leaves the door open for future tests of their validity. Mean shape differences recovered between triangle number suggests that further investigation of the fossil record of *Lemmiscus* could facilitate additional investigation of evolutionary tempo and mode within the species.

A weak signal for modularity between an anterior and posterior module suggests that selection has acted to evolve or preserve some degree of modularity in the lower m1, perhaps aided by increased developmental lability at the anterior end of the tooth. A strong signal of integration supports the hypothesis that there is likely downstream developmental integration (late stage developmental overprinting) of the m1, despite the inclusion of components of the p4 earlier in tooth development. Further, a strong signal of morphological integration suggests that the strength of selection has not been sufficient to overcome the existence of a developmental module encompassing the entire m1. Previous work (Burroughs 2019) suggests that barring a substantial evolutionary event (e.g., regulatory gene duplication) it is unlikely that natural selection can overcome developmental canalization to the extent that the m1 would develop a separate module in the anterior part of this tooth.

Finally, future work should focus on studying the variation recovered at the posterior end of the tooth, which was previously undocumented in descriptions of *Lemmiscus* tooth morphology. This work should investigate the use of an outline based semi-landmark analysis on an internal plane of the tooth instead of the exposed occlusal surface, which would allow a larger sample to be evaluated across a broader geographic range.

Cited

3D Slicer. 2021. https://www.slicer.org/

Adams, D. C., Rohlf, F. J., Slice, D. E. 2004. Geometric morphometrics: ten years of progress folling the ‘revolution’. Italian Journal of Zoology 71: 5-16.

Barnosky A. D., and Bell C. J. 2003. Evolution, climatic change, and species boundaries: Perspectives from tracing *Lemmiscus curtatus* populations through time and space. Proceedings of the Royal Society of London B 270: 2585-2590.

BELL, C.J., AND MEAD, J. I. 1998. Late Pleistocene microtine rodents from Snake Creek BurialCave, White Pine County, Nevada. Great Basin Naturalist 58:82–86.

BELL, C.J., AND C.N. JASS. 2004. Arvicoline rodents from Kokoweef Cave, Ivanpah Mountains, San Bernardino County, California. Bulletin of the Southern California Academy of Sciences 103:1–11.

Bell, C. J., Jass, C. N. Burroughs, R. W. 2019. Dental variation in a collection of *Lemmiscus curtatus* from the northern plains of southern Saskatchewan: implications for morphological evolution. *Western North American Naturalist* 79:219–232.

Burroughs, R.W. 2019. Modeling rodent tooth morphogenesis reveals constraints on mammalian tooth evolution. *Scientific Reports* 9:10902 doi:10.1038/s41598-019-47469-x

Collyer, M. L., and Adams, D. C. 2018. RRPP: An R package for fitting linear models to high-dimensional data using residual randomization. Methods in Ecology and Evolution 9: 1772-1779.

Dumont, M., Wall, C. E., Botton-Divet, L., Goswami, A., Peigné S., Fabre, A. C. 2016. Do functional demands associated with locomotor habitat, diet, and activity pattern drive skull shape evolution in musteloid carnivorans? Biological Journal of the Linnean Society 117: 858-878.

Evans A. R., Wilson G. P., Fortelius M., and Jernvall J. 2007. High-Level Similarity of Dentitions in Carnivorans and Rodents. Nature 445: 78-81.

Fedorov A., Beichel R., Kalpathy-Cramer J., Finet J., Fillion-Robin J-C., Pujol S., Bauer C., Jennings D., Fennessy F.M., Sonka M., Buatti J., Aylward S.R., Miller J.V., Pieper S., Kikinis R. 2012. 3D Slicer as an Image Computing Platform for the Quantitative Imaging Network. Magnetic Resonance Imaging 30(9):1323-1341.

Goswami, A., Watanabe, A., Felice, R., Badua C., Fabre, A. C., and Polly, P. D. 2019. High-density morphometric analysis of shape and integration: the good, the bad, and the not-really-a-problem. Integrative Comparative Biology 59: 669-683.

Guthrie, R. D. 1965. Variability in Characters Undergoing Rapid Evolution, an Analysis of Microtus Molars. Evolution 19: 214-233.

Herrera-Álvarez, S. Karlsson, E., Ryder, O.A., Lindblad-Toh, K. & Crawford, A.J. 2020. How to make a rodent giant: Genomic basis and tradeoffs of gigantism in the capybara, the world's largest rodent. Mol. Biol. Evol. 38(5):1715–1730.

Hlusko, L. J., Sage, R. D., and Mahaney, M. C. 2011. Modularity in the mammalian dentition: Mice and monkeys share a common dental genetic architecture. J. Exp. Zool. B. Mol. Dev. Evol. 316, 21-49.

Jass, C. N. 2011. Caves, arvicoline rodents, and chronologic resolution. *Palaeontologia Electronica* Vol. 14, Issue 3; 40A:21p.

Jernvall, J. and I. Thesleff. 2000. Reiterative signaling and patterning during mammalian tooth morphogenesis. Mechanisms of Development. 92: 19-29.

Kavanagh K. D., Evans A. R., and Jernvall J. 2007. Predicting Evolutionary Patterns of Mammalian Teeth from Development. Nature 449: 427-432.

Klingenberg, C. 2008. Morphological integration and developmental modularity. Annual Review of Ecology Evolution and Systematics 39: 115-132.

Lucas, P. W. (2004). Dental Functional Morphology: How Teeth Work. Cambridge University Press.

Luo, Z-X.. 2007. Transformation and diversification in early mammal evolution. Nature

450, 1011-1019.

Luo, Z-X., Gatesy, S., Jenkins, F., Amaral, W., and Shubin, N. 2015. Mandibular and dental characteristics of Late Triassic mammaliaform *Haramiyavia* and their ramifications for mammal evolution. PNAS 112, E7101-E7109.

Morita, W., Morimoto, N., and Jernvall, J. 2020. Mapping molar shapes on signaling pathways. PLoS Computational Biology 16(12): e1008436.

Nowak, R. M. 1999. Walker's Mammals of the World; 2-Volume Set, Johns Hopkins University Press; 6th Edition.

Oyanagi, T., Takeshita, N., Hara, M., Ikeda, E., Chida, T., Seki, D., Yoshida, M., Seiryu, M., Takano, I., Kimura, S., Oshima, M., Tsuji, T., Takano-Yamamoto, T. 2019. Insulin-like growth factor 1 modulates bioengineered tooth morphogenesis. Sci. Rep. 9: Article Number 368.

Polly P. D. 2007. Development with a Bite. Nature 449: 413-415.

Polly, P. D. 2008. Developmental dynamics and G-matrices: can morphometric spaces be used to model evolution and development? Evol. Biol. 35, 83-96.

Prochazka, J., Pantalucci, S., Churava, S., Rothova, M., Lambert, A., Lesot, H., Klein, O., Peterka, M., Laudet, V., and Peterkova, R. 2010. Patterning by heritage in mouse molar row development. PNAS 107, 15497-15502.

RENSBERGER, J.M., A.D. BARNOSKY, AND P. SPENCER. 1984. Geology and paleontology of a Pleistocene-to-Holocene loess succession, Benton County, Washington. Eastern Washington University Reports in Archaeology and History 100-39:1–105.

Rhoda, D., Polly, P. D., Raxworthy, C., and Segall, M. 2020. Morphological integration and modularity in the hyperkinetic feeding system of aquatic-foraging snakes. Evolution 75: 56-72.

Rodrigues H. G., Renaud S., Charles C., Le Poul Y., Solé F., Aguilar J-P., Michaux J., Tafforeau P., Headon D., Jernvall J., and Viriot L. 2013. Roles of dental development and adaptation in rodent evolution. Nature Communications 4:2504. DOI: 10.1038/ncomms3504. 8 pp.

Rogers, K., Repenning, C., Luiszer, F., and Benson, R. 2000. Geologic History, Stratigraphy, and Paleontology of SAM Cave, north-central New Mexico. New Mexico Geology 22: 89-117.

Rolfe, S., Pieper, S., Porto, A., Diamond, K., Winchester, J., Shan, S., Kirveslahti, H., Boyer, D., Summers, A., and Maga, A. M. 2020. SlicerMorph: An open and extensible platform to retrieve, visualize and analyze 3D Morphology. bioRxiv Preprint: doi:10.1101/2020.11.09.374926.

Ruez, D. R., Gensler, P. A. 2006. Fossil *Lemmiscus curtatus* (Rodentia, Arvicolinae) from the Hagerman Fossil Beds National Monument, Idaho. Northwestern Naturalist 87: 240-245.

Sadier A., Viriot L., Pantalacci S., and Laudet V. 2014. The ectodysplasin pathway: From diseases to adaptations. Trends in Genetics 30: 24-31.

Sadier, A., Twarogowska, M., Steklikova, K., Hayden, L., Lambert, A., Schneider, P., Laudet, V., Hovorakova, M., Calvez, V., and Pantalacci, S. 2019. Modeling Edar expression reveals the hidden dynamics of tooth signaling center patterning. PLoS Biol. 17, e3000064. doi: https://doi.org/10.1371/journal.pbio.3000064

Salazar-Cuidad I., and Jernvall J. 2013. The Causality Horizon and the Developmental Bases of Morphological Evolution. Biological Theory 8: 286-292.

Steppan S. J., Schenk J. J. 2017. Muroid rodent phylogenetics: 900-species tree reveals increasing diversification rates. PLoS ONE 12(8): e0183070. https://doi.org/10.1371/journal.pone.0183070

Ungar, P. 2010. Mammal teeth, origin, evolution, and diversity. Johns Hopkins University Press.

Volume Graphics GmBH. 2021. VGStudioMax Version 3.4.

Woodburne M. O. (Editor) 2004. Late Cretaceous and Cenozoic Mammals of North America: Biostratigraphy and Geochronology. Columbia University Press, New York. 376 pp.

Figure 2.1: Map of *Lemmiscus curtatus* distributions

Map showing the extant (shaded grey) geographic distribution of *Lemmiscus curtatus* and the broader distribution of fossils (dashed circle). Modified from Bell et al. 2019.

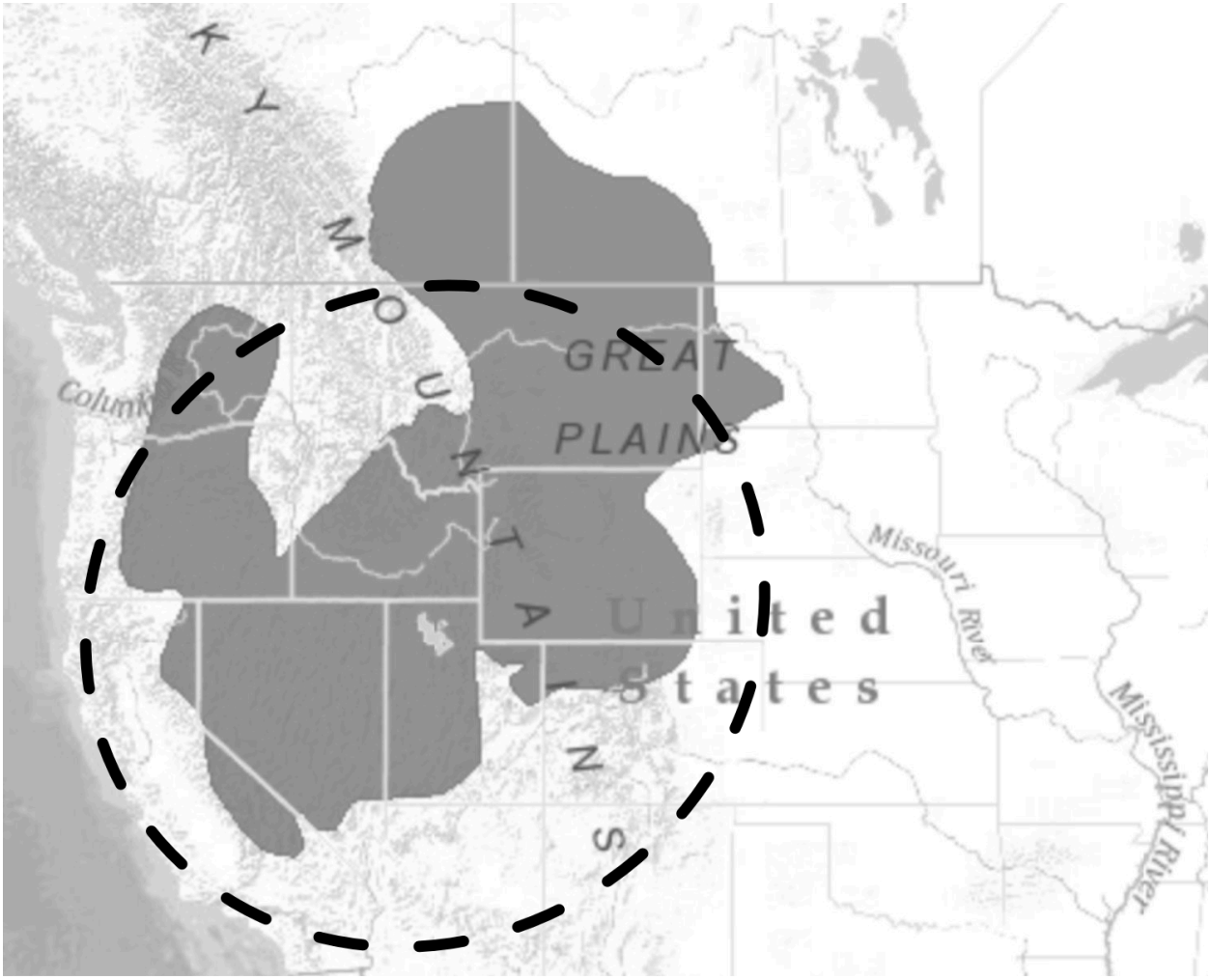

Figure 2.2: Line Drawing of *Lemmiscus* m1

Line drawing of the lower first molar (m1) of *Lemmiscus curtatus* showing relevant morphological features. Enamel shown in bright white, light gray is cementum, and black represents dentin. Enamel triangles are identified in numerical order from the posterior to anterior end of the tooth. Dashed line is the approximate break separating hypothesized anterior (T5, T6, and Anterior Loop) and posterior (Posterior Loop, T1, T2, T3, and T4) modules. Modified from Bell et al. 2019.

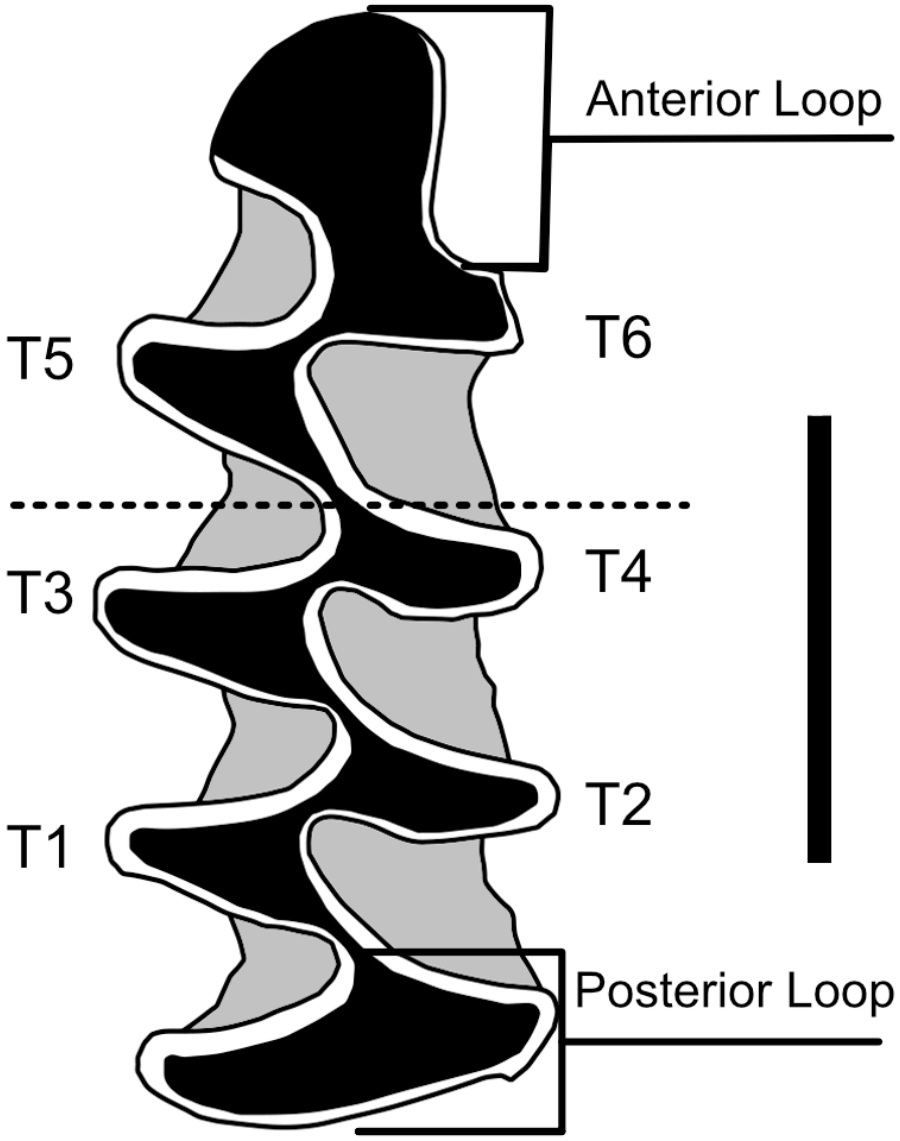

Figure 2.3: Morphometric Methods for *Lemmiscus* m1s

Three-dimensional models showing geometric morphometric landmark scheme employed here. A) 3D model of *Lemmiscus curtatus* lower m1 generated from µCT scans. B) Same model showing positions of 20 fixed landmarks (blue dots). C) Same model showing positions of all 1008 landmarks. Fixed landmarks are blue dots and patch-based sliding semi-landmarks are green dots.

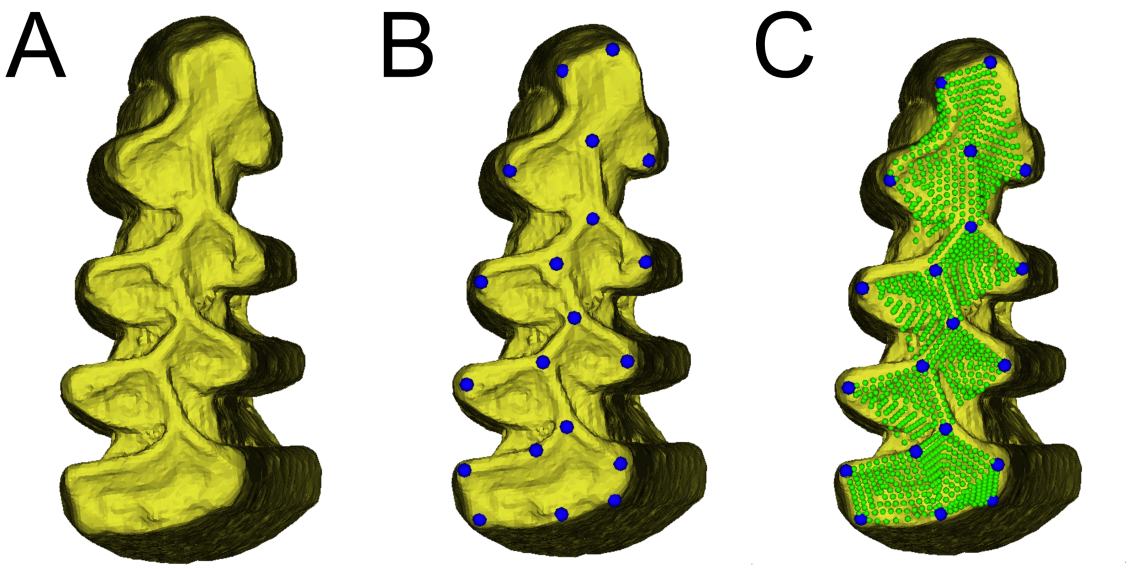

Figure 2.4: PCA Plot of Extant *Lemmiscus* m1s

PCA Plot of PC1 and PC2 that explain the majority of variance. Colored dots correspond to triangle number.

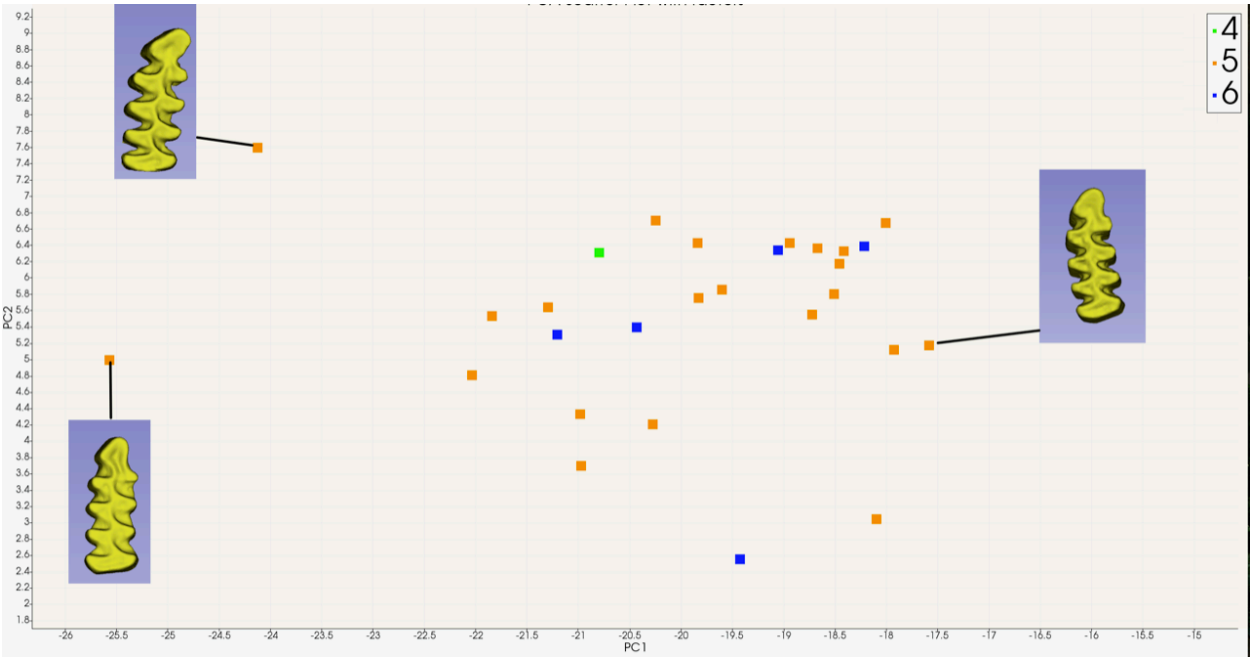

Figure 2.5: Lollipop plots of extant *Lemmiscus* m1s

Warped landmark positions and lollipop plots after generalized procrustes analysis. “Sticks” of the lollipops indicate the magnitude and direction of landmark movement described by that principal component. A) Mean shape of landmarks post-GPA. B) Lollipop vector plot of PC1 on mean shape. C) Lollipop vector plot of PC2 on mean shape. D) Lollipop vector plot of PC3 on mean shape. Dashed lines represent the approximate break between the hypothesized anterior and posterior modules.

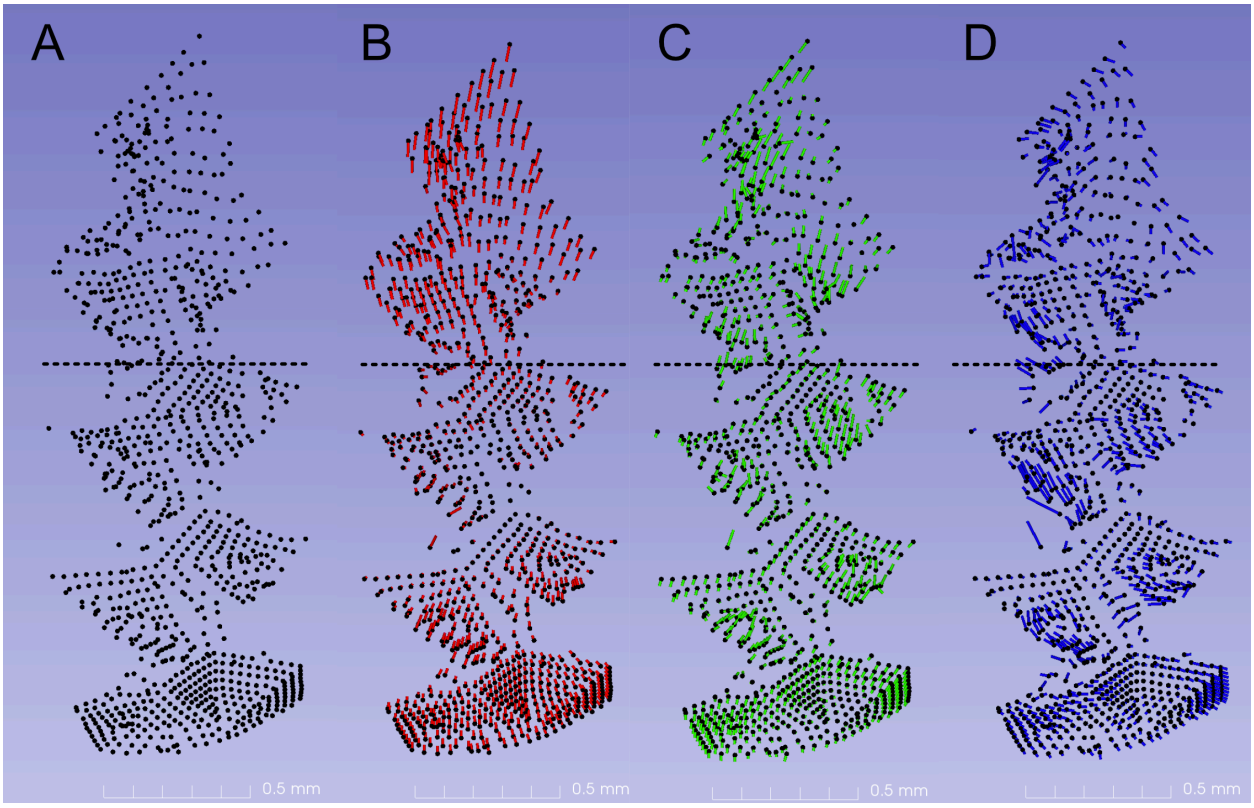

Figure 2.6: Comparison µCT scans of newly identified extant 4T and 5T

Comparison of new 4T form recovered from Nevada (left) and the ‘typical’ 5T form recovered from the same location (right). White arrow points to the open basin between enamel bands that have not yet closed to form the fifth triangle (left). White arrow points to same area now completely closed to form a closed 5T form (right).

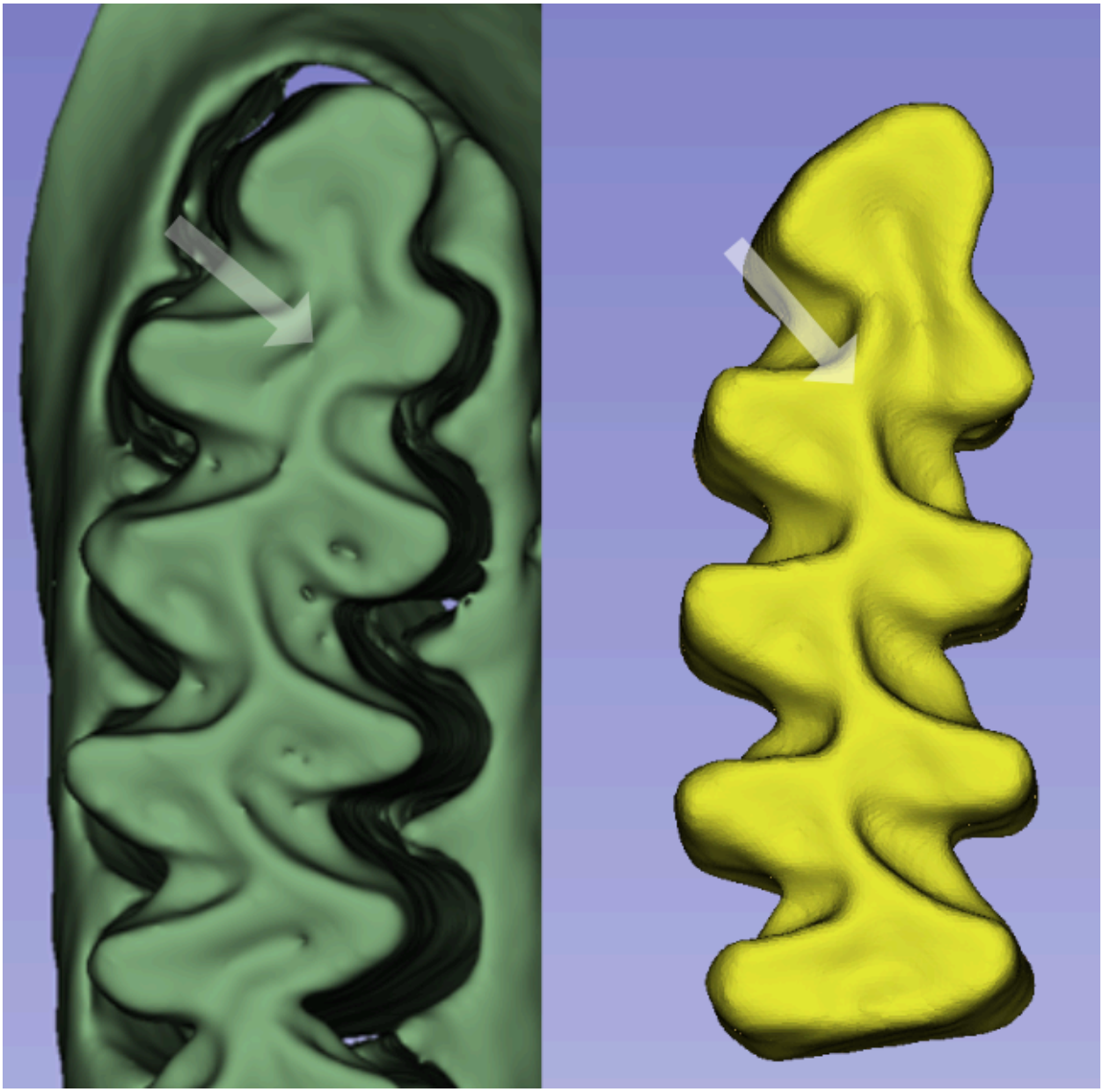

Table 2.1: Summary of Procrustes ANOVAs of extant *Lemmiscus*

Summary of ProcrustesANOVAs based on binning schemes. DF= Degrees of Freedom; SS = Sum of Squares; MS = Mean of Squares; Rsq = R-squared; F = F-statistic; Z = Z-score; Pr(>F) = P-value for r values that are greater than F.

Bin	Df	SS	MS	Rsq	F	Z	Pr(>F)
Locality	9	0.087913	0.0097681	0.33035	0.9867	-0.0044348	0.502
Sub-Species	5	0.059869	0.0119738	0.22497	1.2772	1.0868	0.149
State	3	0.026763	0.0089211	0.10057	0.8945	-0.23947	0.593

Chapter 3: Tooth Triangles II: Secret of the Occlusal Surface

Introduction

Lemmiscus curtatus, the extant Sagebrush Vole, has an extensive fossil record because isolated *Lemmiscus* m1s can be identified to the species level, something that is exceedingly difficult to do within closely related taxa (e.g., *Microtus*) (Bell and Jass 2004). The *L. curtatus* fossil record includes localities that are extralimital to the present-day geographic distribution of the species (Figure 3.1) (Bell and Jass 2004, Bell et al. 2019), and its stratigraphic range could encompass as much as ~4 million years of evolutionary history, based on material from Idaho that is thought to date to the Pliocene (Ruez and Gensler 2006). A critical component of this record is a purported evolutionary transition that is characterized by the addition and closure of enamel triangles on the anterior end of the lower first molar (Figure 3.1), with concomitant changes on the occluding upper third molar (Barnosky and Bell 2003). This large fossil record, with a unique advantage that *L. curtatus* specimens can be reliably identified to the species level, provides an ideal system for investigating patterns of modularity and integration in the context of deep evolutionary history.

I previously described patterns of variation, integration, and modularity on the occlusal surfaces of the lower first molar (m1) of modern (i.e., 'extant') specimens of *Lemmiscus curtatus* (Chapter 2 of this work). There I sought to identify if distinct morphological modules were present in the m1 that corresponded with a hypothesis of developmental modularity. The hypothesis of developmental (and thus morphological)

modularity is based on the addition of cusps on the anterior end of the developing m1 during embryogenesis (Prochazka et al. 2010). Under this model, the m1 incorporates components of a primordial premolar (p4) into the anterior end, which could result in two distinct developmental modules (see: Forward and Chapter 2 of this work, Figure F.1). Alternatively, it is possible that downstream developmental reorganization results in total integration of p4 components into the m1 (Sadier et al. 2019; Figure F.1). I uncovered a very weak signal of modularity and a strong signal of integration in m1s, within extant populations of *Lemmiscus curtatus*, suggesting that developmental integration is present. This suggested that natural selection was insufficiently strong to produce or maintain distinct evolutionary modules on the m1 over the evolutionary history of *Lemmiscus*. However, my previous study did not explicitly investigate modularity, integration, and variation across the stratigraphic range of *Lemmiscus*, which are necessary to fully test that hypothesis. Here, I utilize high-density geometric morphometrics (GMM) to categorize variation and test hypothesis of modularity and integration across the fossil record of *Lemmiscus*, to determine if the patterns of weak modularity and integration recovered from extant population are present during the earlier history of this species.

Methods

Sampling

I sampled lower first molars of 34 individuals of *Lemmiscus curtatus* from a total of four fossil-bearing localities from across the geographic and stratigraphic range of the species (Figure 3.1) to encompass the maximum amount of potential evolutionary varia-

tion that could be reasonably attained. Individuals were μCT scanned and segmented following the same procedures described previously (Chapter 2 of this work). As in the previous study, individuals used here had to be free of damage to the occlusal surface for patch-based semi-landmark analysis. Because there is a high number of semi-landmarks relative to sample size, I also investigated modularity and integration for 20 fixed landmarks as in Chapter 2. A summary table of specimen information, locality, triangle number, and relative age is provided in Appendix 3.1. In addition to the 34 fossil specimens, I conducted a set of analyses combining the dataset of extant individuals (n=28) with the fossils for a 'combined' dataset consisting of 62 specimens. This combined dataset and associated categorical data are provided in Appendix 3.2.

Three of the four fossil localities in this study (Porcupine Cave, Cathedral Cave, Rock Springs Cave) are fossil bearing caves where pack rats nest and form their middens. Pack rat middens are a significant source of fossil data and typically represent the diversity of flora and fauna found within a few hundred meters of their homes (Terry 2008). In the case of *Lemmiscus,* individuals are inferred to have been preyed on by owls, who consume dead individuals whole and subsequently reguritate the skeletal materials which are non-digestable (Terry 2010). Pack rats then drag the regurgitated 'owl pellets' into their middens, where the materials are subsequently buried under successive layers of sediment and additional material brought in by the pack rats. Pack rat middens are maintained for multiple generations, leading to substantial build-up of fossil materials within them (Andrews 1990).

The fourth locality, Kennewick Roadcut, represents a different taphonomic mode. Kennewick Roadcut (KRC) is inferred to be a set of windstorm deposited sediments, with subsequent deposition of calcrete layers in between the windstorm events (Rensberger et al. 1984). These alternating depositional cycles resulted in the deposition of fossils and then subsequent compaction of the sedimentary layers over the fossil bearing sediments (Rensberger et al. 1984). The source of the fossils deposited at KRC is unclear.

The locality bearing the oldest fossils in this analysis is Porcupine Cave (n=21), located near South Park, Colorado (Barnosky et al. 2004). The chronological interpretations from this locality are based on a combination of radiometric and paleomagnetic data, and suggest that fossils from this locality are between 1.6 million and 750 thousand years old (kya). From within Porcupine Cave, *Lemmiscus* fossils were examined from three sub-localities, the 'Pit' (n=18), 'Velvet Room' (n=2), and 'Gypsum Room' (n=1). The chronological sequence provided above is based on data primarily derived from the Pit sub-locality. Addintional age information for the Gypsum Room assigned it tentatively to the Irvingtonian and an unclear age for the Velvet Room, which would make these localities roughly contemporary with the Pit locality ((Barnosky et al. 2004).

The locality with the next oldest fossils in this analysis is Cathedral Cave (n=5), located within the Great Basin in north eastern Nevada, near the Utah border. The chronological interpretations from Cathedral Cave are based on biochronological data

and radiometric dates, and suggest that the fossil-bearing sediments are in the age range of 160-144kya (Jass and Bell 2011). All material examined from Cathedral Cave came from a single excavation in ‘Room 2’ (Jass and Bell 2011).

Kennewick Roadcut (n=8) has substantially less geochronological data available. The initial description of KRC used a biostratigraphic interpretation based on the presence of a four triangle form of *Lemmiscus* and its co-occurrence with *Phaiomys* to date the deposits to between 50-20kya (Rensberger et al. 1984). When this fossil assemblage was first described in 1984, no four-triangle form of *Lemmiscus* had been found in sediments definitively older or younger than this range (Rensberger et al. 1984). However, four triangle forms of *Lemmiscus* subsequently were found at other localities in sediments ranging from 2.6 million years old (Rogers et al. 2000) to ~10,000 years old (Bell and Jass 2004), with individual fossils from Hagerman Fossil Beds of Idaho that potentially range as far back as four million years ago (Ruez and Gensler 2006). At least one other locality (Cathedral Cave) older than the initially proposed dates for KRC also preserves *Lemmiscus* in association with *Phaiomys* (Jass 2011). The top of KRC is capped by an ash fall with a definitive radiometric date of ~5,000 years (Rensberger et al. 1984), establishing a minimum age for all specimens preserved in the KRC section. Recent efforts to reassess the biostratigraphy of KRC are ongoing, but further indicate that the faunal composition of KRC represents a late-Pleistocene aged locality with a maximum age of approximately 50,000 years old (pers. obs.). For the purposes of this study, it is assumed that KRC represents deposits aged from between 50-5kya.

The final locality included in this study is Rock Springs Cave (n=1) located in Utah. This represents the youngest fossil locality in my sample. Rock Springs is inferred to represent a Rancholabrean-Holocene aged fauna (Jefferson et al. 1994). The occurrence of the biostratigraphic index taxon *Ovis canadensis*, the Bighorn Sheep, within the Rock Springs deposits, indicates that this locality is no older than the beginning of the Rancholabrean, about 24-25kya (Jefferson et al. 1994; Bell et al. 2004).

Binning

To evaluate modularity and integration in the context of geologic age, I binned my samples by locality, operating under the assumption that each locality represents a distinct geological age (see discussion of localities above). Because I had only a single individual from Rock Springs Cave, I binned this specimen with the Kennewick Roadcut fossils because of the overlap in interpreted age of these localities. This resulted in three datasets, 'Porcupine', made up of fossils from Porcupine Cave, 'Cathedral' made up of fossils from Cathedral Cave, and 'KRC' made up of fossils from Kennewick Roadcut and the single individual from Rock Springs Cave. To address the potential for low sample size in the 'Cathedral' and 'KRC' bins, I also evaluated a two-bin scheme described as "older" and "younger", where I combined the samples from Cathedral Cave and KRC into the 'younger' bin (n=14) and Porcupine Cave fossils made up the 'older' bin (N=21) (Appendix 3.1, 'Younger/Older'). In addition, to evaluate shape variation in the context of triangle number, I scored all individuals for the number of closed enamel triangles and used these as categorical variables in subsequent analyses (Appendix 3.1, 'Triangle Number'). For 'combined' analyses, I evaluated the dataset by whether or

not individual specimens belonged to the fossil or extant categories (Appendix 3.2, ‘Fossil/Extant’) and by triangle number (Appendix 3.2, ‘Triangle Number’).

Geometric Morphometrics

I utilized the same methods described in Chapter 2 for landmarking and analysis of morphometric data (Chapter 2; this work; Figure 3.2).

Generalized Procrustes Analysis

I followed the same methods described for extant data for the Generalized Procrustes Analysis (GPA), with one exception. Landmarks 876 and 877 were excluded from all analyses. These two landmarks exhibited a large amount of individual variation along the Z-axis for several specimens, resulting in a skewed set of results where virtually all variance on PC1 was described by the positions of these landmarks along the Z-axis. I examined each individual specimen to determine if there was landmark placement error and ultimately concluded the issue arose due to variable presence of dips and divots on the cementum column between T1 and T3.

Tests of Modularity and Integration

I investigated the same modularity hypothesis previously described, which is the bisection of the m1 into a distinct anterior and posterior module (AM and PM, respec-

tively) (Chapter 2; this work) (Figure 3.2). I justify the separation of the AM and PM with the described evolutionary transition within *Lemmiscus* and the developmental modularity hypothesis, where the AM and PM represent the p4 (AM) and m1 (PM) modules respectively (see: Forward and Chapter 2 for detailed review). The AM is defined as all landmarks present on the anterior loop (AL) and triangles 5 and 6 (T5 and T6) if present. The PM is defined as the landmark present on the posterior loop and triangles 1, 2, 3, and 4.

I followed the same procedures described previously (Chapter 2; this work) to test if signals for modularity and integration were present. As described before, the output of the modularity tests was a covariance ratio (CR) value, where values close to 1 indicate a signal for *less* modularity and values close to 0 indicate a signal for *more* modularity. Output values for the integration tests take the form of the r-PLS value, where values close to 1 indicate *more* integration and close to 0 indicate *less* integration. To determine if the CR and r-PLS are statistically significant, random permutations are performed and a P-Value is generated with a $P \leq 0.01$ being viewed as statistically significant (Collyer and Adams 2018).

ProcrustesANOVA

I evaluated morphological variation between localities, by triangle number, and by younger vs. older for fossil data. For combined analyses, I made comparisons between extant and fossil samples, as well as by triangle number, using the same procedures

described in Chapter 2 (This Work). The output from Procrustes ANOVAs represent the degrees of freedom (df), sum of squares (SS), mean of squares (MS), R-squared (Rsq), F-statistic (F), Z-score (Z), and P-value for the Rsq values on a 99% confidence interval.

Results

A principal components analysis of the Procrustes superimposed data resulted in ten principal components describing 1% or more of the variation within the dataset. Of these, the first three principal components represent 76.6% of the total variation (PC1 = 41.6%, PC2 = 22.2%, PC3 = 12.8%). The remaining 23.4% of the variation is spread across the remaining seven principal components. Plots of PCAs are presented in Figure 3.3.

Examination of lollipop vector plots indicates that the shape variation captured by PC1 differentiates individuals with anteroposteriorly shorter anterior loops from those with shorter posterior loops; PC2 differentiates individuals on the basis of the buccal-lingual position of the posterior loop relative to the position of the anterior loop; PC3 primarily differentiates individuals on the basis of the mesial-distal lengths of triangles 2 and 4 relative to triangle 1 and 3 (Figure 3.4).

A very weak signal for modularity was recovered for the total dataset (CR = 0.957, P = 0.01) and a strong signal for integration was recovered (r-PLS = 0.97, P=0.001). For the ‘Fixed LM’ dataset no signal for modularity was present (CR = 0.989, P=0.23) and a strong signal for integration was recovered (r-PLS = 0.854, P=0.001). For

the ‘Porcupine’ dataset a weak signal of modularity was recovered (CR = 0.949, P=0.01) and a strong signal of integration was present (r-PLS = 0.99, P=0.01). For the ‘Cathedral’ dataset no signal for modularity was recovered (CR = 0.999, P=0.04) and the signal for integration was strong (r-PLS 0.99), but not statistically significant (P=0.16). For ‘KRC’ the signal for modularity was very weak (CR=0.997, P=0.01) whereas there was a strong signal for integration (r-PLS 0.992, P=0.002). A weak signal for modularity was recovered from the Combined analyses (CR = 0.948, P=0.01) and a strong integration signal was also recovered (r-PLS = 0.97, P=0.01).

The results of the two ProcrustesANOVAs on fossil datasets found no significant differences in mean shapes between localities, individuals of younger or older relative age, or triangle number. For combined analyses a significant difference in mean shape was detected between fossil and extant datasets (Pr=0.003, with a significant P-value of 0.01). Similarly, a significant difference in mean shape between 4T, 5T, and 6T individuals was recovered (Pr=0.002, P=0.01). The summary statistics for these ProcrustesANOVAs are provided in Table 3.1.

Discussion

The general patterns of modularity and integration recovered in analysis of extant *Lemmiscus* are also recovered within fossil samples of *Lemmsicus*. Overall, a very weak to non-existent signal for modularity was found with a strong signal of integration across the dataset. Although a statistically significant signal for modularity was recovered for the ‘KRC’ dataset, this signal is interpreted to not be accurate. In all cases I

evaluated the CR values recovered from bootstrap permutations of modularity tests. In the case of 'KRC' the bootstrap values contained several permutations with values at or exceeding 1. This indicates that at least one quartile of the distribution would have values in excess of 1 and that the resulting P-Value should be viewed skeptically (Klingenberg 2008). It is likely that the unreliable test for modularity is due to the low sample size for this locality (N=9). Similarly, the lack of significant values for tests of modularity and integration for 'Cathedral' is likely driven by the very low sample size of this bin (N=5). When we evaluate the total dataset for a signal of modularity and integration, effectively doubling the dataset size, the same general pattern is recovered (weak signal of modularity, strong signal of integration), further supporting the idea that this is the signal within fossil specimens of *Lemmiscus curtatus* broadly.

Low sample size could also be a contributing factor in the lack of significant shape differences between specimens assigned to the different geologic age bins, as assessed via ProcrustesANOVA. In this particular instance, however, I am less convinced this is the case. Although ANOVA analyses can be biased by low sample sizes, the use of the 'Older'/'Younger' bins to increase sample size also did not result in significant differences in mean shape. Similarly, no mean shape difference based on triangle number for fossil localities suggests minimal difference between individuals, despite a substantial amount of geological time between localities in this study. Taken together, these results suggest that shape variation in this sample has no strong correlation to the geologic age differences of the specimens.

The combined dataset does find a significant difference in mean shape between fossil and extant individuals. So, although no significant mean shape difference is detected between fossil localities, there does appear to be some difference in mean shape between the extant and fossil records. Similarly, a significant mean shape difference based on triangle number for the combined dataset could be interpreted in two ways. One interpretation is that sample size is a limiting factor for uncovering mean shape difference between triangle number in fossil individuals, and simply expanding the dataset facilitates the recovery of a significant shape difference. In this scenario the fossil dataset contains only 4T and 5T forms and the extant dataset contains effectively only 5T and 6T forms, so pooling these together facilitates mean shape differences that are obscured in the individual datasets.

An alternative explanation is that the significant shape difference detected between the extant and fossil records is also captured within triangle number shape differences. To adequately test this latter interpretation requires more substantial sampling and ideally close to even number of individuals sampled for 4T, 5T, and 6T forms in both the fossil and extant records. Because the interpretations of evolution in *Lemmiscus* are based on relative abundance shifts of the different triangle morphotypes (Barnosky and Bell 2003), even sampling within each time bin is likely impossible. However even sampling between extant and fossil localities should be possible. Previously, this would have been impossible for the supposedly extinct 4T form, but the discovery of a modern 4T specimen now suggests that it may be possible to build a dataset with even sampling between fossil and extant records. At present, though, this lone individual is insufficient

for such analyses, and further collection of new materials from the same extant population would be necessary before such analyses can be done.

Analysis of the fixed landmark dataset suggests that essentially the same morphological signal captured using patch-based semi-landmark analysis can be captured by an outline-type analysis of the enamel ridges of the m1. An advantage of the use of μCT scans is that samples can be digitally 'sliced' to reveal relatively pristine enamel ridges contained within the tooth, and outline-based analyses could be performed on these enamel ridges. This would facilitate increasing the available sample size significantly because specimens with damaged occlusal surfaces could be included, improving the overall statistical power of the analyses. Simultaneously, this would reduce the overall number of landmarks, potentially reducing noise within the dataset by removing a number of landmarks which may vary due to wear (e.g., those associated with the internal 'basin' morphology of the triangles and loops). At this point, it is impossible to say if these results would significantly change the current interpretations. It seems unlikely, though, because both the fixed and semi-landmark analyses reveal largely the same pattern of low modularity and high integration. However, the addition of samples across a broader stratigraphic range may reveal a more fine-scale level of detail.

Taking the results recovered here at their face value, it would appear that patterns of modularity and integration within *Lemmiscus* have been relatively stable over the past 1.6 million years (the oldest potential age of the individuals examined here). This suggests that developmental integration of the m1 has been the dominant force in

evolutionary dynamics within *Lemmiscus* over the past 1.6 million years. This integrative stability reinforces the idea that natural selection has only been able to act on a relatively limited set of phenotypes that are produced due to underlying developmental lability (Chapters 1 and 2 this work). This is consistent with the results of simulations: in cases with strong phenotypic integration natural selection acts in more canalized ways on traits that have the highest amount of variability (Goswami et al. 2014). In the case of *Lemmiscus*, the traits with the apparent highest variability are those associated with increasing enamel triangles on the m1. Similarly, this explanation of developmental and morphological integration serving to limit natural selection can explain why highly similar patterns of increasing closed enamel triangles on the m1 are found in other arvicoline rodents (e.g., muskrat) (Chaline et al. 1999).

Conclusions

Patterns of modularity and integration found within extant populations of *Lemmiscus* are also found within fossil samples of *Lemmiscus*, suggesting long-term stability of a developmental and evolutionary module consisting of the entire m1.

Combined analyses of extant and fossil data further suggest that there are differences between extant and fossil samples. These will require increased sampling and more even sampling across the triangle morphotypes to determine if this signal is accurate or merely a reflection of noise within the dataset.

As with the analyses of extant samples, an outline-based semi-landmark analysis could improve sample size. In the case of *Lemmiscus* would allow a significantly larger

portion of its temporal and geographic ranges to be included in the dataset. This would improve the overall statistical power of analyses, although the similar results between fixed and semi-landmark analyses suggest that major changes in overall interpretations are unlikely. Future work should focus on an outline-based analysis and attempting to sample from the farthest geographic extents of *Lemmiscus.*

Cited

Andrews, P. 1990. *Owls, caves and fossils*. University of Chicago Press, Chicago, IL.

Barnosky A. D., and Bell C. J. 2003. Evolution, climatic change, and species boundaries: Perspectives from tracing *Lemmiscus curtatus* populations through time and space. Proceedings of the Royal Society of London B 270: 2585-2590.

Barnosky, A. D., Bell, C. J., Raynolds, R. G., and Taylor, L. H. The Pleistocene Fossils of Porcupine Cave, Colorado. Spatial Distribution and Taphonomic Overview. In: Biodiversity Response to Climate Change in the Middle Pleistocene: The Porcupine Cave Fauna from Colorado: 6-26.

BELL, C.J., AND C.N. JASS. 2004. Arvicoline rodents from Kokoweef Cave, Ivanpah Mountains, San Bernardino County, California. Bulletin of the Southern California Academy of Sciences 103:1–11.

Bell, C. J., Lundelius, E. L., Barnosky, A. D., Graham, R. W., Lindsay, E. H., Ruez, D. R., Semken, H. A., Webb, S. D., and Zakrzewski, R. J. 2004. The Blancan, Irvingtonian, and Rancholabrean Mammal Ages. In: Late Cretaceous and Cenozoic Mammals of North America: 232-314.

Bell, C. J., Jass, C. N. Burroughs, R. W. 2019. Dental variation in a collection of *Lemmiscus curtatus* from the northern plains of southern Saskatchewan: implications for morphological evolution. *Western North American Naturalist* 79:219–232.

Burroughs, R.W. 2019. Modeling rodent tooth morphogenesis reveals constraints on mammalian tooth evolution. *Scientific Reports* 9:10902 doi:10.1038/s41598-019-47469-x

Chaline, J., Brunet-Lecomte, P., Montuire, S., Viriot. L. & Courant, F. 1999. Anatomy of the arvicoline radiation (Rodentia): palaeogeographical, palaeoecological history and evolutionary data. *Ann. Zool. Fennici* 36, 239-267.

Collyer, M. L., and Adams, D. C. 2018. RRPP: An R package for fitting linear models to high-dimensional data using residual randomization. Methods in Ecology and Evolution 9: 1772-1779.

Goswami, A., Watanabe, A., Felice, R., Badua C., Fabre, A. C., and Polly, P. D. 2019. High-density morphometric analysis of shape and integration: the good, the bad, and the not-really-a-problem. Integrative Comparative Biology 59: 669-683.

Jass, C. N. 2011. Caves, arvicoline rodents, and chronologic resolution. *Palaeontologia Electronica* Vol. 14, Issue 3; 40A:21p.

Jefferson, G. T., Miller, W. E., Nelson, M. E., and Madsen, J. H. 1994. Catalogue of Late Quaternary Vertebrates from Utah. Technical Reports of the Los Angelese County Natural History Museum 9: 34pp.

Klingenberg, C. 2008. Morphological integration and developmental modularity. Annual Review of Ecology Evolution and Systematics 39: 115-132.

Prochazka, J., Pantalucci, S., Churava, S., Rothova, M., Lambert, A., Lesot, H., Klein, O., Peterka, M., Laudet, V., and Peterkova, R. 2010. Patterning by heritage in mouse molar row development. PNAS 107, 15497-15502.

RENSBERGER, J.M., A.D. BARNOSKY, AND P. SPENCER. 1984. Geology and paleontology of a Pleistocene-to-Holocene loess succession, Benton County, Washington. Eastern Washington University Reports in Archaeology and History 100-39:1–105.

Rogers, K., Repenning, C., Luiszer, F., and Benson, R. 2000. Geologic History, Stratigraphy, and Paleontology of SAM Cave, north-central New Mexico. New Mexico Geology 22: 89-117.

Ruez, D. R., Gensler, P. A. 2006. Fossil *Lemmiscus curtatus* (Rodentia, Arvicolinae) from the Hagerman Fossil Beds National Monument, Idaho. Northwestern Naturalist 87: 240-245.

Sadier, A., Twarogowska, M., Steklikova, K., Hayden, L., Lambert, A., Schneider, P., Laudet, V., Hovorakova, M., Calvez, V., and Pantalacci, S. 2019. Modeling Edar expression reveals the hidden dynamics of tooth signaling center patterning. PLoS Biol. 17, e3000064. doi: https://doi.org/10.1371/journal.pbio.3000064

TERRY, R.C. 2008. Modeling the effects of predation, prey cycling, and time averaging on relative abundance in raptor-generated small mammal death assemblages. Palaios 23:402–410.

TERRY, R.C. 2010. On raptors and rodents: testing the ecological fidelity and spatiotemporal resolution of cave death assemblages. Paleobiology 36:137–160.

Figure 3.1: Map showing fossil-bearing *Lemmiscus* localities

Map showing the extant (gray shaded area) and fossil (blue and yellow dots) distribution of *Lemmiscus curtatus*. Localities sampled in this study are shown as yellow dots.

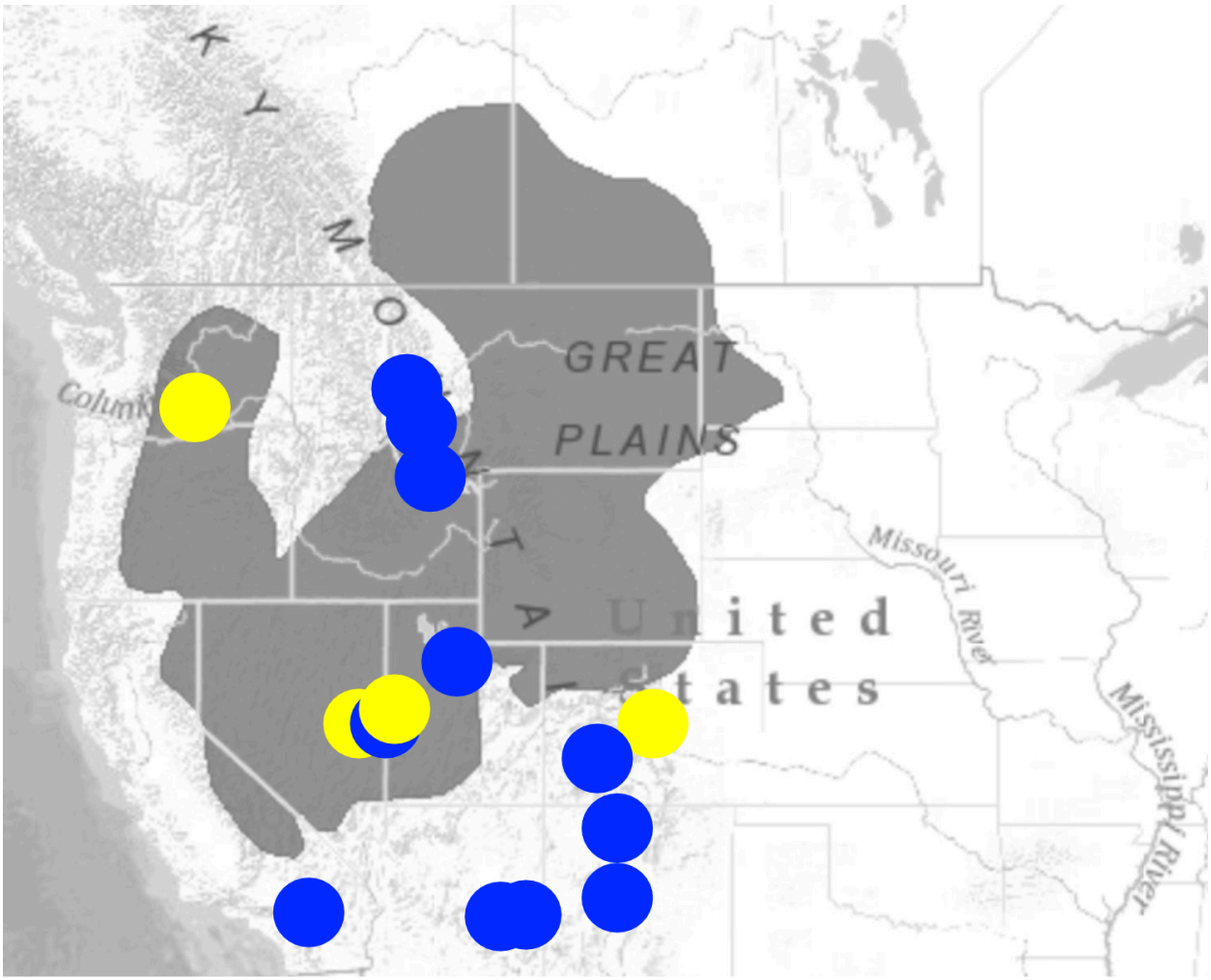

Figure 3.2: Landmarking Regime for *Lemmiscus* m1s

Landmarking Regime of fixed and patch-based semi-landmarks across the occlusal surface of a *Lemmiscus curtatus* m1. A) 3D Model of *Lemmiscus* m1, B) Positions of the 20 fixed landmarks. C) Patch-based semi-landmarks triangled between fixed landmarks.

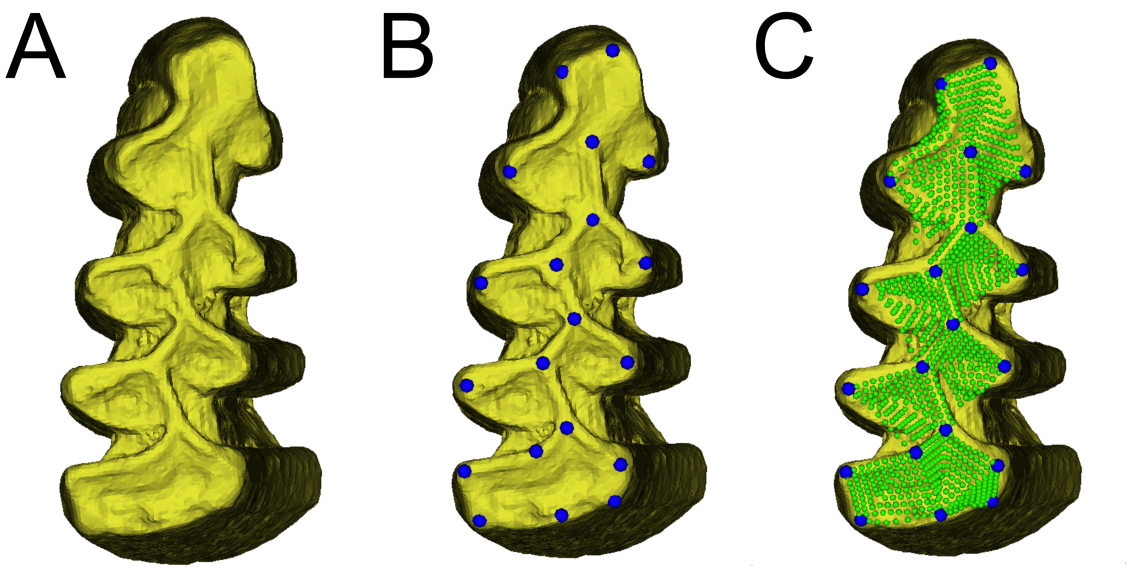

Figure 3.3: PCA Plot of fossil *Lemmiscus* m1s

PCA Plot of PC1 and PC2 the all fossils and semi-landmarks used in this study (n=34).

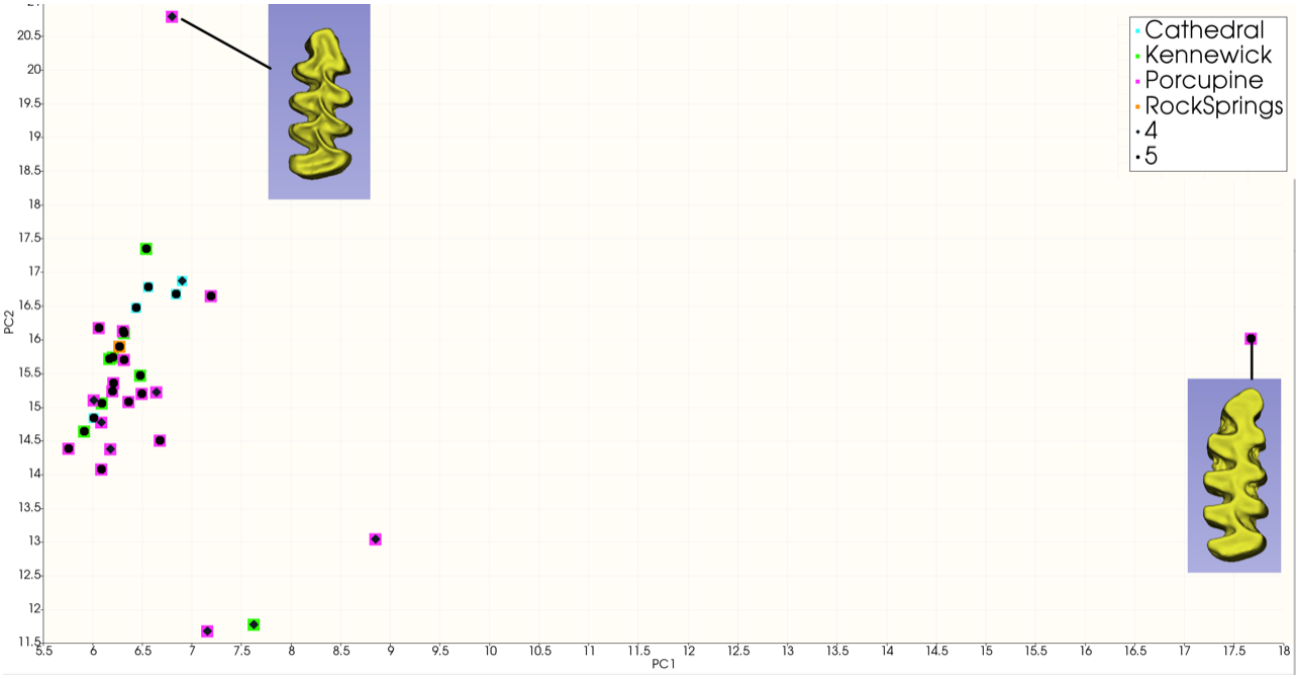

Figure 3.4: Lollipop plots of fossil *Lemmiscus* m1s

Mean warped shape of semi-landmarks (A) and lollipop plots showing variation found on PC1 (B), PC2 (C), and PC3 (D).

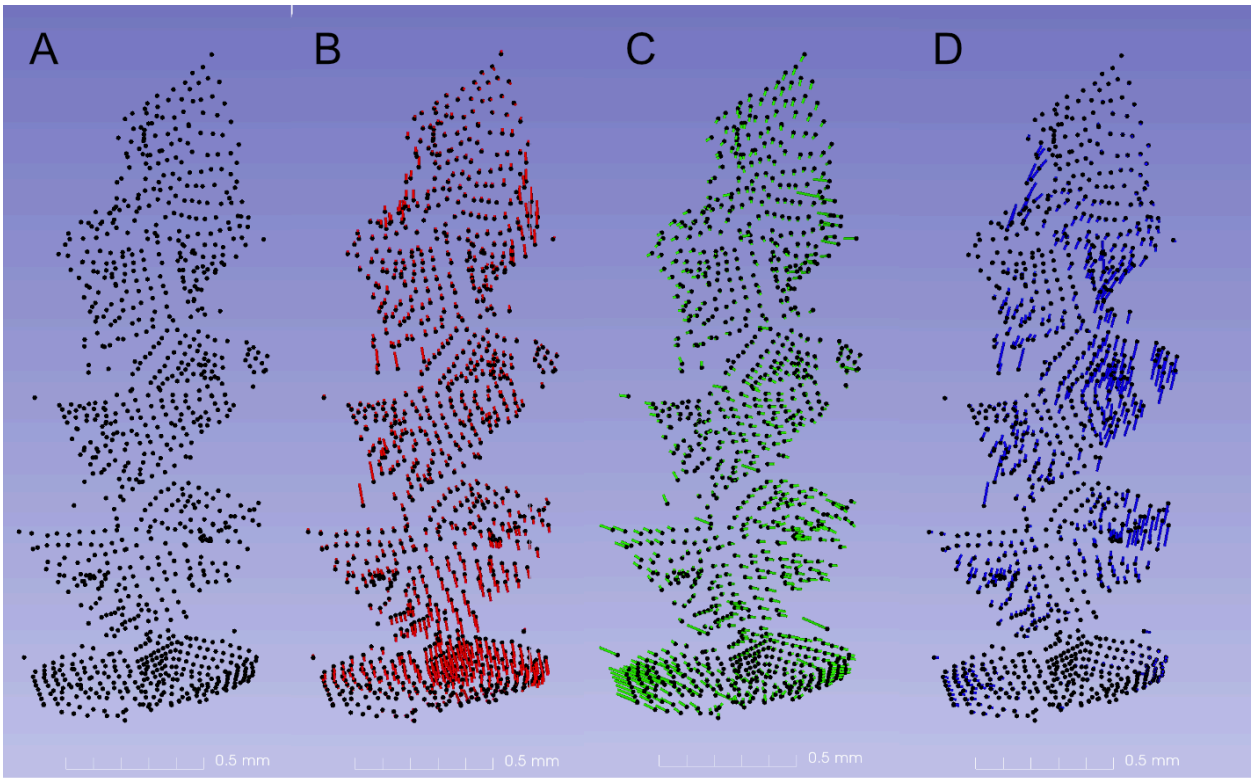

Table 3.1: Summary of Procrustes ANOVA for fossil *Lemmiscus*

Summary of ProcrustesANOVAs based on binning schemes. DF= Degrees of Freedom; SS = Sum of Squares; MS = Mean of Squares; Rsq = R-squared; F = F-statistic; Z = Z-score; Pr(>F) = P-value for r values that are greater than F.

Bin	Df	SS	MS	Rsq	F	Z	Pr(>F)
Locality (Fossils)	2	0.06225	0.031125	0.04945	0.8324	-0.26981	0.591
Younger/Older (Fossils)	1	0.03676	0.036757	0.0292	0.9927	0.12155	0.466
Triangle Number (Fossils)	1	0.01631	0.016314	0.02664	0.8485	-0.20577	0.58
Fossil-Extant (Combined)	1	0.04012	0.040120	0.04375	2.6993	2.7829	0.003
Triangle Number (Combined)	1	0.04636	0.046363	0.05056	3.1417	2.6887	0.002

Appendix 1.1: Supplemental Dataset 1 from Burroughs (2019)

Uploaded Separately on ProQuest

Appendix 1.2: Supplemental Dataset 2 from Burroughs (2019)

Table A1.2.1: Supplemental Data from Burroughs (2019)

Specimen/Species	Cusp Count
Eda null (0 ng/ml EDA)	2.54
Eda null (2.5 ng/ml EDA)	3
Eda null (10 ng/ml EDA)	4
Eda null (25 ng/ml EDA)	4
Eda null (50 ng/ml EDA)	4.92
Eda null (100 ng/ml EDA)	5.29
Eda null (500 ng/ml EDA)	5.4
Eda null (1000 ng/ml EDA)	5.76
Wild type (0 ng/ml EDA)	5.7
~~*Tribosphenomys minutus*~~	5
Anisomys imitator	7
Bunomys coelestis	7
Hydromys chrysogaster	6
Hyomys goliath	9
Leptomys elegans	7

Mallomys rothschildi	7
Niviventer rapit	7
Notes: Strike through = extinct species; No specimen numbers were provided; *EDA* specimens belong to *Mus musculus*	

Appendix 1.3: Supplementary Information from Burroughs (2019)

Supplementary Information is Available Here: https://static-content.springer.com/esm/art%3A10.1038%2Fs41598-019-47469-x/MediaObjects/41598_2019_47469_MOESM3_ESM.pdf

Author's Note: I have reproduced the supplementary information below as it is published in the link above associated with Burroughs (2019). This SI section contains three sets of data, Supplemental Figure 1, Supplemental Table 1, and Supplemental 3. Because this work has been published, it is reproduced exactly as is without formatting changes. For appropriate citation, please cite Supplemental Information (SI) from Burroughs (2019).

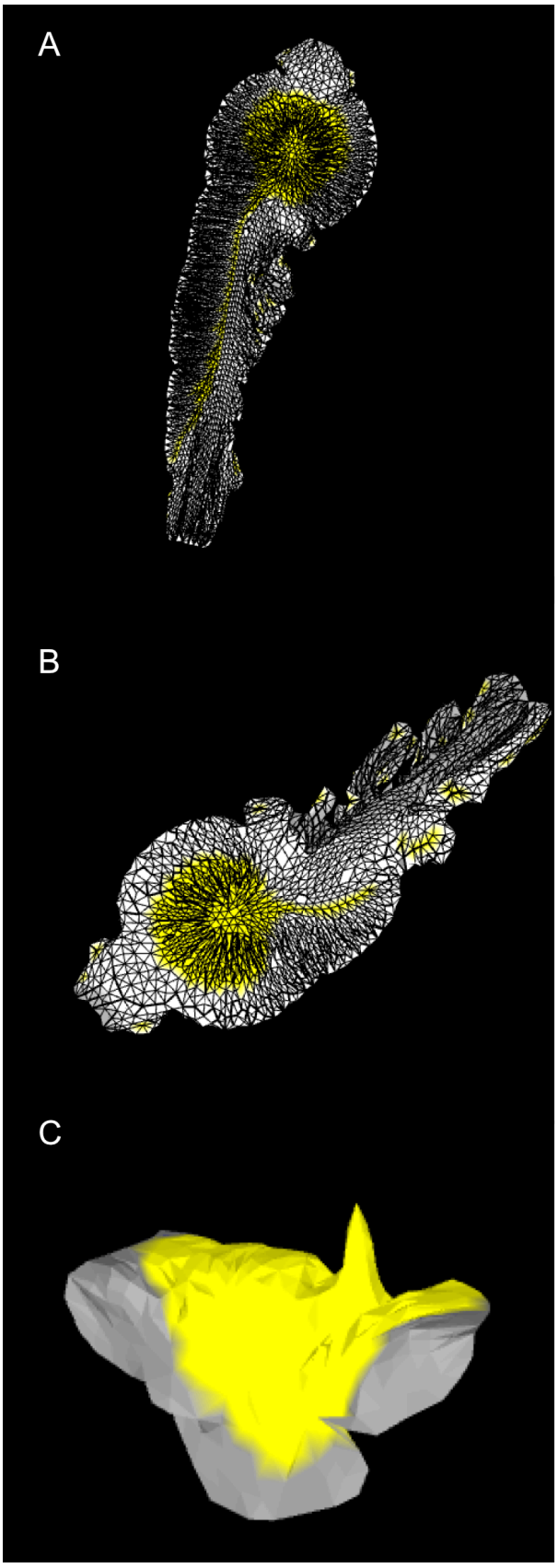
A
B
C

Supplemental Figure 1 (On Previous Page):

(A) “Tooth” from *in silico* modeling with 4.0 ACT and 800 INH values.

(B) “Tooth” from *in silico* modeling using 1.6 ACT and 160 INH values

(C) “Tooth” from *in silico* modeling with 4.0 ACT, 160 INH, and run for 28000 iterations.

Supplemental Table 1: Sampled species and specimens for empirical cusp counts. Fossils de- noted by †. Specimens marked with * are data from Harjunmaa et al. 2014.

Species/ Specimen	**m1 cusp number**	**Tooth Row Cusp Number (Minimum estimate)**	**Maximum straight line m1 length (mm)**	**Maximum straight line Tooth Row Length (mm)**
Castor canadensis	6	23	6.77	27.82
Cavia porcellus	5	19	3.1	13.4
Hydrochoerus hydrochaeris	11	42	17.74	86
Sciurus niger	5	17	2.71	12.14
Marmota flaviventris sierare	4	17	3.72	18.41
Tamiasciurus hudsonicus richardsoni	4	20	1.6	8.8
Tamiasciurus richardsoni	4	20	2	9.1
Petaurista alboufus candidulus	9	28	4	17.5
Petaurista alborufus lena	7	27	3.5	17.1
Iomys horsfieldi	4	17	1.6	9
Callosciurus atrodorsalis	4	18	1.8	9.2

Tamiops swinhoei spencei	4	19	2.2	6.9
Erethizon myops	7	21	5.7	29.22
Lepus californicus	4	20	3.19	17.5
Sylvilagus flordianus	4	21	2.08	13.78
Protophiomys tunisiensis†	6	23	1.63	6.36
Gomphos sp.†	4	19	NA	NA
Mimolagus aurorae†	NA	23	NA	NA
Aethomys hindei	9	9	2.4	6.2
Apodemus agrarius	8	7	0.8	3.8
Arvicanthis niloticus	9	8	2.6	7
Bandicota indica	7	7	3	9.5
Berylmys bowersi	7	8	3.1	8.7
Chiropodomys gliroides	9	9	1.3	4
Crateromys schadenbergi	7	7	6.3	16.3

Dasymys incomtus	8	6	2.2	6.7
Dephomys defua	7	7	1.7	5.5
Grammomys dolichurus	9	9	1.5	4.4
Hybomys univittatus	8	8	2.4	5.7
Hylomyscus stella	8	8	1.7	3.6
Lemniscomys striatus	9	9	1.8	4.8
Leopoldamys sabanus	7	7	3.7	9.2
Malacomys longipes	7	7	2.4	5.5
Mastomys natalensis	7	7	1.8	4.7
Mus musculus	7	6	1.3	3
Nesokia indica	5	6	2.4	7.6
Notomys mitchellii	7	7	2.1	4.6
Oenomys hypoxanthus	7	9	2.7	6.5
Pelomys campanae	6	6	2.1	5.3
Eda null (0 ng/ ml EDA)*	2.54	NA	NA	NA
Eda null (2.5 ng/ml EDA)*	3	NA	NA	NA

Eda null (10 ng/ ml EDA)*	4	NA	NA	NA
Eda null (25 ng/ ml EDA)*	4	NA	NA	NA
Eda null (50 ng/ ml EDA)*	4.92	NA	NA	NA
Eda null (100 ng/ml EDA)*	5.29	NA	NA	NA
Eda null (500 ng/ml EDA)*	5.4	NA	NA	NA
Eda null (1000 ng/ ml EDA)*	5.76	NA	NA	NA
Wild type (0 ng/ ml EDA)*	5.7	NA	NA	NA
Tribosphenomys minutus†*	5	NA	NA	NA
*Anisomys imitator**	7	NA	NA	NA
*Bunomys coelestis**	7	NA	NA	NA
*Hydromys chrysogaster**	6	NA	NA	NA
*Hyomys goliath**	9	NA	NA	NA
*Leptomys elegans**	7	NA	NA	NA
*Mallomys rothschildi**	7	NA	NA	NA

*Niviventer rapit**	7	NA	NA	NA

Supplement 3: Figures showing cusp counts on extant specimens. All scale bars are 10 mm.

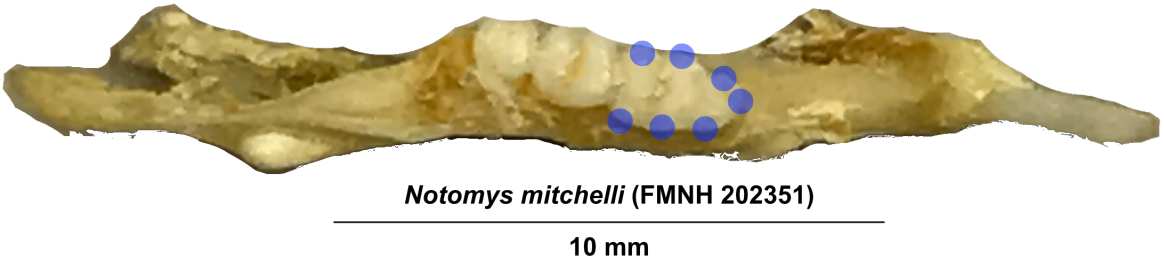

***Notomys mitchelli* (FMNH 202351)**

10 mm

***Lemniscomys striatus* (FMNH 231770)**

10 mm

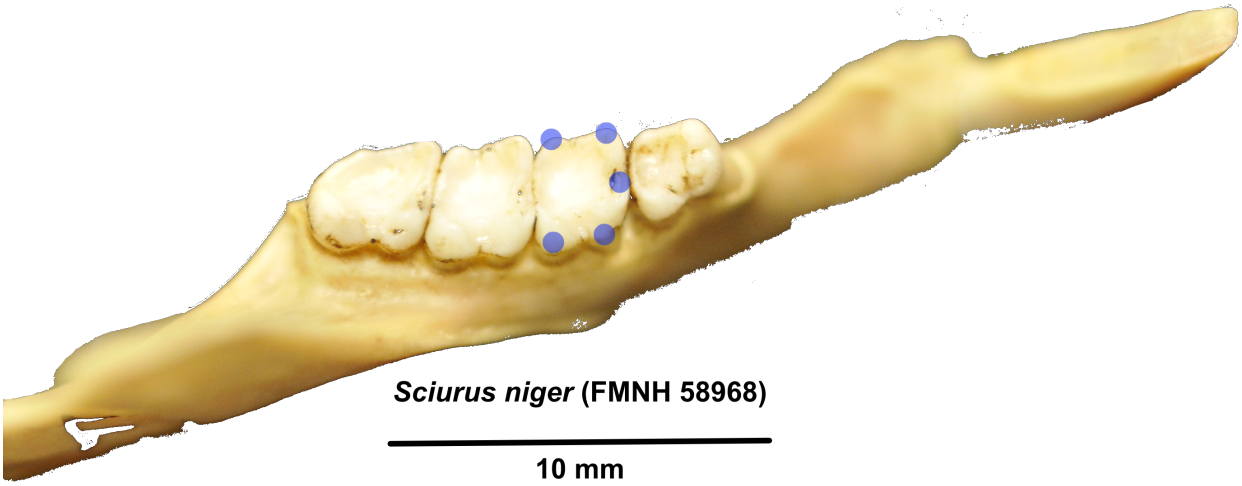

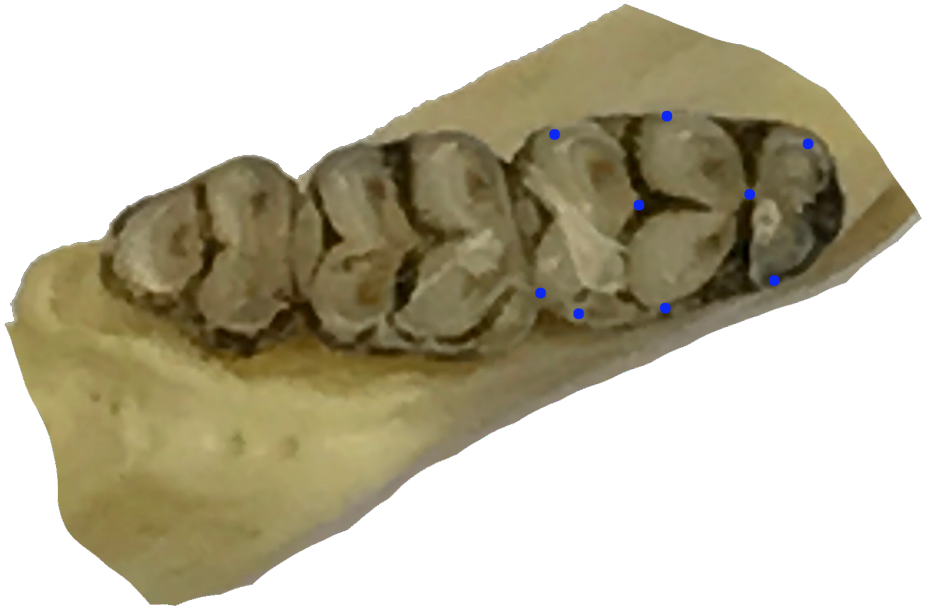

***Aethomys hindei* (FMNH 153217)**

10 mm

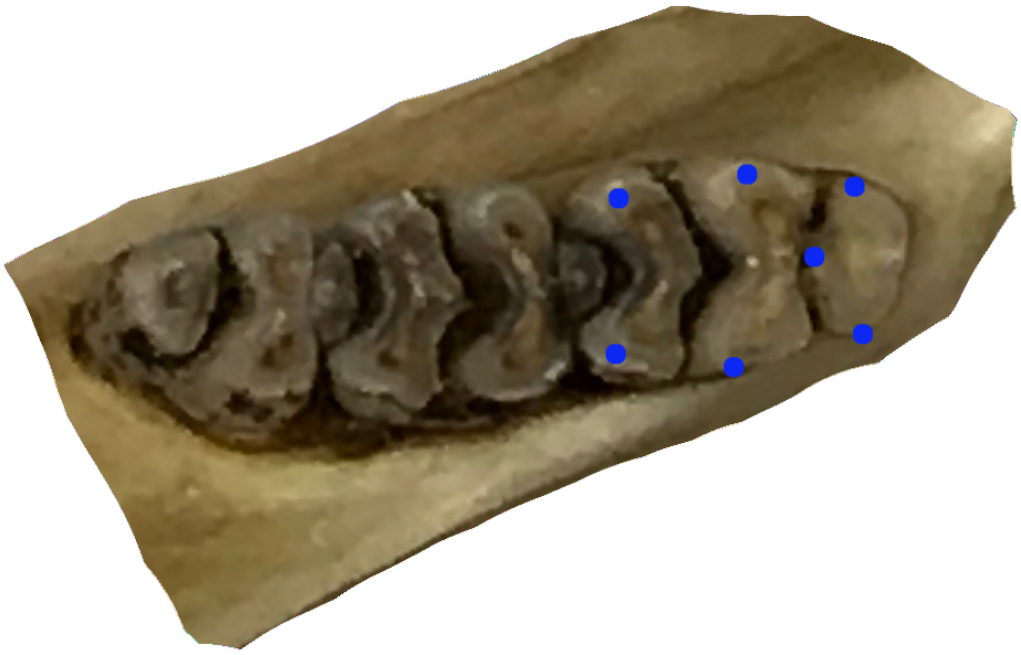

***Leopoldamys sabanus* (FMNH 168675)**

10 mm

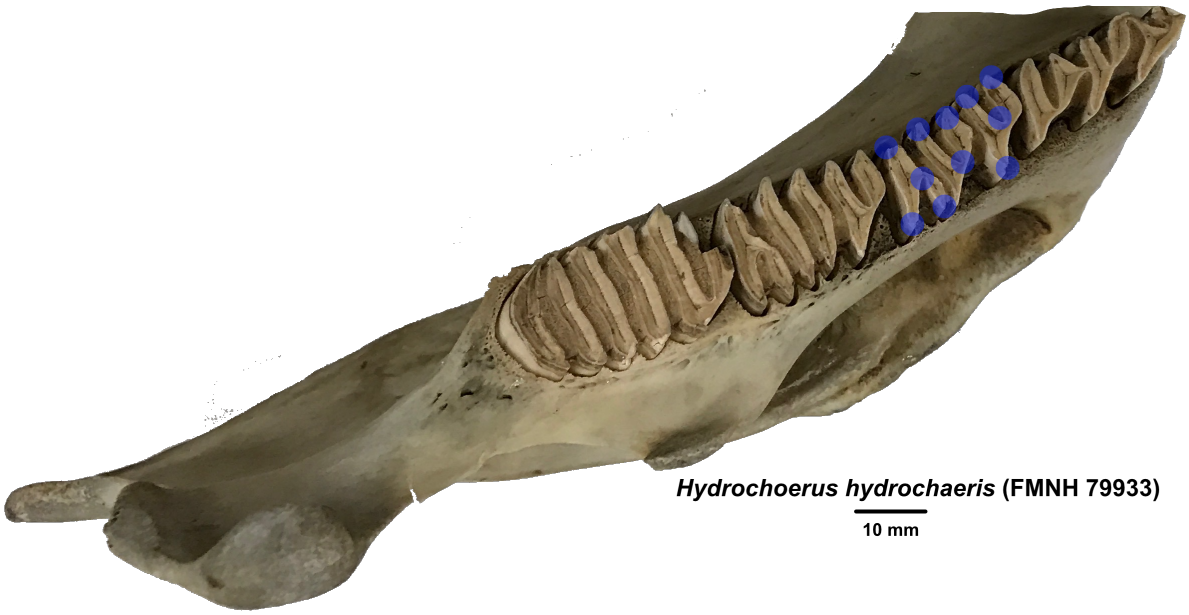
Hydrochoerus hydrochaeris (FMNH 79933)
10 mm

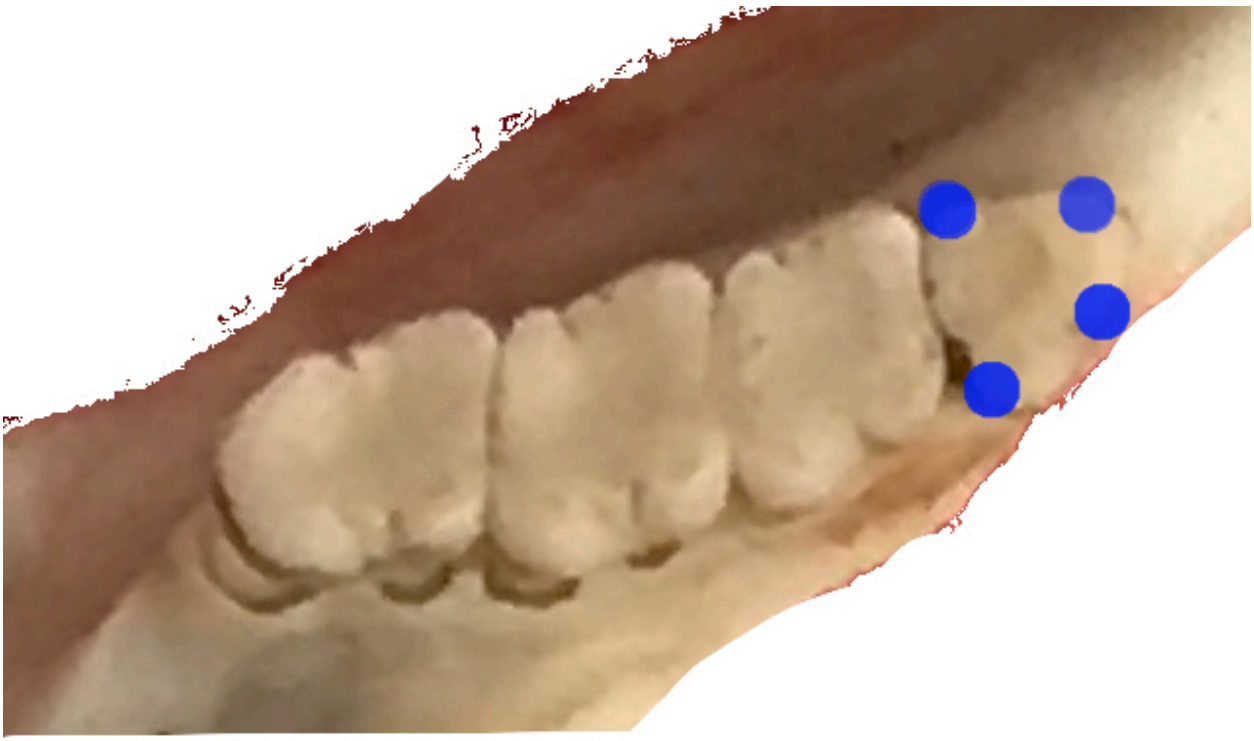

Tamiasciurus hudsonicus richardsoni

(FMNH 90924)

10 mm

***Crateromys schadenbergi* (FMNH 62295)**

10 mm

***Sylvilagus floridanus* (FMNH 16055)**

10 mm

***Berylmys bowersi* (FMNH 76474)**

10 mm

***Petaurista alborufus lena* (FMNH 91636)**

10 mm

***Tamiasciurus richardsoni* (FMNH 5571)**

10 mm

Castor canadensis (FMNH 134455)

10 mm

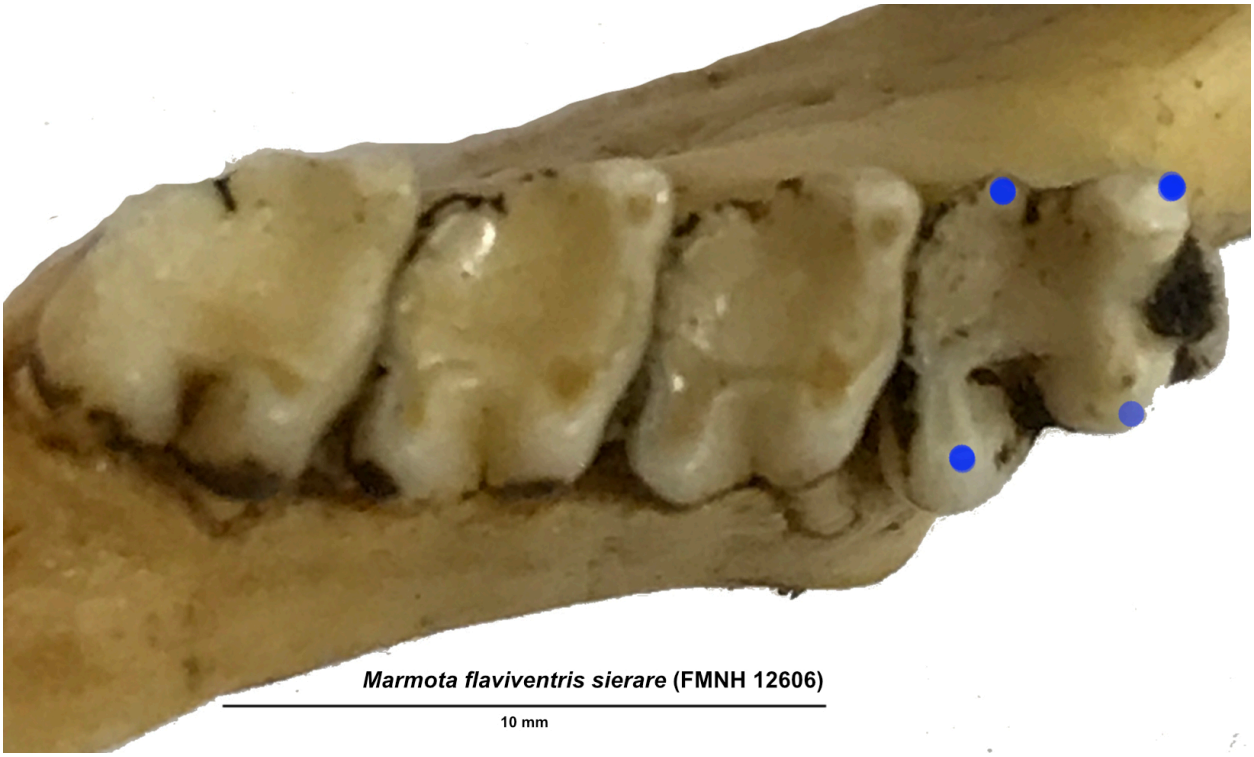

Marmota flaviventris sierare (FMNH 12606)

10 mm

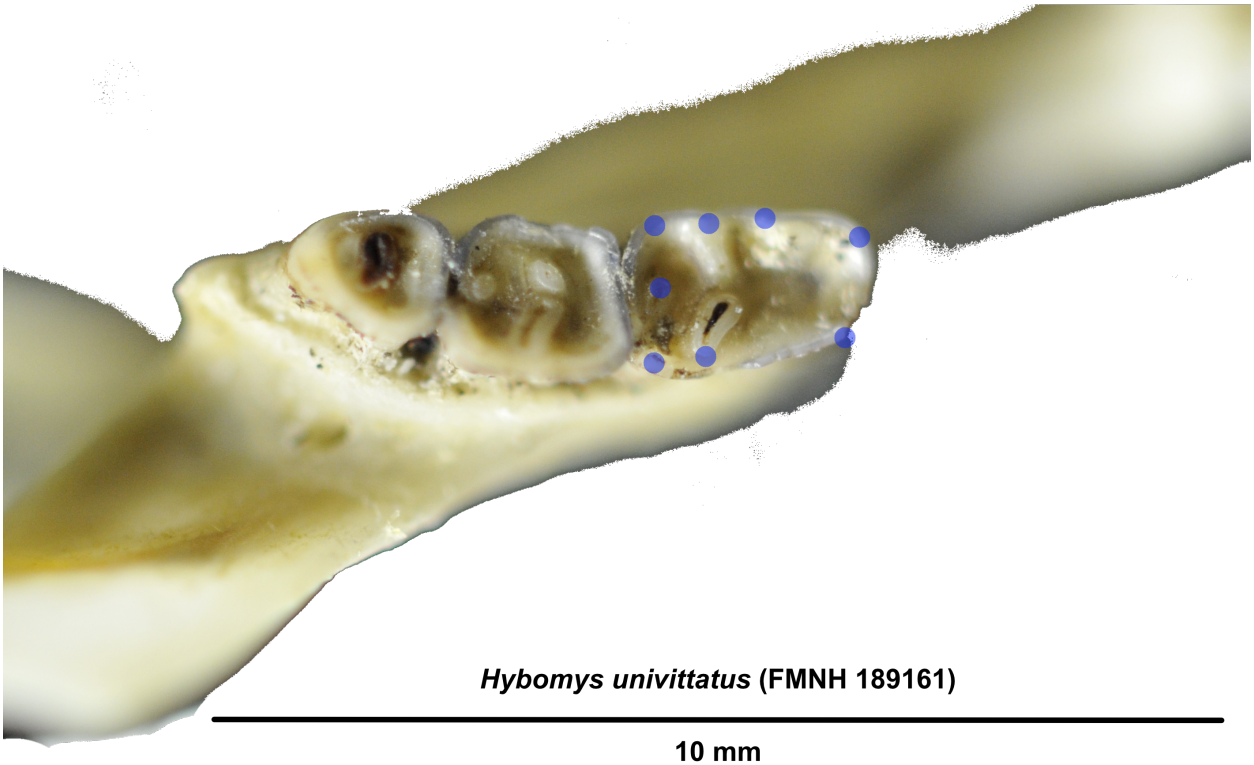

***Hybomys univittatus* (FMNH 189161)**

10 mm

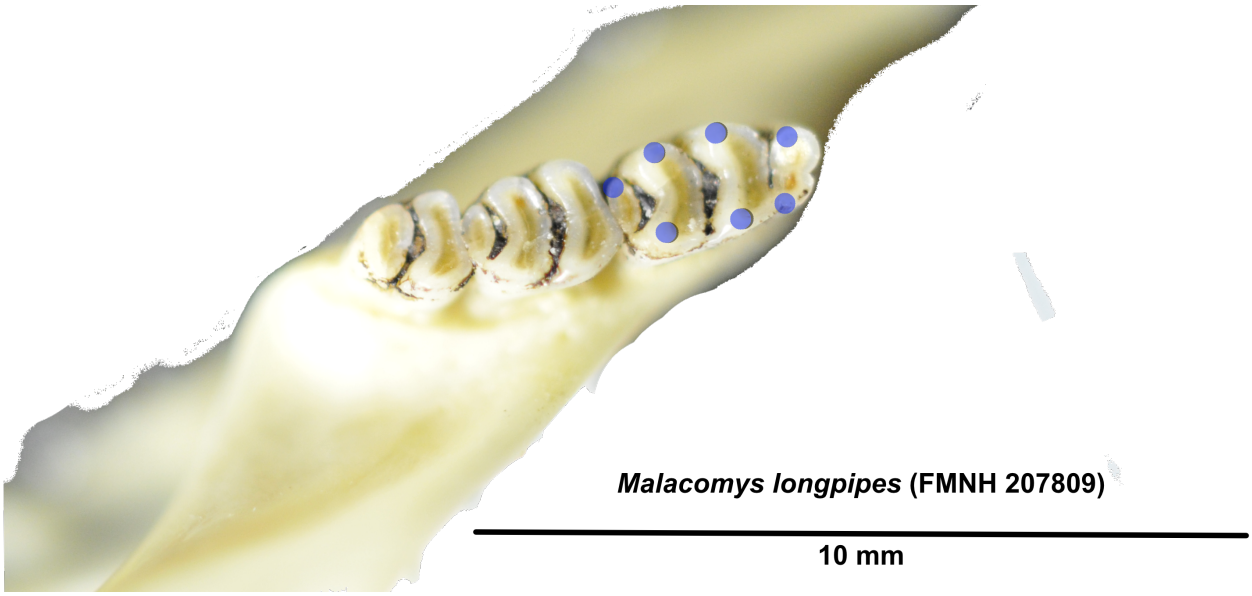

***Malacomys longpipes* (FMNH 207809)**

10 mm

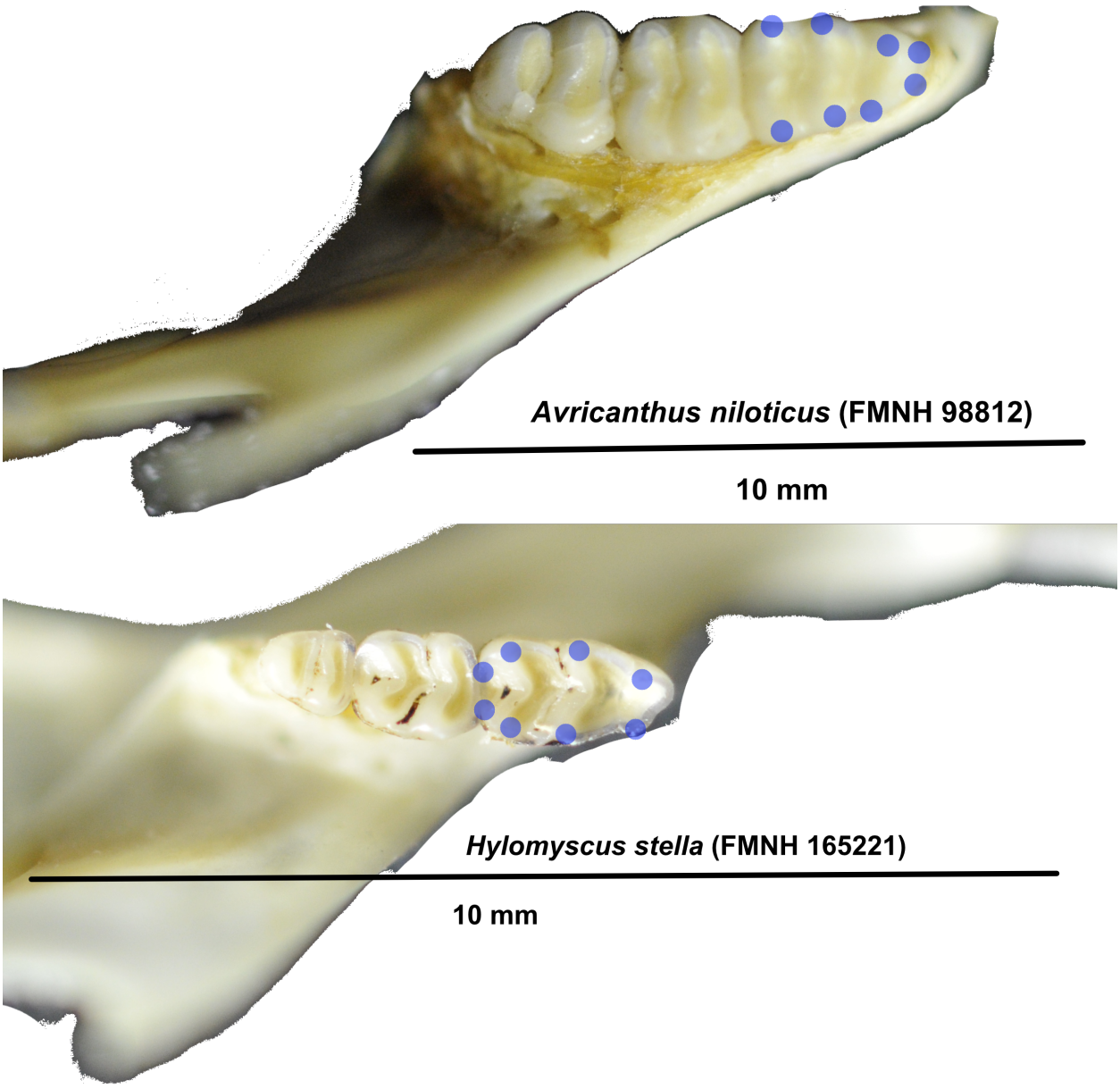
Avricanthus niloticus (FMNH 98812)
10 mm
Hylomyscus stella (FMNH 165221)
10 mm

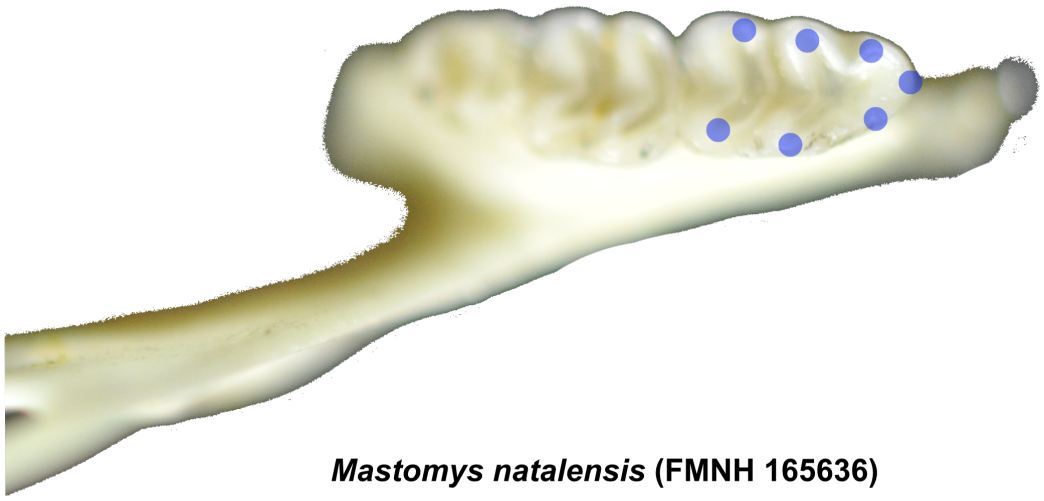

***Mastomys natalensis* (FMNH 165636)**

10 mm

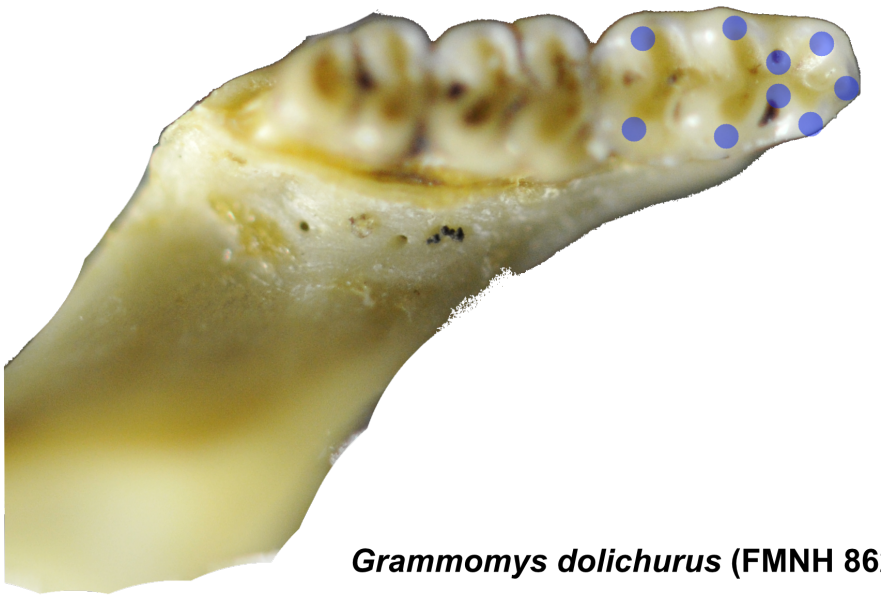

***Grammomys dolichurus* (FMNH 86252)**

10 mm

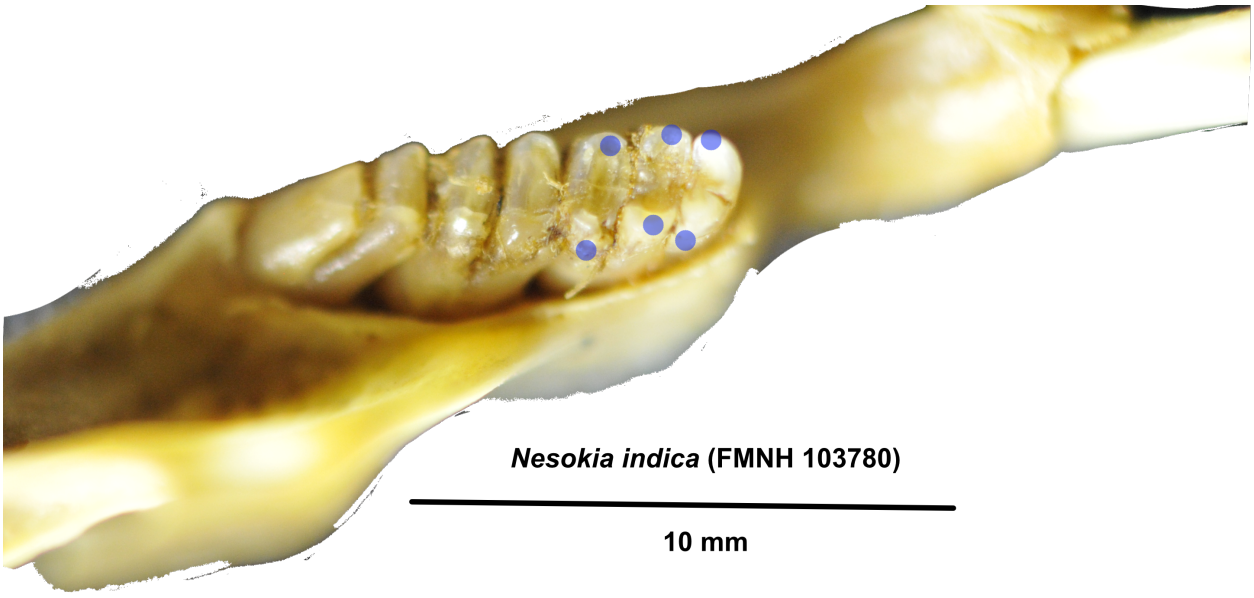

***Nesokia indica* (FMNH 103780)**

10 mm

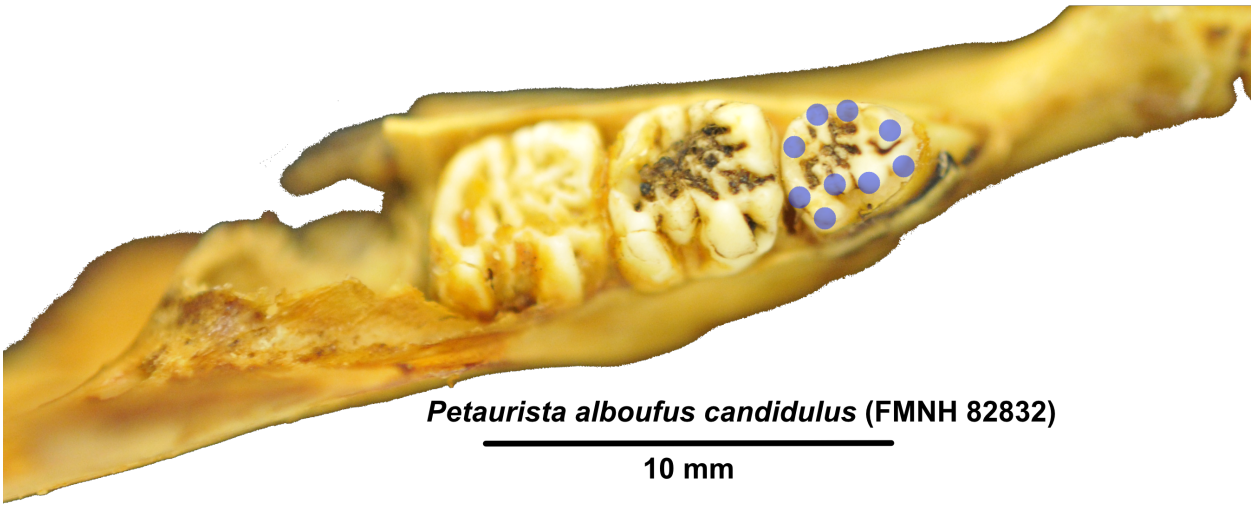
Petaurista alboufus candidulus (FMNH 82832)
10 mm

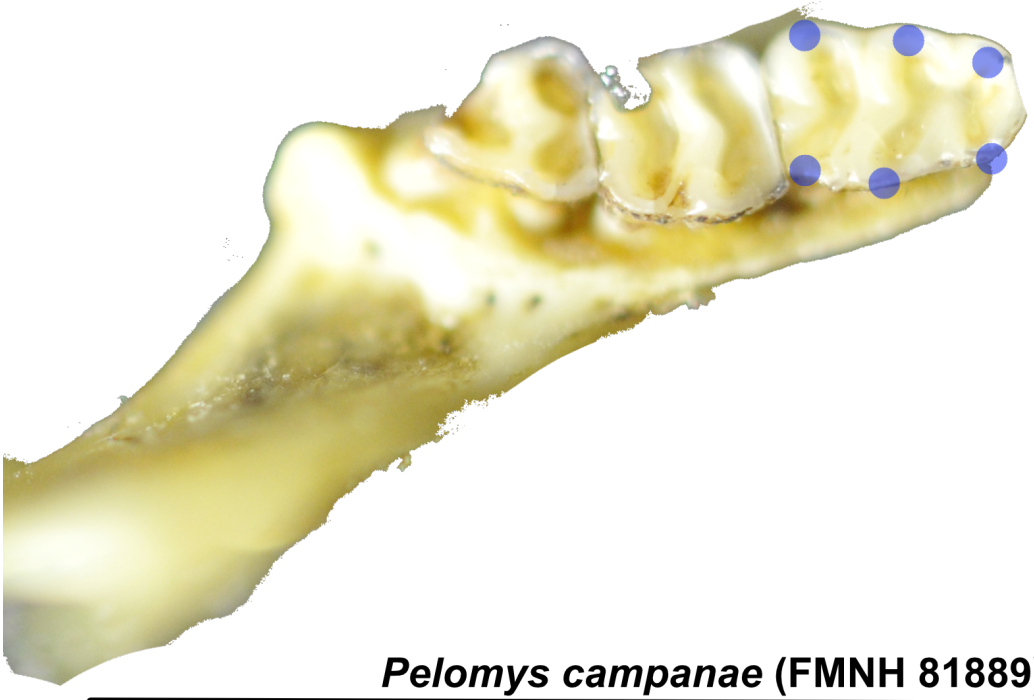

***Pelomys campanae* (FMNH 81889)**

10 mm

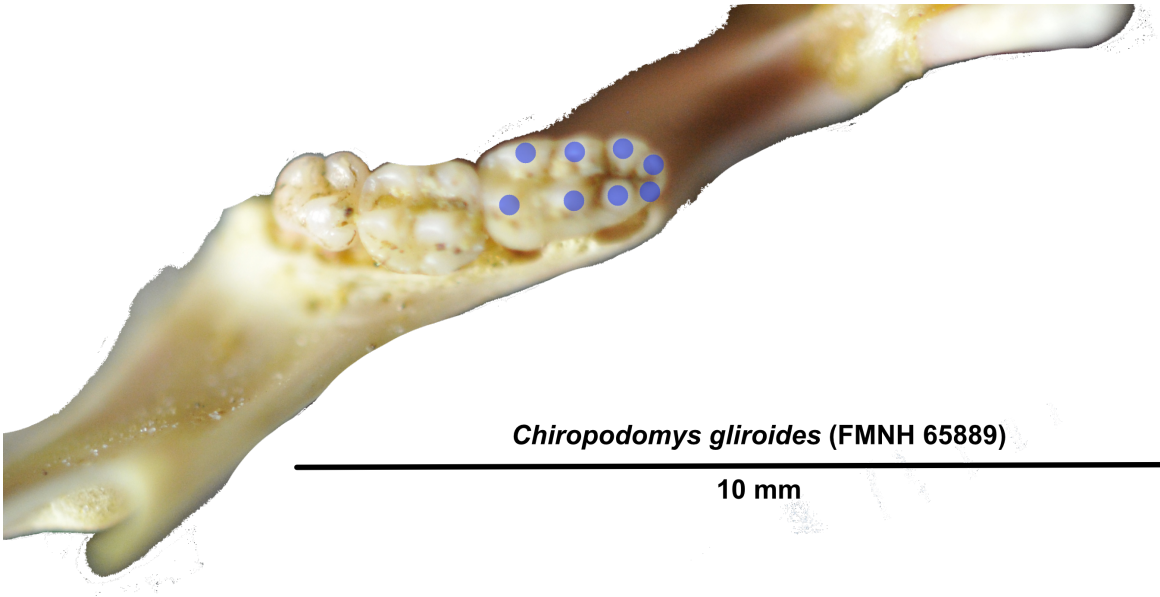

***Chiropodomys gliroides* (FMNH 65889)**

10 mm

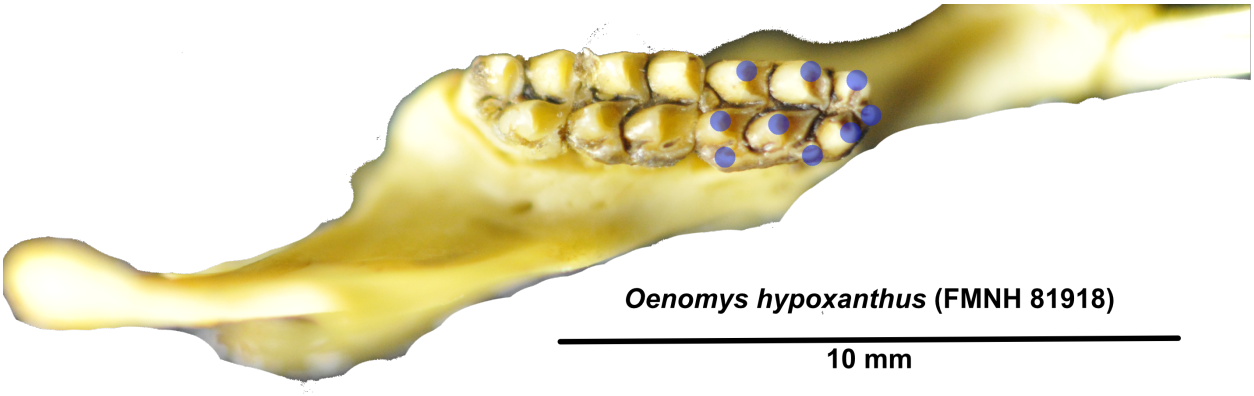

***Oenomys hypoxanthus* (FMNH 81918)**

10 mm

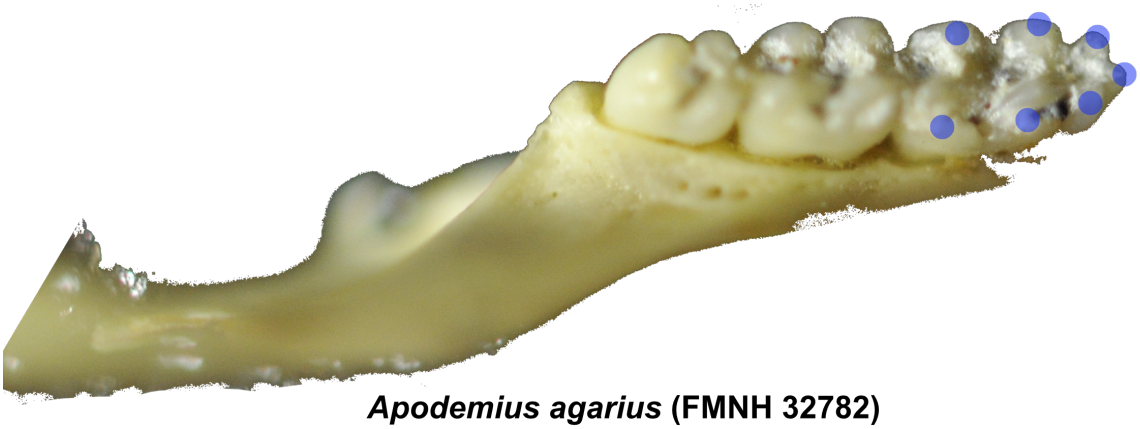

***Apodemius agarius* (FMNH 32782)**

10 mm

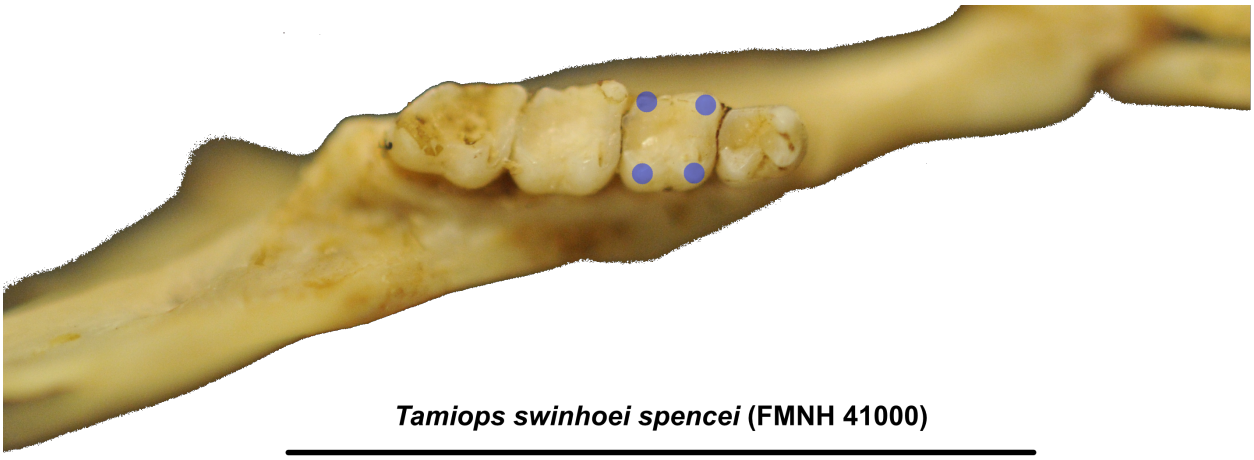

***Tamiops swinhoei spencei* (FMNH 41000)**

10 mm

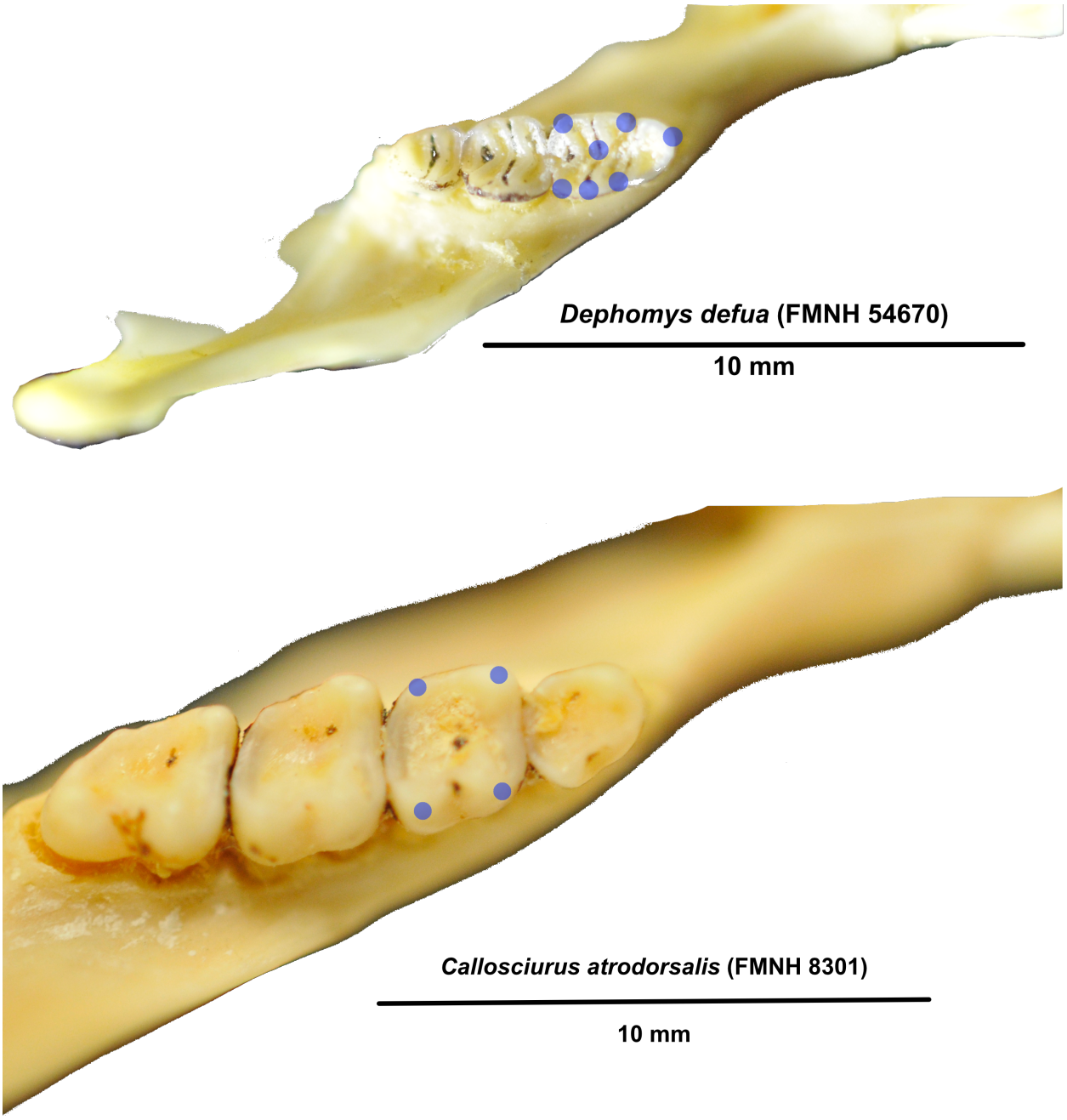
Dephomys defua (FMNH 54670)
10 mm
Callosciurus atrodorsalis (FMNH 8301)
10 mm

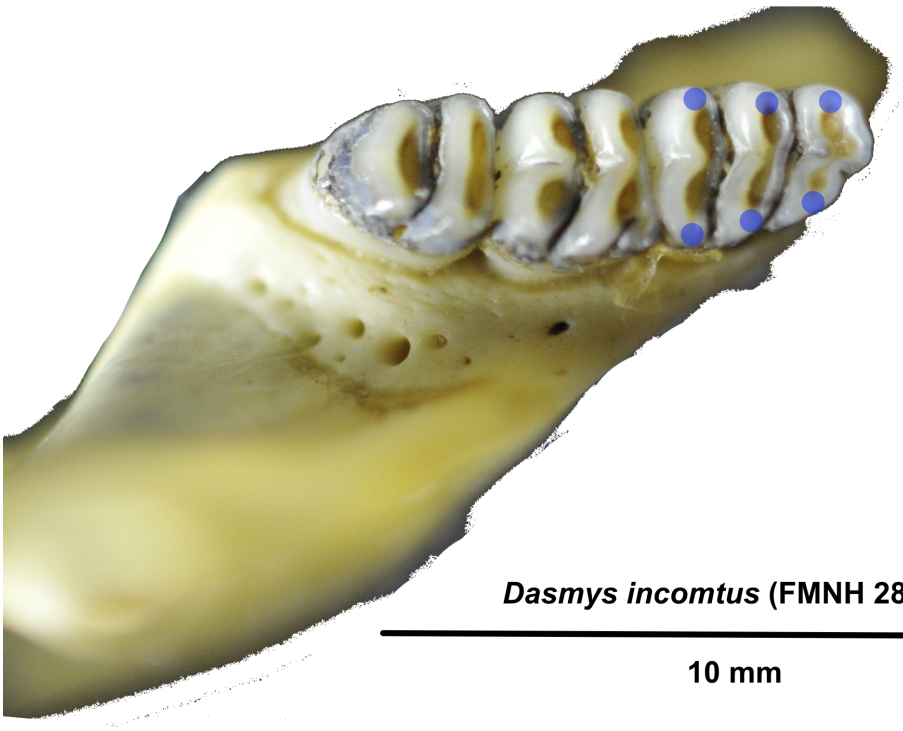

***Dasmys incomtus* (FMNH 28634)**

10 mm

Appendix 2.1: Specimen Data

Table A2.1.1: Extant Specimen Data

Specimen Numbers, Locality, Sub-Species Designation, State, and Triangle Number.

Institution	Locality	Sub-Species	State	Triangle
UMNH_35650	Humboldt_NV	L.c.i.	NV	5
UMNH_35651	Humboldt_NV	L.c.i.	NV	4
UMNH_38730	White_Pine_NV	L.c.i.	NV	5
UMNH_38920	Mineral_NV	L.c.i.	NV	5
UMNH_38924	Mineral_NV	L.c.i.	NV	5
UMNH_39580	White_Pine_NV	L.c.i.	NV	5
UMNH_39581	White_Pine_NV	L.c.i.	NV	6
UMNH_42245	Custer_ID	L.c.l.	ID	5
MVZ_7969	Humboldt_NV	L.c.c.	NV	6
MVZ_26426	Mono_CA	L.c.c.	CA	6
MVZ_26428	Mono_CA	L.c.c.	CA	5
MVZ_26430	Mono_CA	L.c.c.	CA	5
MVZ_26431	Inyo_CA	L.c.c.	CA	5
MVZ_26432	Mono_CA	L.c.c.	CA	5
MVZ_26435	Mono_CA	L.c.c.	CA	5
MVZ_26436	Mono_CA	L.c.c.	CA	5
MVZ_26446	Mono_CA	L.c.c.	CA	5
MVZ_38479	Esmeralda_NV	L.c.c.	NV	5
MVZ_38481	Esmeralda_NV	L.c.c.	NV	5
MVZ_38727	Esmeralda_NV	L.c.c.	NV	5
MVZ_54472	Sasketchewan	L.c.p.	CAN	5
MVZ_54473	Sasketchewan	L.c.p.	CAN	5
MVZ_66430	Lassen_CA	L.c.a.	CA	5
MVZ_121137	Mono_CA	L.c.c.	CA	6
MVZ_121138	Mono_CA	L.c.c.	CA	6

MVZ_208364	Mono_CA	L.c.c.	CA	5
MVZ_218372	Lassen_CA	L.c.i.	CA	5
MVZ_224234	Alpine_CA	L.c.c.	CA	5

Appendix 2.2: Generalized R-Code of analyses conducted

```
## R Markdown


library(Morpho)
library(geomorph)
library(SlicerMorphR)


#This reads in a log file of generalized procrustes analysis from SlicerMorph Extension in 3D-Slicer.


SM.log.file <-file.choose()


SM.log <- parser(SM.log.file)


head(SM.log)


SM.output <- read.csv(file = paste(SM.log$output.path,
                           SM.log$OutputData,
                           sep = "/"))



#This Extracts the number of landmarks no.LM used in the SlicerMorph GPA


PD <- SM.output[,2]
if (!SM.log$skipped) {
  no.LM <- SM.log$no.LM
  } else {
    no.LM <- SM.log$no.LM - length(SM.log$skipped.LM)
  }
PD
no.LM
```

```
#This converts slicermorph landmarks into a 3D array for reading into a geomorph.data.frame format downstream

coords <- arrayspecs(SM.output[, -c(1:3)],
                     p = no.LM,
                     k = 3)
dimnames(coords) <- list(1:no.LM,
                         c("x","y","z"),
                         SM.log$ID)

#Generalized Procrusted Analysis of landmarks in geomorph framework, gpagen.

gpa.fossil <- gpagen(SM.log$LM)

#Data Table with Locality and Sub-Species Information

data.table.fossil<-read.csv(file.choose())

#Subset Each Independent Variable from data.table.fossil

locality <-data.table.fossil$Locality

y_o <-data.table.fossil$Older.Younger

tri_num <-data.table.fossil$Triangle

#Conversion to Geomorph.Data.Frame without info

gdf.fossil <-geomorph.data.frame(gpa.fossil, specimens = SM.log$ID)

#Data.Frame with info
```

```
gdf.fossil <-geomorph.data.frame(gpa.fossil, specimens = SM.log$ID, locality = locality, y.o=
y_o, tri_number = tri_num)


#MorphologicalDisparityTest - Determine if there is a signal for grouping based on either allome-
try or the total dataset without a priori assumption


morphol.disparity.locality <-morphol.disparity(coords ~ Csize, groups = locality, data = gdf.fossil,
iter=99, print.progress=FALSE)


summary(morphol.disparity.locality)


#Triangle Number


morphol.disparity.tri.num <-morphol.disparity(coords ~ Csize, groups = tri_num, data = gdf.fos-
sil, iter=99, print.progress=FALSE)


summary(morphol.disparity.tri.num)


#LandMark Subset for Modularity Analysis - 'a' = anterior, 'p' = posterior - Not the cleanest way,
but this does work.


land.gps<-rep('x', 1006)


land.gps[1:3]<-'a'; land.gps[9:11]<-'a';land.gps[21:200]<-'a'; land.gps[237:275]<-'a';
land.gps[705:784]<-'a';land.gps[809:812]<-'a';


land.gps[4:8]<-'p';land.gps[12:20]<-'p';land.gps[201:236]<-'p'; land.gps[276:704]<-'p';
land.gps[785:808]<-'p'; land.gps[813:875] [878:1008]<-'p'


land.gps


#ModularityAnalysis
```

```
m_test<-modularity.test(gpa.fossil$coords, land.gps, CI=TRUE, iter=99)

CInterval<-m_test$CInterval

CInterval

CRBoot <-m_test$CR.boot

CRBoot

summary(m_test)

plot(m_test)

#IntegrationTest

i_test<-integration.test(gpa.fossil$coords, A2=NULL, partition.gp=land.gps, iter=99)

summary(i_test)

plot(i_test)

#ProcrustesANOVA

fit_locality <-procD.lm(coords ~ locality, data=gdf.fossil, iter=999, turbo=TRUE)

summary(fit_locality)

plot(fit_locality)

#Triangle Number
```

```
fit_tri.num <-procD.lm(coords ~ tri_num, data=gdf.fossil, iter=999, turbo=TRUE)

summary(fit_tri.num)

plot(fit_tri.num)

#Locality Specific Age

fit_y.o <-procD.lm(coords ~ y.o, data=gdf.fossil, iter=999, turbo=TRUE)

summary(fit_y.o)

plot(fit_y.o)


#End
```

Appendix 3.1: Specimen Data for Fossils

Table A3.1.1: Data table of fossil specimens

Locality, general age, stratigraphic age (older vs. younger), and triangle number

Specimen	Locality	General Age	Older/Younger	Triangle
BYU_7726977	RockSprings	50-5	Y	5
TMM_2109	Cathedral	200-150	Y	5
TMM_2112	Cathedral	200-150	Y	5
TMM_2125	Cathedral	200-150	Y	5
TMM_2126	Cathedral	200-150	Y	5
TMM_2133	Cathedral	200-150	Y	4
UCMP_155279	Porcupine	1000-750	O	5
UCMP_155283	Porcupine	1000-750	O	4
UCMP_155284	Porcupine	1000-750	O	5
UCMP_155286	Porcupine	1000-750	O	5
UCMP_155287	Porcupine	1000-750	O	5
UCMP_155356	Porcupine	1000-750	O	5
UCMP_155357	Porcupine	1000-750	O	5
UCMP_155359	Porcupine	1000-750	O	5
UCMP_155361	Porcupine	1000-750	O	5
UCMP_155368	Porcupine	1000-750	O	5
UCMP_155372	Porcupine	1000-750	O	4
UCMP_155376	Porcupine	1000-750	O	4
UCMP_155380	Porcupine	1000-750	O	4
UCMP_155383	Porcupine	1000-750	O	5
UCMP_155386	Porcupine	1000-750	O	5
UCMP_213235	Porcupine	1000-750	O	4
UCMP_213253	Porcupine	1000-750	O	4
UCMP_213366	Porcupine	1000-750	O	4
UW_67283	Kennewick	50-5	Y	5

UW_67284	Kennewick	50-5	Y	5
UW_67285	Kennewick	50-5	Y	4
UW_67286	Kennewick	50-5	Y	5
UW_67290	Kennewick	50-5	Y	5
UW_67292	Kennewick	50-5	Y	5
UW_67376	Kennewick	50-5	Y	5
UW_68224	Kennewick	50-5	Y	5

Appendix 3.2: Specimen Data for All Specimens

Table A3.2.1: Data Table of All Specimens

Locality, whether they are fossil (F) or extant (E) specimens, and closed triangle number (Triangle)

Specimen	Locality	Fossil/Extant	Triangle
BYU_7726977	RockSprings	F	5
MVZ_121137	Mono_CA	E	6
MVZ_121138	Mono_CA	E	6
MVZ_208364	Mono_CA	E	5
MVZ_218372	Lassen_CA	E	5
MVZ_224234	Alpine_CA	E	5
MVZ_26426	Mono_CA	E	6
MVZ_26428	Mono_CA	E	5
MVZ_26430	Mono_CA	E	5
MVZ_26431	Inyo_CA	E	5
MVZ_26432	Mono_CA	E	5
MVZ_26435	Mono_CA	E	5
MVZ_26436	Mono_CA	E	5
MVZ_26446	Mono_CA	E	5
MVZ_38479	Esmeralda_NV	E	5
MVZ_38481	Esmeralda_NV	E	5
MVZ_38727	Esmeralda_NV	E	5
MVZ_54472	Sasketchewan	E	5
MVZ_54473	Sasketchewan	E	5
MVZ_66430	Lassen_CA	E	5
MVZ_7969	Humboldt_NV	E	6
TMM_2109	Cathedral	F	5
TMM_2112	Cathedral	F	5
TMM_2125	Cathedral	F	5

TMM_2126	Cathedral	F	5
TMM_2133	Cathedral	F	4
UCMP_155279	Porcupine	F	5
UCMP_155283	Porcupine	F	4
UCMP_155284	Porcupine	F	5
UCMP_155286	Porcupine	F	5
UCMP_155287	Porcupine	F	5
UCMP_155356	Porcupine	F	5
UCMP_155357	Porcupine	F	5
UCMP_155359	Porcupine	F	5
UCMP_155361	Porcupine	F	5
UCMP_155368	Porcupine	F	5
UCMP_155372	Porcupine	F	4
UCMP_155376	Porcupine	F	4
UCMP_155380	Porcupine	F	4
UCMP_155383	Porcupine	F	5
UCMP_155386	Porcupine	F	5
UCMP_213235	Porcupine	F	4
UCMP_213253	Porcupine	F	4
UCMP_213366	Porcupine	F	4
UMNH_35650	Humboldt_NV	E	5
UMNH_35651	Humboldt_NV	E	4
UMNH_38730	White_Pine_NV	E	5
UMNH_38920	Mineral_NV	E	5
UMNH_38924	Mineral_NV	E	5
UMNH_39580	White_Pine_NV	E	5
UMNH_39581	White_Pine_NV	E	6
UMNH_42245	Custer_ID	E	5
UW_67283	Kennewick	F	5
UW_67284	Kennewick	F	5
UW_67285	Kennewick	F	4

UW_67286	Kennewick	F	5
UW_67290	Kennewick	F	5
UW_67292	Kennewick	F	5
UW_67376	Kennewick	F	5
UW_68224	Kennewick	F	5